DEVELOPMENT OF SPECKLE INTERFEROMETRY FOR SIMULTANEOUS DUAL SENSITIVE MEASUREMENT

by

XIAOWAN ZHENG

A dissertation submitted in partial fulfillment of the requirements for the degree of

DOCTOR OF PHILOSOPHY IN SYSTEM ENGINEERING

2023

Oakland University
Rochester, Michigan

Doctoral Advisory Committee:

Lianxiang Yang, Ph.D., Chair
Gary Barber, Ph.D.
S. Ali Arefifar, Ph.D.
Ankun Yang, Ph.D.
Cunxiang Yang, Ph.D.

© Copyright by Xiaowan Zheng, 2023
All rights reserved

To my mother and father, thanks for their love, help and support.

ACKNOWLEDGMENTS

Firstly, I would like to express my gratitude to my supervisor, Lianxiang Yang, who provided me with tremendous support throughout my entire Ph.D. study. He not only taught me professional knowledge and academic skills, but also led me on the road of both academics and life. Without his guidance and instruction, I would not have been able to complete my doctoral degree and dissertation.

I would also like to thank all the members of my academic committee, including Professor Gary Barber, Professor S. Ali Arefifar, Professor Ankun Yang, and Professor Cunxiang Yang, for their support and help.

Additionally, I am grateful to Zhengzhou University of Light Industry for their enormous support.

Especially, I really appreciate my mother and father, they gave me so much love, help, and great support for all things I want. Furthermore, I am grateful to my husband for his support in my personal life, which allowed me to focus on my studies and research. I also want to express my gratitude to my son for his emotional comfort and support.

Lastly, I want to thank all my colleagues, professors, and faculties who helped me throughout my entire study at Oakland University.

Xiaowan Zheng

PREFACE

Digital speckle interferometric measurement techniques, including digital speckle pattern interferometry (DSPI, also called digital holography) and digital speckle pattern shearing interferometry (also called digital shearography), offer advantages such as high precision, high sensitivity, full-field measurement, non-contact, and real-time capabilities. They are widely applied in the measurement of deformation and the first derivative of deformation as well as in the detection of internal defects in various materials, especially for composite materials, in industrial settings, including the automotive and aerospace industries.

Traditional measurement methods using speckle pattern interferometry can only target one parameter or a single spatial resolution at a time. However, in practical applications, measurements with multiple parameters or multiple spatial resolutions are beneficial to practical applications for material evaluations and nondestructive testing. To reach these goals, the most direct approach is to perform multiple repeated measurements, but this leads to increased time and detection costs. Additionally, in certain situations, repeated measurements are not feasible, therefore, the development of synchronized dual-sensitivity detection methods is useful for industrial applications.

Current research on synchronized dual-sensitivity detection mainly falls into two categories. One category involves synchronously detecting different parameters at a single spatial resolution, while the other focuses on synchronously detecting the same parameter at different spatial resolutions. There is relatively abundant research on the first category, including synchronous dual-direction shearography, in-plane and out-of-plane deformation measurement, and deformation and first derivatives of deformations measurement. However, research on the second category is relatively limited, with few studies found. This research primarily focuses on the second category, namely, simultaneous dual-spatial resolution detection methods.

The key points to achieve simultaneous dual-spatial resolution measurement include the following parts: design of the optical layout, obtaining dual spatial resolution, constructing dual channels, and obtaining phase information. The main challenges are how to design an optical setup which includes different field-of-views (i.e. dual channels) and how to separate the information (i.e. phase information) of the different field-of-views recorded in a single image. An innovative development by using polarization techniques, Fourier and inverse Fourier transforms, and spatial carrier phase-shifting technique was made to solve these challenges. This doctoral dissertation provides an overall introduction to the fundamental methods and principle involved. It also gives a summary of the current relevant research.

The main research of this doctoral dissertation proposes a novel method utilizing digital holography to achieve simultaneous dual spatial resolution sensitivity measurements. This system marks the first application of holography for simultaneous dual spatial resolution sensitivity measurement. It accomplishes dual spatial resolution measurements by observing different-sized fields of view, establishes dual channels using polarization techniques to avoid cross-interference, and employs spatial carrier techniques to separate and extract phase information, thereby successfully achieving simultaneous dual spatial resolution measurements.

In addition, an improvement to overcome the current shortcoming of overlapping spectra in the existing dual-resolution shearography system. This improvement primarily addresses the issue of overlapping spectra only along the x-direction in the frequency domain. By adjusting the shearing direction and controlling the distribution of spectra in the frequency domain, the spectra corresponding to different resolutions are separated along the x and y directions respectively, effectively solving the overlaped spectral information. The development makes the current shearography dual-resolution system much easier and more practical.

ABSTRACT

DEVELOPMENT OF SPECKLE PATTERN INTERFEROMETRY FOR SIMULTANEOUS DUAL SENSITIVE MEASUREMENT

by

Xiaowan Zheng

Adviser: Lianxiang Yang, Ph.D.

Digital speckle interferometry involves two main methods: digital speckle pattern interferometry (DSPI/Digital Holography) and digital speckle pattern shear interferometry (Digital Shearography). This technology allows for non-destructive, full-field, high-precision measurements.

In early stages, speckle interferometry was limited to measuring a single parameter in a single test, like in-plane or out-of-plane deformation or the first derivative of displacement (strain) along horizontal or vertical directions. However, advancements in speckle technology now allow simultaneous measurement of two of above parameters. These measurements systems, though, have limitations—they possess a single spatial resolution, resulting in certain drawbacks during deformation detection and non-destructive testing, such as difficulty in evaluating dense fringes or overlooking smaller defects.

Recent advancements have led to a new study using digital shearography, measuring one parameter with two different spatial resolutions. However, due to its recent emergence, there's limited literature on this method. Both measuring two

parameters with one spatial resolution and measuring one parameter with two spatial resolutions are referred to as dual-sensitive measurement.

This study mainly concentrates on simultaneous measurement of target parameters using speckle pattern interferometry technology. It delves into two key areas: enhancing digital shearography to achieve dual parameters and dual spatial resolution measurements, and developing novel digital holography for dual spatial resolutions.

The novel digital holography method employs different-sized fields of view and polarization techniques to establish independent optical channels. Unlike shearography systems, it uses spatial carrier phase-shifting technology to separate overlapped intensity maps. This method proves more convenient and practical than traditional methods by eliminating the need to adjust shear directions. Ultimately, this technique can simultaneously produce dual-sensitive measurement results at different spatial resolutions, reducing the need for redundant measurements and saving time and labor costs. With ongoing enhancements, this technology holds significant promise for industrial applications and interest researchers focused on experimental mechanics via speckle/holographic interferometry.

TABLE OF CONTENTS

TABLE OF CONTENTS—Continued

LIST OF TABLES

LIST OF FIGURES

LIST OF ABBREVIATIONS

NDT	Non-Destructive Testing
PS	Photographic Shearography
ES	Electronic Shearography
PSPI	Photographic Speckle Pattern Interferometry
ESPI	Electronic Speckle Pattern Interferometry
DSPI	Digital Speckle Pattern Interferometry
DS	Digital Shearography
CCD	Charge-Couple Device
PZT	Piezoelectric Ceramics
OPD	Optical Path Difference
SLM	Spatial Light Modulator
FT	Fourier Transfer
FIT	Fourie Inverse Transfer

CHAPTER ONE

INTRODUCTION AND SCOPE OF WORK

1.1 Background

Speckle interferometry is a full-field, non-contacting, high-precision optical interferometry technique suited for surface deformation and strain measurement as well as for nondestructive testing. Speckle interferometry includes two major technologies, speckle pattern interferometry (SPI) and speckle pattern shearing interferometry (SPSI). In recent decades of development, speckle pattern interferometry can be divided into photographic speckle pattern interferometry (PSPI), electronic speckle pattern interferometry (ESPI, also called TV-Holography) and Digital speckle pattern interferometry (DSPI, also called Digital Holography) [1-3]. Similarly, the speckle pattern shearing interferometry, also called shearography can be divided into photographic speckle pattern shearing interferometry (PSPSI), electronic speckle pattern shearing interferometry (ESPSI/TV-shearography) and digital speckle pattern shearing interferometry (DSPSI/digital shearography) [4-6].

Among the technologies mentioned above, the latest and most widely used are Digital shearography and digital holography. Digital holography directly measures the deformation. While digital shearography directly measures the deformation gradient (strain components). These two technology have been widely used for deformation measurements, strain measurement, and non-destructive testing (NDT) due to its advantages of high sensitivity, high accuracy, and whole-field, non-touch measurements.

The traditional speckle interferometry measurement method can only measure one parameter with a given field of view. If two parameters or one parameter with different fields of view are needed, repeated measurements must be carried out and these measurements are usually acceptable for some common measurements. It is, however, difficult for precise measurements, such as by digital holography and digital shearography which measure submicron deformations or relative deformations because the loading is hardly exactly repeated and, in some cases, repeated measurement are not allowed, which limit the practical applications of holography and shearography where multiple parameters measurement or one parameter with multiple fields of view are needed. Obviously, development of simultaneous measurement for multiple parameters or single parameter but with multiple sensitivities are needed.

1.2 Review of existed research work

This research is focused on the development of speckle interferometry system for simultaneous dual-sensitive measurements, belonging to dual-channel measurements or dual-parameter measurements Reported research on multi-channels measurements can be divided into two categories: one is simultaneously to measure two parameters with same spatial resolution, e.g. to measure deformation and the first derivative of deformation simultaneously the other one is to measure one parameter, but with two fields of view simultaneously, e.g. a large field of view and a small field of view. almost all of the existing methods use the same spatial resolution, i.e., to measure two parameters with a same field of view. There are three kinds of examples of these. The first kind is to measure the first derivative of deformation in the x- and y- directions by digital shearography. In these systems, the two sensitivity results correspond to two shearographic systems, one in the x-shearing direction to measure the first derivative of deformation in the x-direction and the other in the y-shearing direction to measure the first derivative of deformation in the y-direction. Three methods have been reported to separate the information from these two channels in the final results. The first one is to use a two-camera system to record the information of the two channels separately [7]. The second method is to observe different channels on one color camera using RGB channels in combination with different laser wavelengths [8]. The last method is to use one black/white camera based on the polarization technology to avoid cross-interference [9,10]. These types of two-channel digital shearographic systems can be useful for NDT because some defects are sensitive to different directions of the first derivative of deformation. The second example is a two sensitivities measurement system with the same spatial resolution that simultaneously measures the deformation and its first derivative. For these systems, one channel is related to a holographic/electronic speckle pattern interferometry (ESPI) system which can measure deformation and the other is related to a shearographic system which can directly measure the first derivative of the deformation [11–13]. Such kinds of systems are used if both the deformation and its derivative are needed at the same time. The last example is two sensitivity measurement systems with the same spatial resolution that simultaneously measure both out-of-plane and in-plane strains. In these systems, one channel is used for an out-of-plane shearographic system and the other for an in-plane shearographic system for strain measurement [14,15].

Another application of dual-channel measurement is to measure only one parameter, but with different spatial resolutions, e.g. a large field of view to see whole area and a small filed view to see an interested area with an enhanced spatial resolution. A Sagnac interferometer-based digital shearography system has been reported by Boyang Zhang, Xiaowan Zheng, et al. [16]. They used a Sagnac interferometer-based optical layout to enable a dual spatial resolution shearography system to measure the first derivative of deformation. It was the first report of a system that allows two shearograms, one for a large field of view and one for a small field of view, to be obtained simultaneously. The development of this technology advanced digital shearography for NDT. However, a deficiency of the developed technology is the phenomenon of spectrum aliasing because the two shearograms have the same shearing direction, e.g., in the x-shearing direction, and all the spectra lie on the x-axis. In shearography, the orientation and separation of the spectrum are determined by the shearing direction and shearing amounts, respectively.

1.3 Scope of research

Current research is focused on the development of simultaneous dual-sensitivity measurements utilizing speckle interferometry technology. Existing studies on simultaneous dual-sensitivity measurements primarily concentrate on synchronously measuring two parameters at the same spatial resolution. However, research on simultaneously measuring the same parameter at different spatial resolutions is very limited. Additionally, all the reported studies so far have been based on shearography systems, and there have been no documented publications using holography systems. The existing studies regarding simultaneous dual-spatial-resolution measurements also employ shearography technology. Nevertheless, the optical structure of such systems is relatively complex, and due to the spectral distribution only along the x-axis in the frequency domain, spectral overlap is prone to occur. Shearography primarily measures the first derivative of deformation, while holography directly measures deformation. Although measuring the first derivative of deformation has benefits for non-destructive testing, in the field of experimental mechanics, measuring deformation is equally significant, sometimes even more crucial, as deformation represents an object's fundamental behavior under loading. In experimental mechanics and non-destructive testing, achieving high spatial resolution measurements for large-sized objects has always been a pressing issue.

This thesis first improves the method of synchronous dual-spatial-resolution measurement using shearography technology. This enhancement encompasses two aspects: first, transitioning from measuring one parameter to measuring two parameters; second, addressing the issue of spectral overlap caused by the spectral distribution only along the x-axis in the frequency domain.

The primary focus of this paper is on utilizing holography technology to achieve synchronous dual-spatial-resolution measurements. A novel dual-spatial-resolution holography system is proposed for deformation measurement, featuring a relatively simple optical setup that facilitates the easy separation of spectra from two channels. By adjusting the combined focal length, the two holographic sets can observe different fields of view, one with a large field of view and the other with a small field of view. To achieve synchronous measurements, polarization technology is employed to mitigate cross-interference between the two optical layouts [17]. Finally, using spatial carrier frequency technology [18], the reference beam is adjusted by introducing different carrier frequencies, thereby obtaining spatial carrier fringes in different directions in the speckle pattern images captured by the two holographic devices. The distinct spatial carrier fringes in different directions enable easy separation of the spectra of the two interference patterns after FT (Fourier Transformation), overcoming the main drawback of spectral aliasing in dual-spatial-resolution shear imaging systems. By Fourier Transforming the spectra and applying windowing, the phase distributions of the two internal images can be extracted and separated. These phase distributions can then be utilized for deformation analysis and computation. Various application cases will be introduced, and the practicality of this method will be verified through experimental results.

1.4 Dissertation structure arrangement

In this dissertation, Chapter One gives the introduction and scope of works. Firstly, the research background of this paper is introduced, and the speckle interferometry and synchronous double sensitivity detection technology are briefly introduced. The development and research status of speckle interferometry synchronous double sensitivity detection are summarized in detail. Then, the problems in this technique are proposed, and the research in this paper is briefly explained. A measurement method using Shearography technology for simultaneous double spatial resolution is developed, and a new method using Holography for simultaneous double spatial resolution is proposed.

Chapter Two introduces the basic theory of speckle interferometry. The development, basic theory and basic application of laser speckle, digital speckle interferometry (Digital Holography), and digital speckle shear interferometry (Digital shearography) are introduced respectively.

Chapter Three reviews the basic theory and basic method of phase shifting technology. Firstly, the real-time intensity method is introduced. Then the time phase shifting technique is explained. Finally, the space phase shift technology is introduced, with emphasis on the space carrier frequency phase shift technology.

Chapter Four introduces the simultaneous sensitive measurement. In this chapter, recent research on dual sensitive measurement are reviewed. And the method to achieve the dual resolution is presented. Also, how to achieve the simultaneous dual resolution measurement is introduced in detail.

In the Fifth chapter, an improvement of digital shearography for dual sensitivity simultaneous measurement is introduced. A method to solve the issue of overlap spectrum is introduced.

Chapter Six introduces a development of simultaneous dual resolution digital holography system. This system presented a novel holography system to achieve dual resolution measurement simultaneously.

In the end, Chapter Seven gives the conclusion.

CHAPTER TWO

BASIC THEORY OF SPECKLE INTERFEROMETRY

2.1 Speckle interferometry

The physical basis of speckle interferometry is optical speckle phenomenon. Speckle can be simply described as follows: when a laser illuminates a rough surface, it will decompose into numerous coherent wavelet waves due to scattering phenomenon on the surface. These wavelets will interfere with each other. According to their phase difference, different bright spots or dark spots will appear randomly (phase difference leads to accumulation or elimination). This random distribution of bright spots or dark spots is called Speckle, and this optical phenomenon is called optical speckle phenomenon. Figure n shows the laser speckle pattern. This optical phenomenon was first discovered and proposed by Gordon and Rigden of Bell Laboratories in the United States in 1962 [19]. With the further study, people found that speckle looks random, but it conforms to the statistical law, and has measurable intensity and definite phase. This lays a theoretical foundation for speckle interferometry.

Speckle interference technology can be divided into digital speckle interference technology and digital shear speckle interference technology. The difference lies in the fact that the reference light of digital speckle interferometry is not diffusing reflected by the surface of the object, while the reference light of digital shear speckle interferometry is mutual reference light. This difference makes the quantity measured by the two different, where the quantity measured by the digital speckle interferometry is the out-of-plane or in-plane deformation, while the quantity measured by the digital shear speckle interferometry is the first derivative of the deformation.

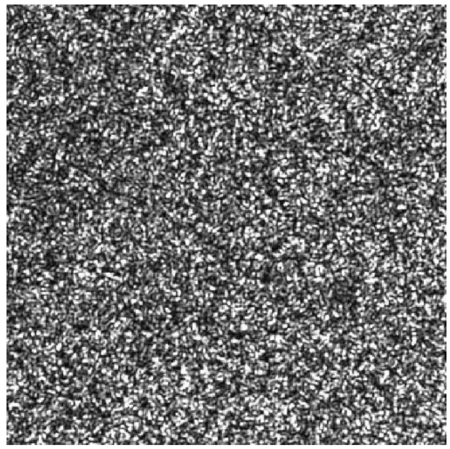

Fig 2.1 Schematic of laser speckles

The basic principle of speckle interference was first proposed by J.M.Burch and J.T. okardki in 1968, and has been successfully applied in the field of fatigue detection [20]. Subsequently, in 1970, British scientist Leendertz proposed a new method to monitor surface deformation of rough objects based on speckle interference principle, which was named speckle interferometry technology [21]. In 1973, on the basis of the traditional speckle interference technique, Y.Y.Hwang and C.E.Taylor proposed a new speckle interference technique named shear speckle interference technique by introducing shear amount into the optical path to change the optical path characteristics. So, speckle interferometry includes two technology speckle pattern interferometry-holograpy and speckle pattern shearing interferometry shearography. The basic idea of speckle interferometry is to generate coherent beam by laser and irradiate it to the surface of rough object to form original speckle field, which is collected by digital acquisition equipment. After the object state changes, the new speckle field is collected again by digital acquisition equipment. By comparing the speckle field collected before and after the state change of the object, the speckle interference fringe pattern carrying the state change information of the object can be generated, and then obtain the state change information of the object through the follow-up processing of the digital image.

However, the speckle interferometry technology has a great defect at the beginning of its appearance: that is, the speckle interferogram collected must be printed on the holographic dry plate, and it needs to go through complex subsequent physical processing such as development, fixing and reproduction. These subsequent processing processes must be carried out in strict darkroom, so the application of speckle interferometry technology is strictly limited.

After the 1980s, due to the rapid development of computer technology and electronic technology, integrated electronic storage equipment, electronic collection equipment, computer processing equipment widely appeared in various fields. Their combination with speckle interferometry makes digital speckle interferometry come into being. Digital speckle interference technology is based on the traditional interference technology, through electronic acquisition equipment (such as industrial cameras) to collect the light intensity signal, and in the form of lattice into electrical signal storage. The acquisition equipment is connected with the computer system through the image acquisition card, and the electrical signal is transmitted to the computer as a digital signal, and the digital speckle interferogram is processed through the computer software, thus solving the limitation of the traditional speckle interferogram technology requiring holographic dry plate for image recording, and its application is greatly expanded. Later, Yamaguchi in Japan and W.H. eter and W.F.Anson in the United States proposed and studied the digital speckle correlation calculation method. Pedrini from the University of Stuttgart in Germany has conducted in-depth research on the application of various electronic (digital) speckle interferometry technologies [22,23]. Hung conducted electronic and digital research on shear speckle interferometry. At the same time, Chinese scholars have also started to study the digital speckle interference technology. Wang Kaifu of Nanjing University of Aeronautics and Astronautics, He Xiaoyuan of Southeast University and other scholars have explored the application of speckle interference technology in the field of measurement [24].

Now days, the digital speckle interferometry (DSPI) and digital speckle pattern shearing interferometry (DSPSI) are used wildly.

2.2 The review of holography

2.2.1 Brief introduction of digital holography

Digital Holography has the advantages of large measuring range, measuring rough objects, multi-dimensional deformation and displacement measurement. The principle is that speckle is generated on the surface of the object by laser irradiation and interferes with the reference light on the CCD target surface. The light intensity of the object before and after deformation is collected by the CCD camera, and the intensity of the two interferogram before and after deformation is subtracted to obtain the deformation fringe field of the object in the sensitive direction of the optical path. In this way, the general information of the overall deformation of the object can be quickly obtained, and the general range of the deformation of the object can be determined through fringe order [25].

Common digital holographic speckle interferometry optical paths are divided into in-plane deformation measurement optical paths and out-of-plane deformation measurement optical paths [26,27].

2.2.2 The principle of digital holography

The digital speckle interferometry (holography) measures the deformation of the object. The deformation of the object usually presents a three-dimensional distribution, in which the deformation perpendicular to the surface of the object is called out-of-plane deformation, which corresponds to the z direction and is represented by w, and the deformation along the horizontal and vertical directions of the surface of the object is called in-plane deformation, which corresponds to the x direction and y direction and is represented by u and v. Digital speckle interferometry can be used to measure out-of-plane or in-plane deformation through different measurement optical paths.

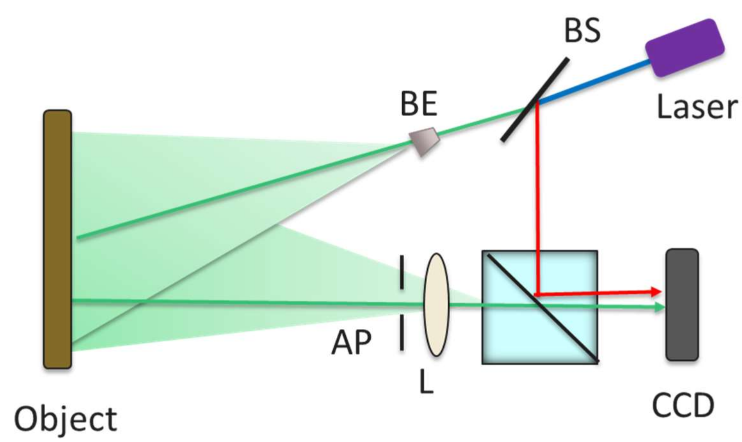

Fig 2.2 Sketch of digital holography setup to measure out-of-plane deformation

The principle of measuring out-of-plane deformation by digital speckle interferometry is shown in Figure 2.2. The laser emitted from the laser is divided into object light and reference light by Beam splitter (BS1). The object light is irradiated through the Beam expander (BE1), and the scattered light of the object is imaged on the CCD target plane through the spectroscopic prism (BS2). The reference light is introduced into the optical path through the beam splitting prism (BS2) after the beam expanding mirror (BE2), and interferes with the object light to form a speckled interferogram, which is recorded by the CCD camera in the form of intensity. Reference light and object light can be described

$$u_1 = a_1 e^{i\varphi_1} \tag{2.1}$$

$$u_2 = a_2 e^{i\varphi_2} \tag{2.2}$$

Where a_1 and a_2 are the amplitudes of reference light and object light, respectively. φ_1 and φ_2 are the random phases of reference light and object light, respectively.

Since the reference light and object light are both received by the CCD camera, their light wave superposition can be expressed as

$$u_t = u_1 + u_2 = a_1 e^{i\varphi_1} + a_2 e^{i\varphi_2} \tag{2.3}$$

The intensity expression of speckle interferogram formed by the interference between reference light and object light is

$$
\begin{aligned}
I = u_t u_t^* &= \left(a_1 e^{i\varphi_1} + a_2 e^{i\varphi_2}\right)\left(a_1 e^{i\varphi_1} + a_2 e^{i\varphi_2}\right)^* \\
&= \left(a_1 e^{i\varphi_1} + a_2 e^{i\varphi_2}\right)\left(a_1 e^{-i\varphi_1} + a_2 e^{-i\varphi_2}\right) \\
&= ({a_1}^2 + {a_2}^2) + a_1 a_2\left[e^{i(\varphi_1-\varphi_2)} + e^{-i(\varphi_1-\varphi_2)}\right] \\
&= ({a_1}^2 + {a_2}^2) + 2a_1 a_2 \cos(\varphi_1 - \varphi_2) \\
&= A + B\cos\varphi
\end{aligned}
$$

2.4

Where * denotes complex conjugation.

$e^{i(\varphi_1-\varphi_2)} + e^{-i(\varphi_1-\varphi_2)} = 2\,cos(\varphi_1 - \varphi_2)$ is euler's formula. $A = {a_1}^2 + {a_2}^2$, $B = 2a_1 a_2$. $\varphi = (\varphi_1 - \varphi_2)$ is the phase difference between reference light and object light.

When the object is deformed, the phase difference between the reference light and the object light changes to φ'. Therefore, the intensity expression of the speckle interferogram after the object deformation is

$$I' = A + B\cos(\phi + \Delta)$$

2.5

Where Δ is the relative phase change of the object light relative to the reference light caused by the deformation of the object.

By subtracting the intensity of the speckle interferogram before and after the object deformation, the expression of the speckle phase diagram can be obtained as

$$\Delta I = |I' - I| = A + B|\cos(\phi + \Delta) - \cos\emptyset|$$

2.6

When $\Delta = 2n\pi, n = 0, \pm 1, \pm 2, \cdots$, the light intensity is 0, and the speckle phase pattern appears as dark fringe. When $\Delta = (2n+1)\pi, n = 0, \pm 1, \pm 2, \cdots$, the light intensity reaches the maximum value and appears as a bright stripe on the speckle phase diagram.

Thus, the speckle phase pattern appears as a pattern of alternating light and dark stripes. In addition, since the relative phase change between two adjacent fringes Δ is 2π, the phase value at each fringe can be determined by calculating the fringe order, and the deformation information of the object can be obtained according to the expression of the relationship between the phase change and the deformation.

Suppose that the Angle α between the illumination direction and the observation direction is equal to or close to 0, then the relative phase change Δ is only related to the out-of-plane deformation w, whose expression is

$$\Delta = \frac{4\pi}{\lambda} w$$

2.7

An experimental result of measuring out-of-plane deformation by digital speckle interferometry is given as shown in Figure 2.3. Figure 2.3(a) is the speckle interferogram recorded before the object deformation, and Figure 2.3(b) is the speckle interferogram recorded after the object deformation. Intensity subtraction is applied to the speckle interferogram before and after the object deformation, and the speckle phase diagram can be obtained, as shown in Figure 2.3(c). The deformation component w in the z direction is shown as a circular stripe pattern with alternating light and dark.

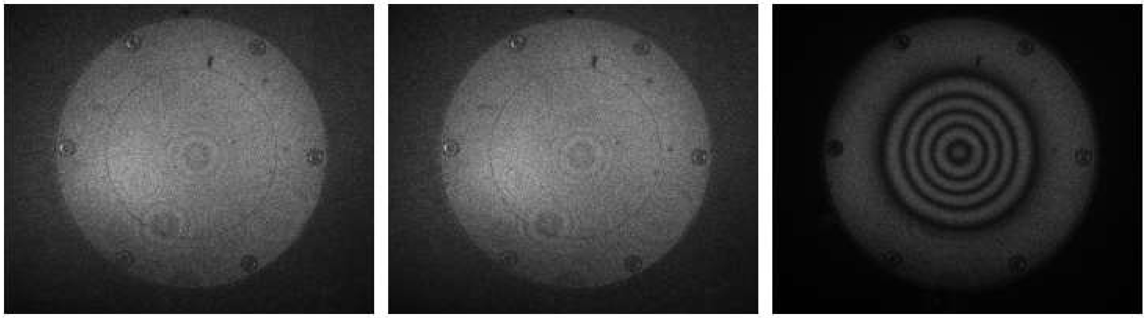

(a) (b) (c)

Fig 2.3 (a) speckle interferogram before deformation; (b) speckle interferogram after deformation; (c) Speckle phase map

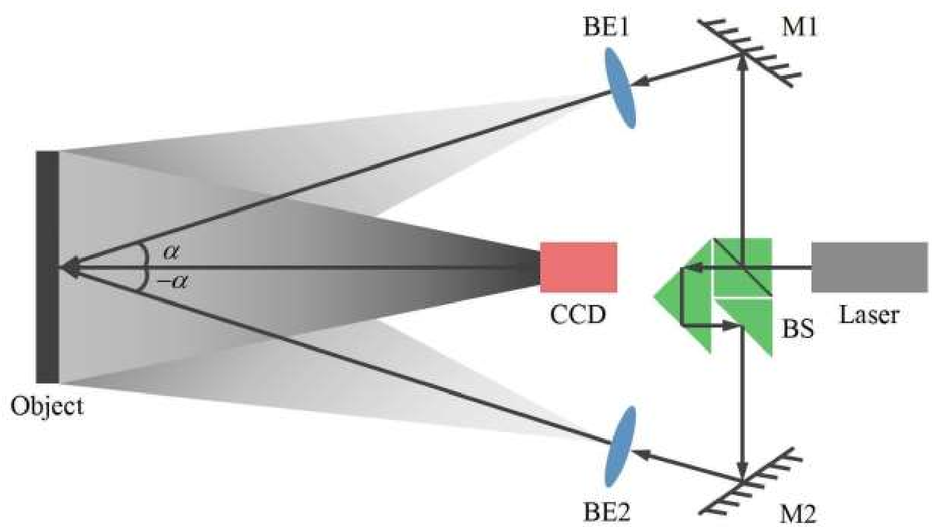

Fig 2.4 Schematic of digital speckle pattern interferometry for the measurement of in-plane deformation.

The principle of digital speckle interferometry for measuring in-plane deformation is shown in Figure 2.4. The laser beam emitted by the laser is divided into two beams by the beam splitter mirror (BS), and after the beam expansion mirror (BE1, BE2), the measured object is irradiated at the same Angle. The light scattered by the object is imaged on the CCD target surface by the imaging system and interferes with each other to form a speckle interferogram recorded by the CCD camera in the form of intensity.

The intensity expression of the speckle interferogram before the object deformation is

$$I = A + B\cos(\phi + \Delta) \tag{2.8}$$

The intensity expression of speckle interferogram after object deformation is

$$I' = A + B\cos(\phi + \Delta) \tag{2.9}$$

Where the relative phase change is $\Delta = \Delta_1 - \Delta_2$, where Δ_1 and Δ_2 are the phases of two beams of light caused by the deformation of the object, respectively

When the illumination direction and the observation direction are in the XOZ plane and the Angle between them is α, Δ_1 andΔ_2 are represented as

$$\Delta_1 = \frac{2\pi}{\lambda}[\sin\alpha \cdot u + (1 + \cos\alpha)w] \tag{2.10}$$

$$\Delta_2 = \frac{2\pi}{\lambda}[-\sin\alpha \cdot u + (1 + \cos\alpha)w] \tag{2.11}$$

At this time, the relative phase change Δ is only related to the in-plane deformation u, whose expression is

$$\Delta = \frac{4\pi}{\lambda}\sin\alpha \cdot u \tag{2.12}$$

When the illumination direction and the observation direction are located on the YOZ plane and the Angle between them is α, then Δ1 and Δ2 can be expressed as

$$\Delta_1 = \frac{2\pi}{\lambda}[\sin\alpha \cdot v + (1 + \cos\alpha)w]$$

2.13

$$\Delta_2 = \frac{2\pi}{\lambda}[-\sin\alpha \cdot v + (1 + \cos\alpha)w]$$

2.14

At this time, the relative phase change Δ is only related to the in-plane deformation v, whose expression is

$$\Delta = \frac{4\pi}{\lambda}\sin\alpha \cdot v$$

2.15

The experimental results of measuring in-plane deformation are shown in Figure 2.5. Figure 2.5(a) is the speckle interferogram recorded before the object deformation, and Figure 2.5(b) is the speckle interferogram recorded after the object deformation. By intensity subtraction of the speckle interferogram before and after the object deformation, the speckle phase diagram can be obtained as shown in fig. 2.5(c) The deformation component u in the x direction shows a horizontal stripe pattern between light and dark, while the deformation in the y direction. The component v appears as a pattern of vertical stripes alternating between light and dark.

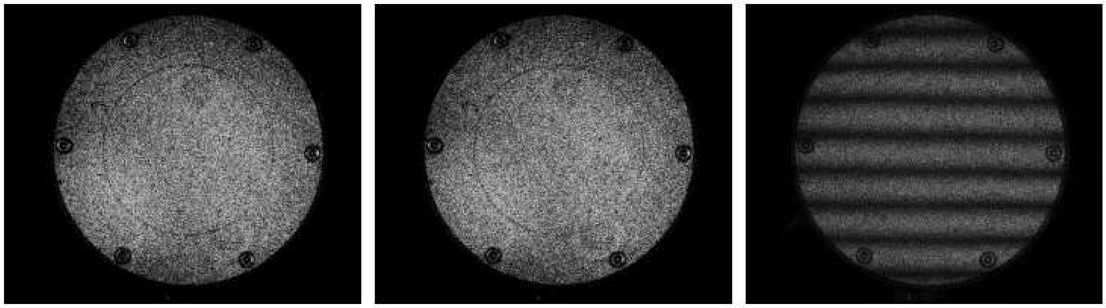

(a) (b) (c)

Fig 2.5 (a) speckle pattern image before deformation; (b) speckle pattern image after deformation; and (c) speckle pattern phase map.

2.3 The review of shearography

2.3.1 The development of digital shearography

In 1970, Leendertz laid the foundation for speckle interferometry, outlining its fundamental principles. This method entails projecting laser light onto rough surfaces to create speckle patterns, and introducing a secondary reference beam for interference. By capturing speckle interference patterns before and after deformation, and performing phase subtraction, valuable information about surface deformation can be extracted. Subsequently, in 1971, Leendertz and Buttes harnessed cameras to record these interference patterns, paving the way for Electronic Speckle Pattern Interferometry (ESPI) after electronic processing [28,29].

In 1973, Leendertz and Buttes introduced Speckle Pattern Shearing Interferometry, colloquially known as Shearography [30]. Differing from ESPI, this technique splits the light reflected from an object's surface into two beams. One beam undergoes a shear process while the other remains unaffected, and their recombination generates a speckle interference pattern on the camera's surface. Analyzing the alterations in speckle interference patterns before and after deformation allows for the computation of the first-order derivative of the object's surface deformation distribution. Due to its self-interferometric nature, shearography doesn't necessitate an additional reference beam, making it more resistant to external environmental disturbances. In 1982, y.y.h Hong further enhanced shearography, creating real-time shearography with significantly improved resolution, although this required a time-consuming wet chemical development process. This drawback significantly impeded its practical implementation.

Post the 1990s, Television Shearography (TV Shearography) emerged, utilizing TV displays for real-time monitoring of fringe pattern changes. In 1990, C. Joenathan employed phase-shifting techniques with dual-beam illumination and TV cameras to quantify object strain. This approach enabled real-time observation of detection results and broadened the technology's application in industrial contexts. Nevertheless, this method was plagued by discernible limitations in spatial resolution.

As the 21st century dawned and CCD and CMOS camera technologies advanced, the digitization of shearography images gave birth to Digital Shearography [31]. By subtracting recorded speckle intensity data from the camera, the first-order derivative of material deformation could be directly visualized on a computer screen, referred to as the intensity mode. This digital approach made phase-shifting techniques feasible, elevating sensitivity and reducing operational complexity in digital shearography applications. This breakthrough facilitated the practical integration of digital shearography in industrial environments.

Currently, grounded in the application of phase-shifting techniques, shearography has branched into two main classifications: Temporal Phase Shift Shearography (TPS-DS) and Spatial Phase Shift Shearography (SPS-DS) [32, 33].

2.3.2 The principle of digital holography

Digital shear speckle interferometry Measurement is the first derivative of the deformation of an object. This is due to the digital shear speckle interferometry technique which uses a shear device to introduce a shear amount so that the light reflected by two adjacent points on the surface of an object interferes with each other in the image plane. The measured phase change corresponds to the relative deformation of the two adjacent points, and can be further approximated as the first derivative of the deformation. The commonly used shear devices are optical wedge, Mahzand interference, Michelson interference and so on. Michelson interference is the most widely used shearing device because of its simple structure and easy to change the shearing quantity and shearing direction. Therefore, taking Michelson interferometry as an example, the basic principle of digital shear speckle interferometry is introduced.

The principle of digital shear speckle interferometry to measure the first derivative of deformation is shown in Figure 2.6. The light scattered by the measured object is divided into two beams by the shear device and interferes with each other to form a speckle interferogram, which is recorded by the CCD camera in the form of intensity. By tilting one of the Michelson interference mirrors (Mirror, M1), the object light reflected by the mirror has a slight shift, so that it is misaligned with the object light reflected by the other mirror (M2). This dislocation is called shear, and the distance between two dislocated objects is called the shear on the image plane, which is equivalent to the shear on the object plane. In general, shear refers to the amount of shear on the plane of the object.

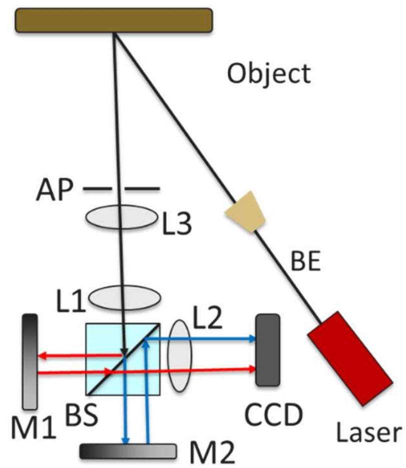

Fig 2.6 Schematic of digital shearography setup

As the Figure 2.6, the laser passes through the beam expander and illuminate the object. The light reflected back can be represented as the equation below.

$$U = ae^{i\theta}$$

2.16

U is the intensity of the light, i is the imaginary number, a is the light amplitudes and θ is the random phase angle of the beam. While the light is divided into two waves by mirrors, the two beams can be written by the following equations.

$$U_1 = a_1 e^{i\theta_1}$$

2.17

$$U_2 = a_2 e^{i\theta_2}$$

2.18

θ_1 and θ_2 are the random phase angles and a_1 and a_2 represent the light amplitudes of the two beams. The total light field U_t can be described as:

$$U_t = U_1 + U_2 = a_1 e^{i\theta_1} + a_2 e^{i\theta_2}$$

2.19

The intensity can be expressed by:

$$I_t = U_t U_t^* = (a_1^2 + a_2^2) + 2a_1 a_2 \cos(\theta_1 - \theta_2)$$

2.20

U_t^* is the complex-conjugate of U_t. There are two forms to simplify the equations.

$$I_1 = A + B\cos\phi = I_0(1 + \gamma\cos\phi)$$

2.21

ϕ represents the phase difference ($\theta_1 - \theta_2$) between the light waves. A represent the average intensity or background intensity of the light while B is the term related to the amplitude of the interference. In another form, I_0 is the background intensity and γ is the contrast.

The phase becomes $\phi + \Delta$ while the object is loaded. The new Intensity equation is:

$$I_2 = A + B\cos\phi = I_0(1 + \gamma\cos(\phi + \Delta))$$

2.22

As the recorded intensity is digitized and stored in a computer. It is easy to calculate the intensity subtraction before and after loading. A highly visible fringe pattern can be directly generated and even can be real-time observed from computer screen. The absolute value of intensity subtraction can be expressed by the subtraction from

$$I_s = I_0\gamma[\cos(\phi + \Delta) - \cos(\phi)]$$

2.23

When the Δ=2nπ and n equals to 0, 1, 2, 3..., Is becomes 0, which forms the dark fringes. Hence, a visible shearographic fringe pattern can be generated. The experimental results of measuring the first derivative of deformation by digital shear speckle interferometry are shown in Figure 2.8. Figure 2.8(a) is the speckle interferogram recorded before the object deformation, and Figure 2.8(b) is the speckle interferogram recorded after the object deformation. The intensity subtraction of the speckle interferogram before and after the object deformation can obtain the speckle phase diagram as shown in Figure 2.7(c), which is manifested as a butterfly stripe pattern with alternating light and dark. The first derivative component in the x direction appears as a horizontal butterfly stripe pattern, while the first derivative component in the y direction appears as a vertical butterfly stripe pattern.

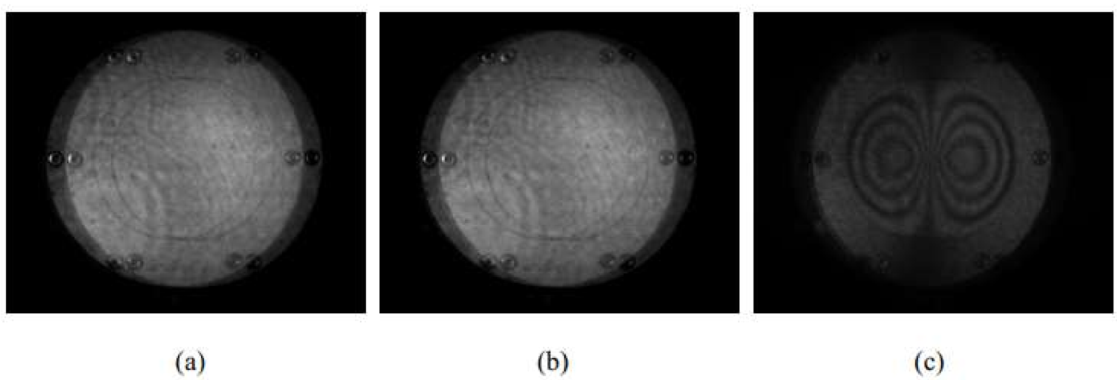

Fig 2.7 (a) speckle pattern image before deformation; (b) speckle pattern image after deformation; and (c) speckle pattern phase map.

The shearogram pattern looks like a 'butterfly', it is also called butterfly pattern. The phase difference of the adjacent fringes is 2π. Based on the optical geometry derivative, the relationship between phase and first derivative of deformation can be figured out as the equation below.

$$\Delta = \frac{2\pi}{\lambda}[(U_1 \sin\alpha) + w_1(1+\cos\alpha)] - [(U_2 \sin\alpha) + w_2(1+\cos\alpha)]$$

2.24

Simplifying the equation and the new form is as the following.

$$\Delta = \frac{2\pi}{\lambda}[\delta u(\sin\alpha) + \delta w(1+\cos\alpha)]$$

2.25

Since, Digital Shearography measures the relative displacement of the adjacent two points. Here, u, v, w are the displacement components in x, y, z direction respectively on the first point. u_1, v_1, w_1 are the displacement components in x, y, z direction respectively on the second point. δu, δv, δw are the difference of the displacement components in x, y, z direction respectively between two pints. If we assuming the shearing direction is in x-direction with the shearing amount of Δx, it divides the both sides of the equation above by Δx and Δx is very small, the equation above becomes.

$$\Delta_x = \frac{2\pi}{\lambda}\left[(\sin\alpha)\frac{\partial u}{\partial x} + (1+\cos\alpha)\frac{\partial w}{\partial x}\right]\delta x$$

2.25

If the device is in y shearing direction, the equation turns to be

$$\Delta_y = \frac{2\pi}{\lambda}\left[(\sin\alpha)\frac{\partial u}{\partial y} + (1+\cos\alpha)\frac{\partial w}{\partial y}\right]\delta y$$

2.26

If the angle between the illumination direction and the observation direction is 0, the equations can be shorted as:

$$\Delta_x = \frac{4\pi\delta x}{\lambda}\frac{\partial w}{\partial x}$$

2.27

$$\Delta_y = \frac{4\pi\delta y}{\lambda}\frac{\partial w}{\partial x}$$

2.28

Based on the equation, it can be found the phase change and the first derivative of deformation have a linear relationship in ideal assumption. Usually, the illumination angle is very small which can be ignored, so the Eq. 2.15 and Eq. 2.16 are the most common equations used. Since ESPI is earlier developed than the Shearography, it is necessary to make a comparison between two technologies to explain why the shearography is more popular.Figure 2.5 shows the difference between the ESPI and Shearography. A loading like thermal method or vacuum will make a buckling on the object surface. Since ESPI detects a defect by looking for displacement anomalies while Shearography looks for the strain anomalies. To demonstrate the concept described above, a square aluminum plate subjected to a point-load at the center of the backside is utilized to test by ESPI and Shearography. Figure 2.6(a) and Figure 2.6(b) show the ESPI fringe pattern andShearography fringe pattern respectively. Figure 2.7(a) shows the holographic application where some circular anomalous fringes appear at the position of delamination. Figure 2.7(b) shows the shearography application and the shearograms appear at the surface with inner defects. ESPI measures the deformation directly which is more sensitive but with an independent reference light, which is easily affected by the external vibration. Without a good vibration isolated environment, ESPI cannot be applied. However, vibration isolated device could highly increase the cost and the space of the device, which limit ESPI industrialized process. In opposite, Digital Shearography measures the relative deformation between two adjacent points, and it is a self-interference technology. External disturbance could be cancelled by the two beams with the same vibration mode, which becomes the most important advantages in speckle pattern interferometry in industry application.

Digital speckle interferometry has the advantages of full-field measurement, non-destructive measurement, non-contact measurement, high sensitivity, etc. Due to the different measurement optical path principles of Holography and shearography, their applications are different. Since the measured value is directly related to the displacement of the object, Holography can easily measure the displacement, deformation and other information of the object directly. Therefore, this technology is widely used to measure the deformation of the object or small rigid body displacement. Although shearography can not directly provide the result of the deformation of the object, instead to obtain the first derivative of the deformation of the object, it is widely used in the field of material nondestructive testing requiring qualitative measurement because it is insensitive to measuring the rigid body displacement of the object and has good anti-interference performance.

CHAPTER THREE

PHASE SHIFT TECHNOLOGIES

According to the principle of digital speckle interferometry, the phase value of the light reflected by the surface of the measured object changes due to the deformation of the surface. In order to measure the deformation of a surface, it is necessary to obtain its phase information. Therefore, obtaining phase information from speckle is the most important step of digital speckle interferometry. According to the different phase extraction technology, three kind of the phase extraction methods are commonly used, they are real-time intensity subtraction technology, time phase shift technology and space phase shift technology.

3.1 Real-time intensity subtraction technology

Among the methods of phase extraction, the most direct and simplest method is intensity phase subtraction. In this method, the speckle interferograms recorded before and after the object deformation, that is, the recorded intensity map, are subtracted to get the speckle phase map, so as to extract the required phase information. According to the formula (Chapter 2), the phase value at each fringe is determined by calculating the fringe order, and the phase difference is calculated by subtracting the different phase value. The phase measurement sensitivity of real-time intensity subtraction method is only one fringe and can only reach 2π. Moreover, this method can only obtain the phase information at the fringe, and the phase information between the fringes cannot be obtained, so that the real full-field measurement cannot be carried out, and the measurement information between the fringes can only be obtained by interpolation or estimation. This makes the method very limited in practical application [34]. In general, the real-time strength subtraction technique is very practical and reliable, but the sensitivity of deformation measurement is relatively low. Therefore, this method is generally only used for qualitative detection during defect detection.

$$I_d = I' - I = B[\cos(\theta + \Delta) - \cos\theta] \tag{3.1}$$

When $\Delta = 0, 2\pi, 4\pi, \ldots = 2N\pi$, $N = 0, 1, 2, 3, \ldots$ called as fringe order, $I_d = 0$, which correspond to dark fringe lines

Fig 3.1 shows an example: A circular plate clamped all around loaded at center position. A fringe pattern is formed after taking a subtraction of I from I'.

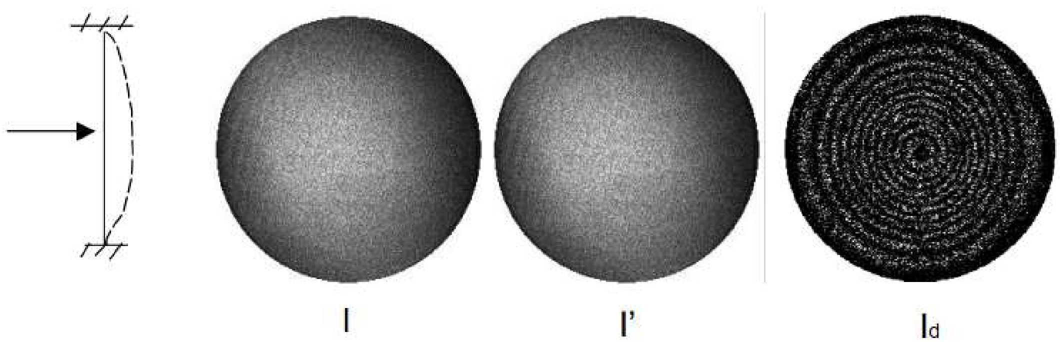

Fig 3.1 Sketch of real-time intensity subtraction

Due to the low sensitivity of intensity subtraction method, in order to improve the measurement sensitivity and phase image quality of speckle interferometry, a variety of phase shifting techniques have been proposed. Phase shifting technology can be mainly divided into two categories: time phase shifting technology and space phase shifting technology [35-40]. The temporal phase shift technique is suitable for static measurement, while the spatial phase shift technique is suitable for dynamic measurement. Phase shift technology is a new technology developed and applied since 1980s. It can extract full-field phase information from the light intensity field of interferogram, so as to achieve full-field accurate measurement, effectively improve the fringe measurement accuracy and obtain full-field phase information. Its implementation principle is to introduce the known phase offset through the phase shift device to obtain the intensity value of the measurement point when the multiple phase offset, so as to solve the phase information in reverse. Through phase shifting technology, the phase information of the whole field is directly obtained, and the phase subdivision is carried out between fringes to obtain more phase information, and at the same time, the problem that too few fringes affect the measurement accuracy is solved [41-43].

3.2 Temporal phase shift technology

In order to obtain a higher quality shearogram and increase the measurement sensitivity, the phase is generally obtained by phase shift technique. Catalog by phase-shift techniques, the phase shift shearography can be divided into temporal phase shift shearography and spatial phase shift shearography. Among them, the temporal phase shift technology uses error averaging in time and in the actual measurement system, the aperture is relatively large, and the amount of information acquired by the camera is more, so it has better fringe quality.

3.2.1 Introduction of temporal phase shift technology

The temporal phase shift technique is the most widely used and precise phase extraction method in shear speckle interferometry. In this method, a dynamic phase shifter is introduced into the optical path while keeping the test object stable. This phase shifter introduces a fixed phase value to the image formed on the camera surface. Multiple interferograms with different phase shifts are captured and solved using phase shifting formulas. This technique was originally proposed by Carré in 1966 and introduced to optical testing by Bruning et al. in 1974. Currently, commonly used methods include piezoelectric ceramic method, grating phase shifting method, and tilted glass method.

Among them, the most commonly used method involves connecting a piezoelectric ceramic (PZT) to a reflective mirror in the shear part and controlling the movement of the PZT by applying a fixed voltage to introduce a fixed phase shift. Piezoelectric ceramics are materials that can convert mechanical energy into electrical energy and vice versa. The piezoelectric ceramic actuator is based on its inverse piezoelectric effect, which converts the voltage applied to the internal electrodes of the piezoelectric crystal into a small displacement. It drives the attached reflective mirror on its surface, thereby changing the optical path length of one of the light beams in the coherent light, thus achieving the phase shift.

This method offers high displacement resolution, fast response, compact size, relatively low cost, and no heat generation. It has advantages such as simplicity of use, stable operation, good repeatability, and nanometer-level step displacement capability. In the introduction of phase shifting in speckle interferometry, it finds extensive applications [44].

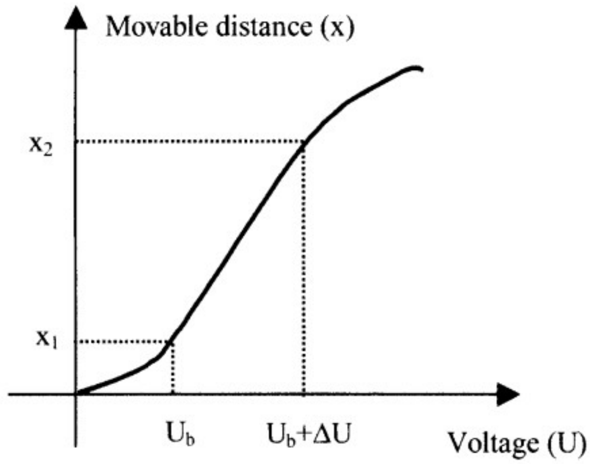

Figure 3.2 Voltage-to-displacement relationship o f a PZT mirror

Piezoelectric ceramics (PZT) are the crucial components for implementing phase shifting. They are voltage-controlled devices capable of generating nanometer-level displacements. By altering the optical path, a certain phase value can be introduced. The relationship between voltage and displacement for each specific PZT element (as shown in Figure 3.2) should be provided by the manufacturer, where x_1 is the beginning position of the PZT, x_2 is the end position of the PZT. U_b is the voltage at the beginning position, ΔU is the voltage increment to make this change of the position of PZT.

As depicted in Figure 3.2 (V-x curve), the overall relationship between displacement and voltage is not linear. However, certain segments of the V-x curve follow a linear relationship. For practical purposes, we typically only utilize the linear portion of the V-x curve. The *k* sensitivity factor of PZT can be expressed as follows:

$$k = \frac{x_2 - x_1}{\Delta U} \tag{3.1}$$

After the calibration, k is a known constant for the PZT. Then, the displacement is brought by the move of the PZT under given voltage increment can be calculated by:

$$d = k\Delta U \tag{3.2}$$

As shown in Figure 3.3, assuming the incident light reach the PZT mirrors with an incident angle of α. The displacement d is achieved with a ΔU voltage applied on the PZT, ΔL is the change of the physical light path, which equals to the amount ab and ac, which is double ab. The displacement d brings the optical path change ΔL_n, which can be written as:

$$\Delta L_n = n\Delta L = n\frac{2d}{\cos\alpha} = n\frac{2k\Delta U}{\cos\alpha} \tag{3.3}$$

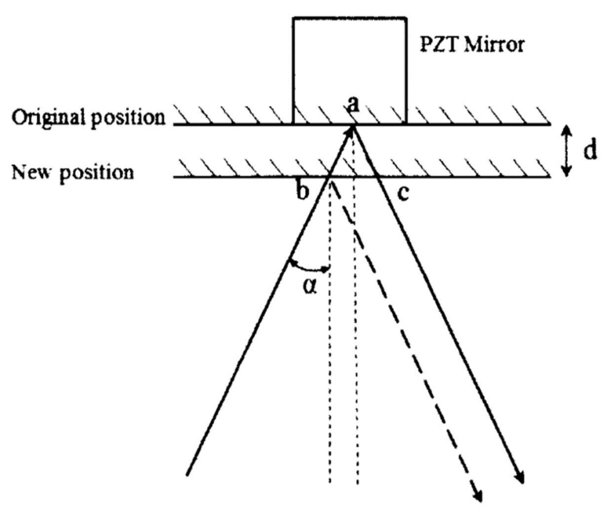

Figure 3.3. Optical path analyses on PZT mirror

The relationship between phase difference and optical path difference is as equation 3.4, Substitute formula 3.3 into formula 3.4, the phase value can be extracted from equation 3.5.

$$\Delta\phi = \frac{2\pi}{\lambda}\Delta L_n \tag{3.4}$$

$$\Delta\phi = \frac{2\pi}{\lambda}\Delta L_n = \frac{2\pi}{\lambda}\left(n\frac{2k\Delta U}{\cos\alpha}\right) = \frac{4\pi nk}{\lambda\cos\alpha}\Delta U \tag{3.5}$$

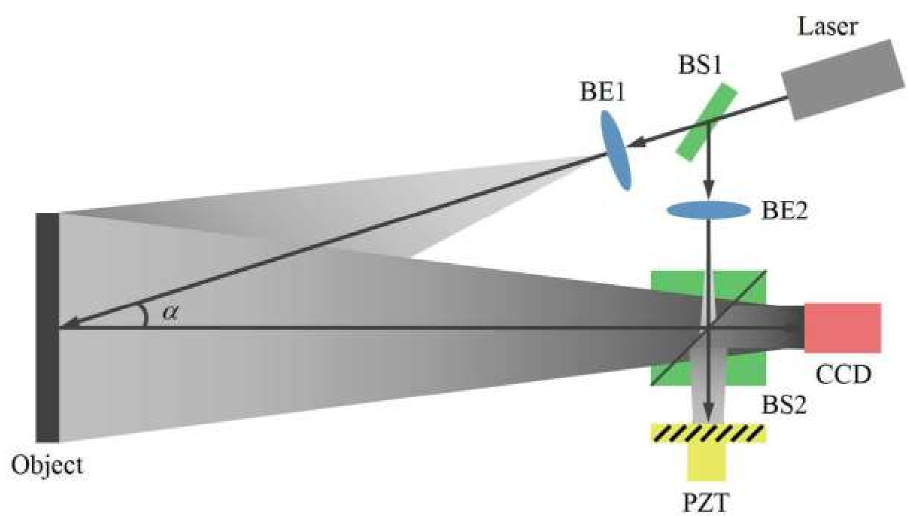

Figure 3.4. The schematic of Digital Holography with PZT

Figure 3.4 shows a digital speckle interferometry system using PZT for out-of-plane deformation measurement. It utilizes the PZT to introduce different phases by reflecting the reference light. The laser beam emitted by the laser source is split into object light and reference light using a beam splitter (BS1). The object light is expanded by a beam expander (BE1) and then illuminates the test object. The scattered light from the test object is imaged onto a CCD camera by a beam splitter (BS2). On the other hand, the reference light is expanded by another beam expander (BE2) and then reflected by a mirror driven by a piezoelectric ceramic (PZT). The reference light, after reflection by the PZT-controlled mirror, also enters the CCD camera through the same beam splitter (BS2) and interferes with the object light to form a speckle interferogram, which is recorded by the CCD camera in intensity form.

The intensity expression of the speckle interferogram formed by the interference of the reference light and the object light is given by the following equation which is discussed in chapter 2:

$$I = A + B\cos\varphi \tag{3.6}$$

Where A and B represent the background intensity and modulation intensity of the speckle interferogram, respectively. φ represents the phase difference between the reference light and the object light. These three parameters are all unknown, and theoretically, at least three equations are needed to form a system of equations to solve for the specific phase values. In other words, at least three phase-shift values need to be introduced, and three intensity images need to be captured in order to calculate the phase values.

For speckle interferometry, subtracting the phase values before and after loading the object allows obtaining the phase distribution of the object deformation. In time phase-shift techniques, the phase values before and after loading the object can be obtained separately using the method mentioned above to construct the system of equations. Commonly used methods include the 3+3 time phase-shifting algorithm and the 4+4 time phase-shifting algorithm. The numbers 3 or 4 refer to the number of introduced phase-shift values during the phase calculation. The part before the plus sign refers to the algorithm used before deformation, while the part after the plus sign refers to the algorithm used after deformation. In theory, any number of phase-shift values greater than or equal to 3 can be introduced before and after deformation. However, in practical applications, the three-step phase-shifting algorithm and the four-step phase-shifting algorithm are more commonly used [s64, 65]. The following section will mainly introduce the principles of the three-step and four-step phase-shifting techniques.

3.2.2 3+3 temporal phase-shift algorithm

Based on the aforementioned, in order to calculate the phase value φ using equation 3.6, we must introduce at least three phase-shift values, which can be achieved using the PZT technology mentioned earlier. The phases introduced in time phase-shifting techniques typically have fixed differences between them, known as fixed-step phase shifts. For the three-step phase-shifting technique, the individual step phase shift is 2π/3, and the system of equations they form is as follows:

$$I_1 = A + B\cos\varphi$$

$$I_2 = A + B\cos\left(\varphi + \frac{2\pi}{3}\right)$$

$$I_3 = A + B\cos\left(\varphi + \frac{4\pi}{3}\right)$$

3.7

Solve 3.7, φ can be obtained. Equation 3.8 shows the result:

$$\varphi = \tan^{-1}\frac{\sqrt{3}(I_3 - I_2)}{2I_1 - I_2 - I_3}$$

3.8

One small issue with this algorithm is that it needs to consider the final phase position, as the same arctangent value may produce two answers ranging from 0 to 2π. It is essential to consider the signs of both the numerator and denominator to determine the exact phase value. The rule is as follows: when both the numerator and denominator are positive, the phase value lies in the first quadrant; for a positive numerator and negative denominator, it lies in the second quadrant; for both a negative numerator and denominator, it lies in the third quadrant; and when the numerator is negative and the denominator is positive, the resulting phase value is in the fourth quadrant.

Then the object under test is loaded, and the same method is used to introduce three individual step phase shifts, and the interference results are collected accordingly, leading to the following equations:

$$I_1' = A + B\cos\ \varphi'$$

$$I_2' = A + B\cos\left(\ \varphi' + \frac{2\pi}{3}\right)$$

$$I_3' = A + B\cos\left(\ \varphi' + \frac{4\pi}{3}\right)$$

3.9

By solving these equations 3.9, we can obtain the phase value φ' of the object after deformation.

$$\varphi' = \tan^{-1}\frac{\sqrt{3}(I_3' - I_2')}{2I_1' - I_2' - I_3'}$$

3.10

By subtracting the phase values before and after deformation, we can obtain the phase distribution of the object under test caused by deformation. Equation 3.11 shows the result:

$$\Delta\varphi = \varphi' - \varphi \qquad for\ = \varphi' > \varphi$$

$$\Delta\varphi = \varphi' - \varphi + 2\pi \qquad for\ = \varphi' < \varphi$$

3.11

3.2.3 4+4 temporal phase shift algorithm

In theory, using three equations is sufficient to obtain the required phase values. However, using four equations for computation is faster, simpler, and results in greater accuracy. Therefore, the algorithm that uses four equations for computation, known as the 4+4 phase-shifting algorithm, is the most widely applied technique in time phase-shifting technology. This algorithm requires capturing four interference patterns of the object, both before and after deformation, with each pattern having a phase shift increment of π/2.

The intensity expression for the interference pattern of the object before deformation is as follows:

$$I_1 = A + B\cos\varphi$$

$$I_2 = A + B\cos\left(\varphi + \frac{\pi}{2}\right)$$

$$I_3 = A + B\cos\left(\varphi + \frac{3\pi}{2}\right)$$

$$I_4 = A + B\cos\left(\varphi + \frac{4\pi}{2}\right)$$

3.12

The phase difference for the object before deformation can be obtained by solving the equations as follows:

$$\varphi = \tan^{-1}\frac{I_4 - I_2}{I_1 - I_3}$$

3.13

Similarly, the intensity expression for the speckle interferogram of the object after deformation can be obtained by loading the object and introducing the phase shifts of π/2, 3π/2, and 2π. It is given by:

$$I_1' = A + B\cos\ \varphi'$$

$$I_2' = A + B\cos\left(\ \varphi' + \frac{\pi}{2}\right)$$

$$I_3' = A + B\cos\left(\ \varphi' + \frac{3\pi}{2}\right)$$

$$I_4' = A + B\cos\left(\ \varphi' + \frac{4\pi}{2}\right)$$

3.14

The phase difference for the object before deformation can be obtained by solving the equations as follows:

$$\varphi = \tan^{-1}\frac{I_4' - I_2'}{I_1' - I_3'}$$

3.15

By subtracting the phase values before and after deformation, we can obtain the phase distribution of the object under test caused by deformation. Equation 3.16 shows the result:

$$\Delta\varphi = \varphi' - \varphi \qquad for\ = \varphi' > \varphi$$

$$\Delta\varphi = \varphi' - \varphi + 2\pi \qquad for\ = \varphi' < \varphi$$

3.16

The 4+4 time phase shift method is the most commonly used time phase shift technique in speckle interferometry due to its simplicity in calculation.

Similarly, in practical measurements, to improve the detection speed, there are also 4+2 or 4+1 step phase shift algorithms. As mentioned in privious section , using 4+2 or 4+1 steps can increase the detection speed, but the corresponding calculation results have lower quality compared to the 4+4 step phase shift algorithm.

3.2.4 Other temporal phase shift algorithm

The 3+3 phase shift algorithm is suitable for static loading tests. The 4+4 time phase shift algorithm provides simple calculations and highly accurate phase extraction results. However, this algorithm requires capturing four interferograms for each deformation state of the object, which takes enough time for multi-step phase shifting.

Moreover, it demands the object to remain stationary during the data acquisition process. Different phase shifting devices have varying operating speeds. For most mechanism-based phase shifters, achieving dynamic or continuous loading poses a challenge to their shifting speed. Hence, the 4+4 algorithm is only suitable for static measurements [45-47].

To adapt to continuous or dynamic deformation scenarios, improvements have been made to the time phase shift algorithm, leading to the development of fast time phase shift algorithms, such as 3+1, 3+2, 4+1, and 4+2, time phase shift algorithms [48-50]. These algorithms still require capturing three or four interferograms before object deformation to ensure adequate phase map quality. However, after deformation or during deformation, they achieve dynamic measurements by reducing the number of acquired images to some extent. Among them, the 4+1 time phase shift algorithm only needs one interferogram to be captured after deformation and enables dynamic measurements. However, the phase maps obtained by this algorithm usually contain a significant amount of speckle noise, making it suitable only for qualitative measurements and not suitable for high-precision quantitative measurements, thus limiting its application scope. On the other hand, the 4+2 time phase shift algorithm requires capturing two interferograms after deformation or during deformation, enabling dynamic measurements with a lower dynamic range. Although the phase map quality of this algorithm is significantly improved compared to the 4+1 time phase shift algorithm, it still lags behind the 4+4 time phase shift algorithm. Similarly, there are other time phase shift algorithms as shown in Table 2.1.

Table 3.1 Temporal phase shift algorithms.

Phase shift step N	Algorithms	Formula
3	3+3	$\Delta = \arctan\frac{\sqrt{3}(I_3' - I_2')}{2I_1' - I_2' - I_3'} - \arctan\frac{\sqrt{3}(I_3 - I_2)}{2I_1 - I_2 - I_3}$
	4+4	$\Delta = \arctan\frac{I_4' - I_2'}{I_1' - I_3'} - \arctan\frac{I_4 - I_2}{I_1 - I_3}$
4	4+2	$\Delta = \arctan\frac{A - I_2'}{I_1' - A}, A = \frac{I_1 + I_2 + I_3 + I_4}{4}$
	4+1	$\Delta = \arctan\frac{\tilde{I}_4^2 - \tilde{I}_2^2}{\tilde{I}_1^2 - \tilde{I}_3^2}, \tilde{I}_n^2 = (I_n - I')^2, n = 1,2,3,4$
5	5+5	$\Delta = \arctan\frac{2I_2' - I_4'}{2I_3' - I_1' - I_5'} - \arctan\frac{2I_2 - I_4}{2I_3 - I_1 - I_5}$

In actual use, selection should be made according to the needs of detection.

In simple terms, the time phase shift digital speckle interferometry technique involves capturing multiple interferograms with different phase shifts before object deformation and then solving them using the phase shift formula to obtain the full-field phase value θ before deformation. After object deformation, the same measurement process is repeated, and the new full-field phase value $\theta + \Delta$ after deformation is also calculated. By subtracting the phases, the relative phase difference Δ representing the object deformation information is obtained. Based on the characteristics of different optical paths, the corresponding measurement values for the specific measurement path can be calculated.

Although time phase shift technique has many advantages, it also has the following drawbacks: From a design perspective, to ensure the correct implementation of phase shifting by the phase shifter, it is necessary to design matching drive control circuits and establish communication with the computer system (such as the PZT drive circuit in the piezoelectric ceramic method, and the motor drive circuit in the tilt glass method), which increases the design complexity and cost. From an application perspective, in time phase shift technique, the phase shifter requires some time to complete the physical process of multi-step phase shifting and the acquisition of multiple frames under the same object deformation state. As a result, it can only measure static or quasi-static object deformations, and dynamic measurements of object deformations cannot be achieved. Spatial phase shift technique and spatial carrier phase shift technique can overcome the above limitations of time phase shift technique.

3.3 Spatial phase shift technology

The time phase shift technique improves the measurement sensitivity by about 10 to 30 times compared to the traditional intensity subtraction method. However, time phase shift technology requires the object under test to remain stationary and introduces fixed phase shifts multiple times, capturing multiple speckle interferograms before and after object deformation. Therefore, it is typically suitable for static measurements, which leads to low data acquisition rate and low phase map quality [51-55]. In practical applications, the state of the object under test may be continuously changing in real-time, and in such cases, using time phase shift technique may result in significant errors. Although fast time phase shift algorithms have been developed, their phase map quality and measurement range are still limited. Therefore, a new phase extraction method called spatial phase shift technique has been proposed.

Spatial phase shift is a completely new approach that can generate a phase map from a single frame of speckle interferogram. This technique enables dynamic measurements by extracting phase information from a single frame of speckle interferogram, and the data acquisition rate is only limited by the camera's acquisition rate [56-61]. Spatial phase shift technique introduces a fixed phase shift value continuously in space for the light reflected from the object under test. By performing a Fourier transform on the single interferogram and solving the phase information from the Fourier transform result, the surface phase information of the object under test can be obtained. Therefore, using spatial phase shift technique allows obtaining deformation information of the object under test even when it undergoes dynamic changes [62-63]. Spatial phase shift technique can be further divided into two categories: multi-channel spatial phase shift technique and spatial carrier technique.

3.3.1 The multichannel spatial phase shift method

The early approach to solving dynamic loading problems was to use the multi-camera spatial phase shift method. The multi-camera spatial phase shift technique has both multi-camera and single-camera configurations.

According to equation $I = A + B\cos\varphi$, A, B and φ are all unknowns. To solve for the value of the phase φ , at least three equations are required. Following this idea, three or more CCD cameras can be placed at different positions, and fixed phase differences can be introduced at these positions. Multiple cameras simultaneously capture speckle interferograms with known fixed phase shifts [64]. Figure 3.5 shows a multi-camera multi-channel spatial phase shift system.

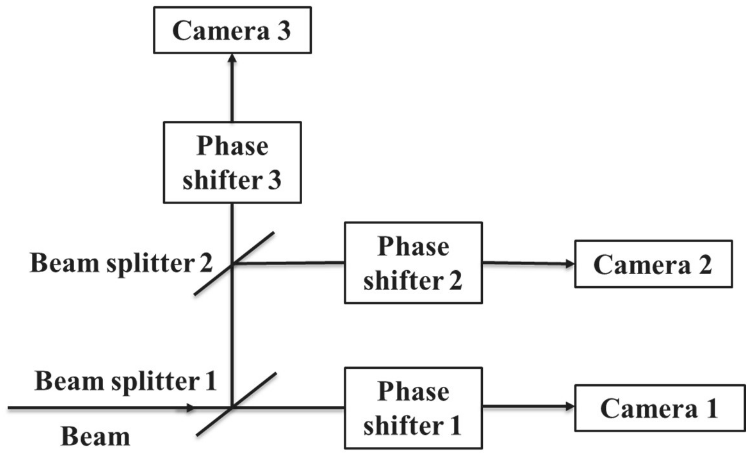

Fig 3.5 Schematic of the multi-camera multichannel spatial phase shift system

Although the multi-camera approach enables dynamic measurements, introducing phase shifts between cameras is challenging, and the system becomes complex with difficult adjustments. Vibrations or temperature changes can introduce significant errors between different cameras, and the use of multiple cameras increases the system cost [65]. As a result, this system had some applications in early dynamic testing, but currently, it is less commonly used in practical applications.

Therefore, to reduce system complexity and cost, a single-camera configuration was proposed, which uses a single CCD camera to capture speckle interferograms and extract phase information [66]. In this method, each individual pixel is treated as a channel, and a certain optical path difference (OPD) is introduced between adjacent pixels by adjusting the incident angle α of the reference light, as shown in Figure 3.6. The optical path difference between adjacent pixels can be further converted into phase changes, thus introducing a determined phase shift between pixel points. Then, by using intensity data from three or more adjacent pixels and applying the phase shift algorithm, the required phase values can be calculated, obtaining the relative phase difference caused by deformation before and after loading on the object [67, 68]. The prerequisite for this technique is that one speckle pattern needs to cover the corresponding number of pixel points [69-74].

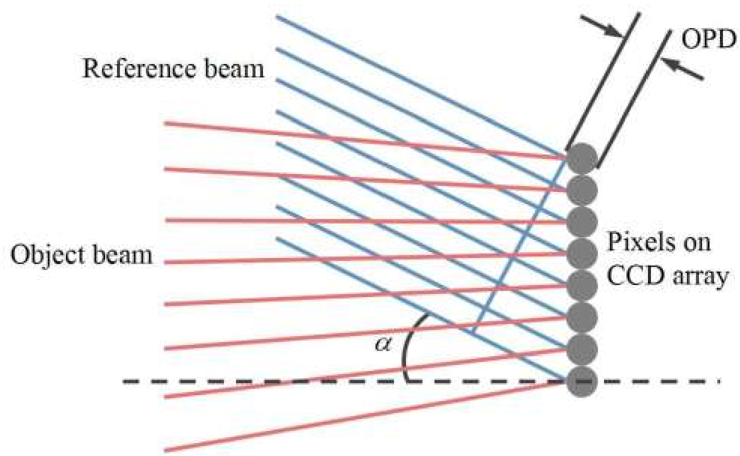

Fig 3.6 Schematic of single-camera multi-channel spatial phase shift system

To utilize the multi-channel spatial phase shifting method for phase extraction, several algorithms are available. The basic algorithms are similar to the time phase shifting method and can be roughly categorized into three-step, four-step, and arbitrary five-step algorithms. The difference lies in the requirement for a specific phase difference between adjacent pixels (three-step requires 120 degrees, four-step requires 90 degrees), while the arbitrary five-step method only requires that adjacent pixels have the same phase difference without a specific value. Different algorithms have different optical setups and image qualities.

Figure 3.6 shows the schematic diagram of the multi-channel method used to generate spatial phase shifting between pixels. The red lines represent object light, the blue lines represent reference light, and the circular speckles are pixel points on the CCD plane. OPD represents the optical path difference between two pixel points, denoted as ΔL, and S represents the distance between pixel points or the size of pixel points. The angle between the incident angle of the reference light and the normal direction of the camera plane is represented as α. Equation 3.17 describes the relationship between ΔL, pixel size S, and the illumination angle α.

$$OPD = \Delta L = S \sin \alpha$$

3.19

If the laser wavelength used is λ, the relationship between the optical path difference ΔL and the phase difference Δ between two pixel points can be expressed as:

$$\frac{\Delta L}{\lambda} = \frac{\Delta}{2\pi}$$

3.20

Due to equation 3.19 and 3.20, the required phase difference between two adjacent pixel points can be represented as:

$$\Delta = 2\pi \frac{S \sin \alpha}{\lambda}$$

3.21

As shown, by adjusting α, we can obtain the desired fixed phase difference Δ. Taking the three-step phase shifting method as an example, we calculate the phase information to obtain the phase map. By adjusting the aperture size to cover three pixels for each speckle, and adjusting α to introduce the fixed phase difference (2π/3), required for the three-step phase shifting method. we can use the recorded intensity information of speckle interferograms by the camera to extract the phase information using the three-step phase shifting method. The intensity of the adjacent three pixels recorded by the camera can be represented as:

$$I_1 = A + B\cos\varphi$$
$$I_2 = A + B\cos\left(\varphi + \frac{2\pi}{3}\right)$$
$$I_3 = A + B\cos\left(\varphi + \frac{4\pi}{3}\right)$$

3.22

In the equation, $I1$ to $I3$ represent the intensities of four pixels. A and B are parameters related to the background information. φ corresponds to the phase information of the corresponding speckle pattern. Therefore, the phase information of the speckle interferogram can be represented as:

$$\varphi = \tan^{-1}\frac{\sqrt{3}(I_3 - I_2)}{2I_1 - I_2 - I_3}$$

3.23

This method allows obtaining at least three phase information from a single speckle interferogram. In practical measurements, before and after deformation, only one image of the object needs to be captured to calculate the phase information of these two status respectively, then the subtraction of the two phase images yields the phase map of the object.

The single-camera structure of the multi-channel spatial phase-shifting technique also has its limitations. This method requires using intensity data from at least three pixels to determine the phase information, which significantly reduces the spatial resolution of the results. Additionally, the precision of adjusting the incident angle of the reference light with respect to the camera plane's normal direction also affects the measurement accuracy.

3.3.2 The carrier frequency spatial phase shift method

To overcome the limitations of the multi-channel spatial phase-shifting technique, another spatial phase-shifting technique suitable for dynamic measurements has been proposed, known as spatial carrier phase-shifting technique [75-77]. Compared to the multi-channel spatial phase-shifting technique, the spatial carrier phase-shifting technique can provide higher spatial resolution and extract and separate multiple phase information from a single speckle interferogram. Its method is simple, computationally convenient, and has a wide range of applications, making it a hot topic in speckle interferometry phase extraction methods.

The frequency carrier technique is a traditional and mature technology in the field of communication. The general principle of this method is to modulate the signal carrying the target information with a high-frequency carrier frequency and propagate it in space. At the signal receiving end, the modulation information is demodulated to separate the signal with the target information [78, 79]. In spatial carrier phase-shifting technique, Fourier transform and inverse transform are used to convert and obtain the phase information. In 1996, G. Pedrini first applied this method to a Mach-Zehnder shear speckle interferometry system and obtained the surface phase information of the tested object using spatial carrier phase-shifting technique [80].

The measurement using spatial carrier phase-shifting technique can be divided into three steps. First, the carrier information is introduced into the optical system, and a CCD records an intensity image. Unlike time phase-shifting technique and multi-camera multi-channel spatial phase-shifting technique, the spatial carrier phase-shifting technique does not require additional phase-shifting devices; instead, the phase shift process is achieved through the carrier. In digital speckle interferometry, the basic principle of introducing the carrier is to tilt the illumination angle of the reference light to generate a specific angle with another beam of laser light that enters vertically. Second, the intensity image is Fourier transformed to obtain the frequency domain spectrum, thus achieving the conversion from spatial domain to frequency domain. In the detection optical path, the mathematical expression of light intensity and carrier information can be formulated, and then Fourier transform can be applied to obtain the mathematical expression of light intensity after Fourier transformation. Third, in the frequency domain, the spectrum containing the target information is selected, and the inverse Fourier transform is used to convert the spectrum back to the required phase map. Figure 3.7 shows the results obtained in each step of this process.

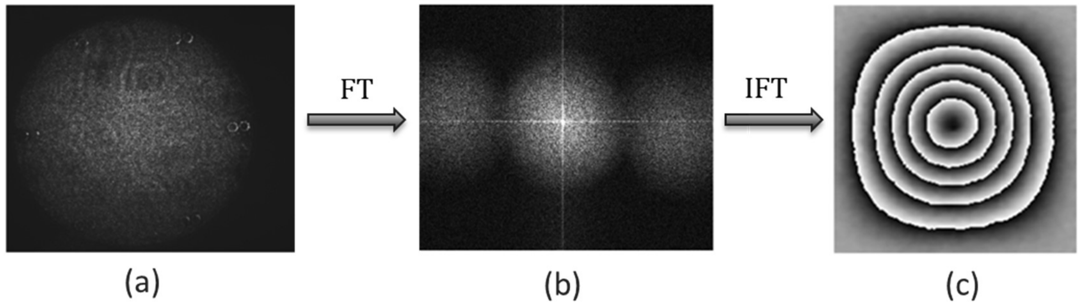

Fig 3.7 The images of carrier frequency spatial phase shift method: (a) the intensity image with spatial carrier frequency, (b) Fourier spectrum distribution from the intensity image, (c) Phase map

As shown in Figure 3.8, it illustrates the spatial carrier phase-shifting technique based on the system schematic. Let's use this system as an example to explain the spatial carrier phase-shifting technique.

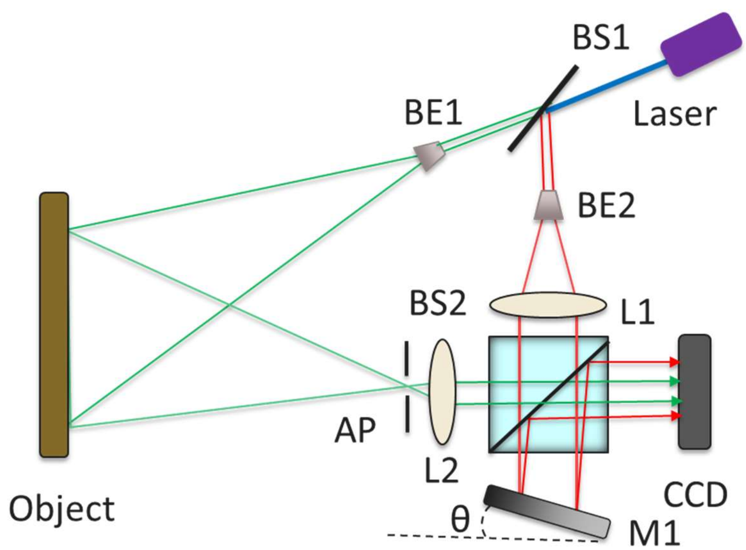

Fig 3.8 DSPI system based on spatial carrier phase-shifting

In the system, the laser emitted from the laser source is divided into object light and reference light by the beam splitter (BS1). The object light passes through the beam expander (BE1) to expand and illuminate the tested object. The light scattered by the tested object goes through an aperture (AP), imaging lens (L2), and another beam splitter (BS2) before forming an image on the CCD target surface.

The reference light, after passing through the beam expander (BE2), passes through a collimating lens (L2) and BS2 before reaching the reflecting mirror M1. By adjusting the angle θ of M1, a spatial carrier is introduced. The modified reference light then reflects off BS2, enters the CCD, and interferes with the object light to form a speckle interferogram, which is recorded by the CCD camera in the form of intensity.

In this way, the spatial carrier phase-shifting technique utilizes the spatial modulation introduced by the reflecting mirror M1 to achieve phase shifting in a single frame of the speckle interferogram. This technique provides higher spatial resolution and allows for the extraction of multiple phase information from a single image, making it a widely used and popular approach in speckle interferometry phase extraction.

The reference light and object light can be represented as follows:

$$u_0 = |u_0(x, y)| \exp[i\phi(x, y)] \tag{3.23}$$

$$u_{\mathrm{r}} = |u_r(x + \Delta x, y + \Delta y)| \exp\{ i[\phi(x + \Delta x, y + \Delta y) + 2\pi(f_{\alpha_x} x + f_{\alpha_y} y)]\} \tag{3.24}$$

where u_o and u_{r} are the object light and reference wave fronts. Tilted M1， Δx and Δy are the shearing distances in the x- and y-direction, respectively, while f_α, which represents the component of the spatial frequency introduced by shearing angle α, can be expressed as Equations (3.25) and (3.26):

$$f_{\alpha_x} = \frac{sin\alpha_x}{\lambda}$$

(3.25)

$$f_{\alpha_y} = \frac{sin\alpha_y}{\lambda}$$

(3.26)

where x and y are the x-direction and y-direction respectively.

The intensity can be expressed as Equation (3.27):

$$I = (u_0 + u_r)(u_0{}^* + u_r{}^*) = u_0 u_0{}^* + u_r u_r{}^* + u_0 u_r{}^* + u_r u_0{}^*$$

3.27

The * denotes the complex conjugate of u_o, and u_r. The Fourier Transform converts the image from the spatial domain to the Fourier domain. Application of the Fourier Transform to Equation (3.27) transforms the equation into the following form:

$$FT(I) = U_0(f_x, f_y) \otimes U_0(f_x, f_y)^* + U_r[(f_x + f_{\alpha_x}), (f_y + f_{\alpha_y})] \otimes U_r[(f_x + f_{\alpha_x}), (f_y + f_{\alpha_y})]^* + U_0(f_x, f_y) \otimes U_r[(f_x + f_{\alpha_x}), (f_y + f_{\alpha_y})]^* + U_r[(f_x + f_{\alpha_x}), (f_y + f_{\alpha_y})] \otimes U_0(f_x, f_y)^*$$

3.28

Here $\otimes$ is the convolution operation.

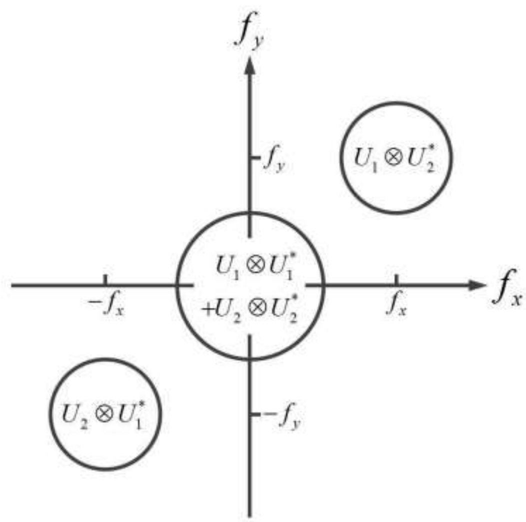

Fig 3.9 Schematic of Fourier spectrum

The schematic diagram of the Fourier spectrum is shown in Figure 3.9. The central low-frequency component $U_1 \otimes U_1^* + U_2 \otimes U_2^*$ contains scene information, while the frequency components $U_1 \otimes U_2^*$ and $U_2 \otimes U_1^*$ contain the required phase information. The frequency components are symmetric about the origin and located at positions (f_x, f_y) and $(-f_x, -f_y)$ in the Fourier spectrum. The width of the frequency components is determined by the aperture size. By appropriately adjusting the incident angle of the object light and selecting an appropriate aperture size, the Fourier domain can completely separate the spectrum containing various types of information.

By extracting the frequency component $U_1 \otimes U_2^*$ and performing an Inverse Fourier Transform (IFT), we can obtain $u_1 u_2^*$. From there, we can calculate the phase difference between the reference light and the object light as follows:

$$\theta + 2\pi\left(f_{\alpha_x}x + f_{\alpha_y}y\right) = tan^{-1}\frac{Im[u_1u_2^*]}{Re[u_1u_2^*]}$$

3.28

$$\theta = \phi(x + \Delta x, y + \Delta y) - \phi(x, y)$$

3.29

Here, *Im* and *Re* denote the imaginary and real part of the complex numbers respectively, and θ is the phase difference between the two tilted beams reflected from M1 and M2.

With the same method, another phase distribution can be obtained after the object is loaded using the recorded images:

$$\theta' + 2\pi\left(f_{\alpha_x}x + f_{\alpha_y}y\right) = tan^{-1}\frac{Im[u_1u_2^*]}{Re[u_1u_2^*]}$$

3.30

The relative phase difference due to a deformation can then be calculated as:

$$\Delta\theta = \theta - \theta'$$

Spatial carrier phase-shifting technique requires only one frame of speckle interferogram to extract the phase information before and after object deformation, and its acquisition rate is not limited by the phase step but solely determined by the camera's capabilities, enabling high-speed dynamic measurements. However, this method suffers from spectral truncation and leakage, which can affect the measurement accuracy to some extent. To provide a more intuitive comparison of the phase quality achieved by different phase extraction methods, experimental results obtained using intensity subtraction, time phase-shifting technique, and spatial carrier technique are shown in Figure 3.9. Figure 3.10(a) represents the speckle phase obtained by intensity subtraction of the speckle interferograms before and after object deformation, Figure 3.10(b) shows the speckle phase obtained using the 4+4 time phase-shifting algorithm, and Figure 3.10(c) displays the speckle phase extracted through Fourier transform of the speckle interferogram. It can be observed that the phase quality obtained by intensity subtraction is the poorest, while the time phase-shifting technique yields the best phase quality. However, the time phase-shifting technique is only suitable for static measurements. On the other hand, the spatial carrier technique, while applicable for dynamic measurements, shows a slight decrease in phase quality within a reasonable range, making it a more advantageous method compared to the other two phase extraction methods.

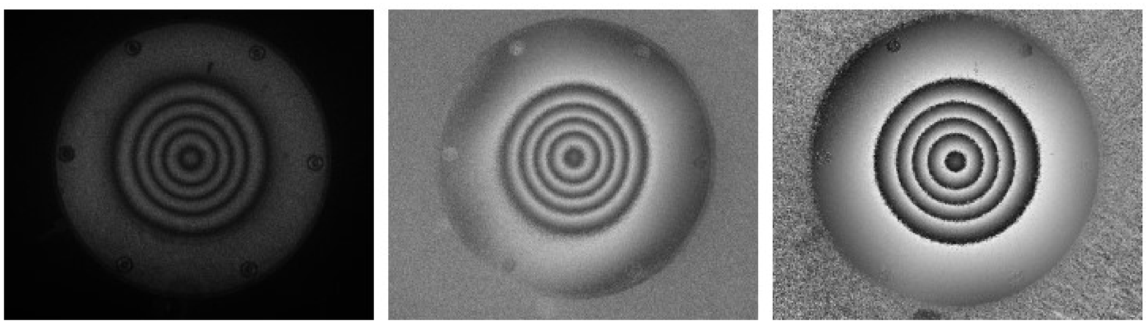

Fig 3.10 Comparison of experimental results of phase extraction methods: (a) intensity subtraction; (b) temporal phase shift; and (c) carrier-frequency spatial phase shift.

CHAPTER FOUR

SIMULTANEOUS DUAL SENSITIVE MEASUREMENT

4.1 Introduction of simultaneous dual sensitive measurement

In industrial testing, in some cases, multiple object parameter results are needed to evaluate the properties of materials. Such as surface deformation and strain, in-plane displacement and out-of-plane displacement, the strain of x direction and y direction, measurement results at different spatial resolution sand so on. Using traditional speckle interferometry methods, only one parameter result can be obtained per measurement. To obtain multiple measurement results, multiple repeated measurements must be carried out. Doing multiple measurements have many drawbacks. First, the loading amount and loading time of each measurement cannot be exactly the same, which leads to certain errors in the obtained results. Second, repeated measurement requires more labor costs and time costs, resulting in an increase in measurement costs. In addition, there are some situations in which repeated measurements cannot be performed, such as destructive experiments. So, the simultaneous dual sensitivities are needed for industrial measurements.

4.1.1 The review of dual simultaneous sensitive measurement

Current existed research on simultaneous double sensitivity can be divided into two broad categories. One is to measure two object parameters at the same time, and the other is to measure one object parameter at different spatial resolutions.

Up till now, many studies on measuring the parameters of two objects simultaneously have been published. In 2003, proposed for the first time, Steinchen W and Yang L a digital shear imaging system based on temporal phase shift technology to measure strain in the both x and y directions to realize strain measurement in the double shear direction[A5-7]. In 2016, Wang et al. introduced a Michelson interferometer-based spatial phase-shift digital shear imaging system to achieve strain measurement in both shear directions. In 2020, Boyang Z et al. propose a dual shearing shearography system based on a spatial light modulator (SLM) [81]. For the research on the simultaneous measurement of the first derivative of surface deformation and deformation, In 2013, Xin Xie et al introduced a method using digital Shearography technology and spatial phase shifting technology to achieve simultaneous measurement of surface deformation and strain [82] In 2019, Qihan Zhao et al. introduced the simultaneous measurement of surface deformation and strain in x, y, and z directions using multiple lasers. [83]. To research on simultaneous in-plane and out-of-plane displacement measurements. In 2019, Hooshmand-Ziafi et al. published a method of simultaneous measurement of in-plane and out-of-plane displacement using dual lasers and spatial phase-shifting techniques [84] In 2019, Dong Jie proposed a digital Shearography system using a single laser and spatial phase-shifting technique to measure in-plane and out-of-plane displacements simultaneously.

At the same time, there are few researches on the measurement of the same measurement object under different fraction rates. In 2021, Boyang Zhang et al proposed a digital Shearography measurement system based on spatially proportional double spatial resolution, which realizes the measurement of double spatial resolution at the same time.

4.1.2 The review of dual simultaneous special resolution sensitive measurement

Currently, most optical inspection systems use a single camera with a fixed field of view to record images, resulting in only one resolution sensitivity per measurement. These systems for measuring a limited area of a specific object are efficient and simple. However, these systems have poor resolution and other drawbacks when measuring objects with internal defects of unknown size, and may overlook small size defects. In order to solve this problem, repeated measurements using multiple sets of equipment with different resolutions are necessary. However, this not only increases labor costs and test time, but also complicates measurement operations. In addition, in some cases, multiple measurements may not be possible. A measurement system with simultaneous spatial resolution is needed.

How can dual spatial resolution measurement be achieved? One method is to use CCDs with different resolutions and change the resolution by switching CCDs, for example, utilizing a digital zoom camera, as shown in Figure 4.1. However, this approach depends on the characteristics of the equipment, and multiple CCD switches would increase time and cost.

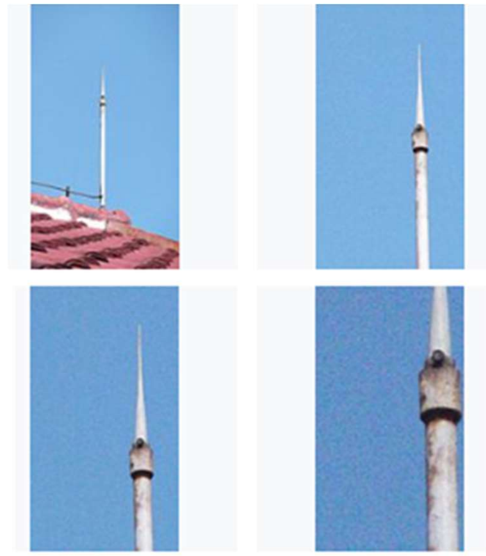

Fig 4.1 Images recorded by digital zoom camera

Another approach is to adjust the optical path by using different lenses to alter the observed field of view, thereby changing the spatial resolution. Figure 4.2 illustrates different fields of view, with Figure 4.2a representing a large field of view with relatively lower resolution, and Figure 4.2b representing a small field of view with relatively higher spatial resolution. By measuring the test object under different fields of view, different spatial resolutions can be achieved. Here, the concepts of large field of view and small field of view are relative. A large field of view for speckle pattern refers to a speckle pattern that can be clearly observed over the entire field. A small field of view is relative to the large field of view, representing a magnified view of a specific region's speckle pattern. As shown in Figure 4.2, if the deformed surface area is much smaller than the field of view, a small speckle point might be overlooked in the large field of view. However, it can be observed in the small field of view.

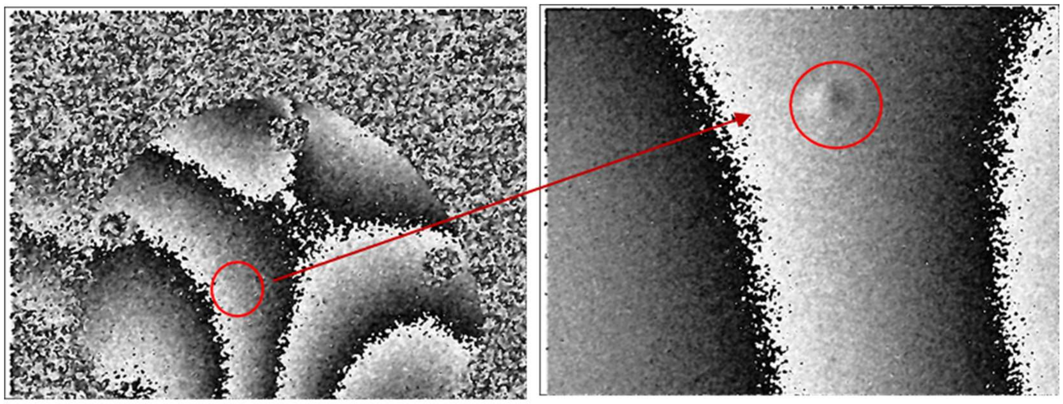

Spackle pattern under large field of view **Spackle pattern under small field of view**

Fig.4.2 Large field of view and small field of view

4.2 The method to achieve dual sensitive measurement

In order to realize the measurement of synchronous double sensitivity, this section summarizes the different methods that have emerged successively. These methods mainly include using two cameras to construct two physical channels, using a single camera and constructed two optical channels superimposed together, using a single camera and constructed two optical channels independent of each other.

4.2.1 Dual camera with two physical channels

In 2003, Steinchen W and Yang L first proposed a dual shear direction digital shear imaging system based on time-phase shift technology [85-87]. The system uses two individual cameras as two interferometric systems, and the two cameras record the dual shear direction information at the same time in the corresponding shear direction, x and y direction. As shown in Figure 4.3, in this system, it stacks two Michelson interferometer, and three reflective mirrors are used, the large one is used as the PZT mirror which has no shearing and utilized to generating phase shift. The other two mirrors are sheared in the x and y directions respectively. In the configuration shown in Figure 4.3, the laser is spread out to illuminate the object and then incident into the top and bottom beam splitters, respectively. The top Michelson interferometer has a y-direction shear, while the bottom beam splitter has an x-direction shear. The two cameras are connected to the frame collector and can record images independently and simultaneously as two physical channels. All images will finally be transferred to the computer for processing with pre-input parameters. In theory, different spatial resolutions can be obtained by adjusting the two cameras. This method is simple and direct, without additional design of measuring optical path, relatively easy to implement, and has been applied for a long time.

However, there are some obvious problems with the system, such as the two CCDs having different coordinates and different shooting positions and angles. This is due to the fact that the two Michelson interferometers are stacked together, the incident lights enter from different angles. In the imaging plane, the two images of the two CCDs channels have different viewing angles. If the object is far away from the setup, this angle is negligible. However, if within a limited measurement area, especially in quantitative testing, the two images may present different surface information. In addition, the beam splitter can be used as a field diaphragm, reducing the field of view, so that the field of view is fixed or limited. Moreover, the two kinds of image acquisition equipment not only require high cost, but also introduce the problem of equipment consistency. Since different cameras have their own characteristics, even if triggered at the same time, system error cannot be avoided. In order to solve these problems, the first consideration is to reduce the number of image acquisition equipment, using a single camera to measure two optical channels at the same time is a better optical structure.

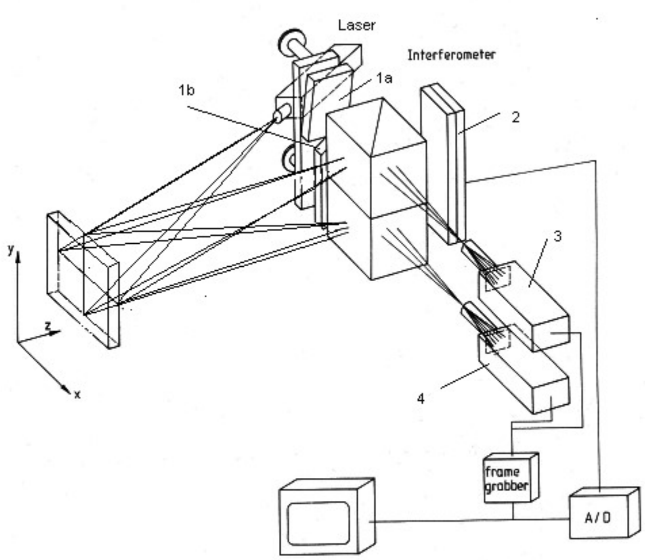

Fig, 4.3 The schematic of dual shearing shearography of two stacked interferometers

<u>4.2.2 Single camera with two mixed optical channels</u>

Due to the limitation of using multiple cameras to achieve simultaneous dual sensitive measurement, the method of using single camera to achieve simultaneous dual sensitive measurement has been developed. The key technology of this method lies in the design of the measuring optical path. With the reduction in the number of measuring cameras, the measurement cost is significantly lowered.

The paper mentioned above, authored by Xin Xie et al., titled "Simultaneous measurement of deformation and the first derivative with spatial phase-shift digital shearography," utilized this single-camera synchronized dual-sensitivity measurement method. In this paper, the system used a Michelson interferometer as the shear device and employs a single wavelength laser and a single CCD camera as the light source and recording element, respectively.

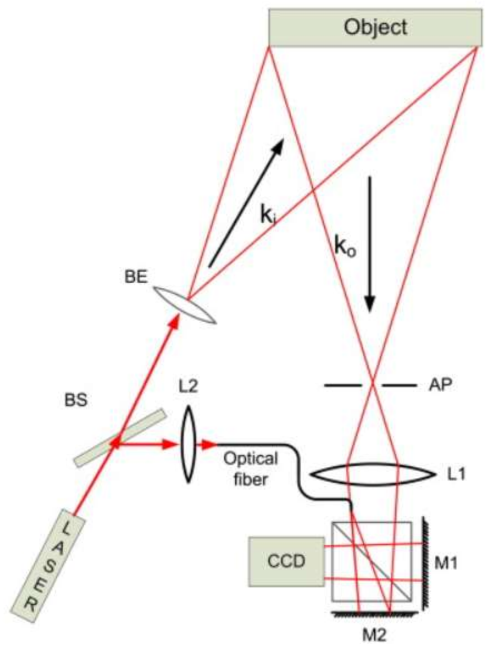

Fig 4.4 Schematic of the multiplexed measurement method based on Michelson interferometer

The principle of the multiplex measurement method based on Michelson interferometry is shown in Figure 4.4. The laser emitted by the laser source is split into object light and reference light by a beam splitter (BS). The object light, after being expanded by a beam expander (BE), illuminated the tested object. The scattered light from the object passes through an aperture (AP), imaging lens (L1), and shear device before being received by the CCD camera. The reference light is guided through an optical fiber, exits behind the lens (L1), and is introduced into the optical path before the shear device, and then it was also received by the CCD camera. The results of digital speckle interferometry (Hologram) were obtained from the interference of the reference light with either of the object lights, while the results of digital shear speckle interferometry (Shearogram) are obtained from the interference of the two object lights produced by the shear device. Both sets of results are simultaneously recorded by the CCD camera in the form of intensities.

This method also employs spatial carrier phase-shifting techniques. The original speckle image captured by the CCD camera contains information from both the hologram and shearogram. A Fourier Transform (FT) is applied to this image to separate the hologram and shearogram information. Then, a Fourier Transform is applied to the intensity image to obtain the Fourier spectrum containing the phase information, as shown in Figure 4.5a. Finally, the inverse Fourier Transform is performed to extract the speckle information (hologram and shearogram) from different optical channels using a single image. In summary, the method described in this paper utilizes spatial phase-shift digital shearography with a Michelson interferometer, a single wavelength laser, and a single CCD camera to perform simultaneous measurement of deformation and the first derivative with synchronized dual-sensitivity testing using spatial carrier techniques. But from figure 4.5, only two pairs of spectrum were used to evaluate, the other spectrums are not needed.

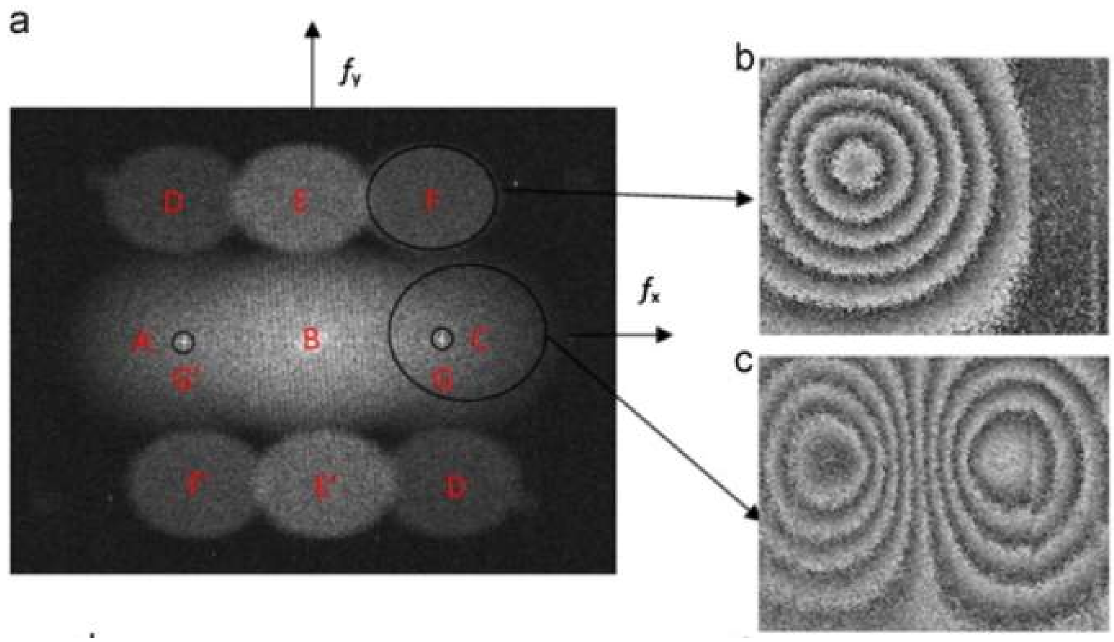

Fig 4.5 (a) Spectrum after Fourier Transform (FT); (b) Phase map of a hologram due to a deformation after Windowed Inverse Fourier Transform (WIFT) operation from Section F′; (c) Phase map of a shearogram due to a deformation after WIFT operation from Section C. [88]

This method using single camera with multiple mixed optical channels primarily involves designing the optical path, constructing multiple optical channels, using a single camera to record intensity images, applying spatial phase-shifting techniques through Fourier transformation to obtain the frequency spectrum, and then using inverse Fourier Transform to extract the speckle information, thus achieving synchronized dual-sensitivity measurement.

While this method overcomes the drawbacks of multi-camera systems by using a single camera for data recording, it also has its limitations. Multiple optical channels are mixed together, and there may be interference between these channels, leading to overlapping of the frequency spectrum or the presence of irrelevant spectral components during spatial phase-shifting, making the extraction of frequency spectra more challenging.

A relatively independent, cross-interference-free synchronized dual-sensitivity measurement method needs to be developed to address these issues.

4.2.3 Single camera with two independent optical channels

To avoid mutual interference between multiple optical channels, methods for constructing relatively independent optical channels have been developed. Currently, there are two main approaches in research to achieve relatively independent optical channels.

The first method involves using multiple lasers with different frequencies as the illumination sources for detection. By using lasers with distinct frequencies, the interference between the optical channels can be minimized, ensuring that each channel remains relatively independent.

The second method involves utilizing polarization techniques to split a single-frequency laser into two beams of incoherent light. This creates two relatively independent and non-cross-interfering optical channels.

These approaches allow researchers to overcome the challenges associated with cross-interference among optical channels, enabling more precise and accurate synchronized dual-sensitivity measurements.

4.2.3.1 Dual frequency laser beam

Qihan Zhao and his team proposed a method for synchronously measuring three parameters of objects. This method utilizes three lasers with different wavelengths as light sources and a single color camera as the recording element. By solving phase change equations that include different angular components, it obtains three-dimensional deformation and its first derivative information. The method is illustrated in Figure 4.6.

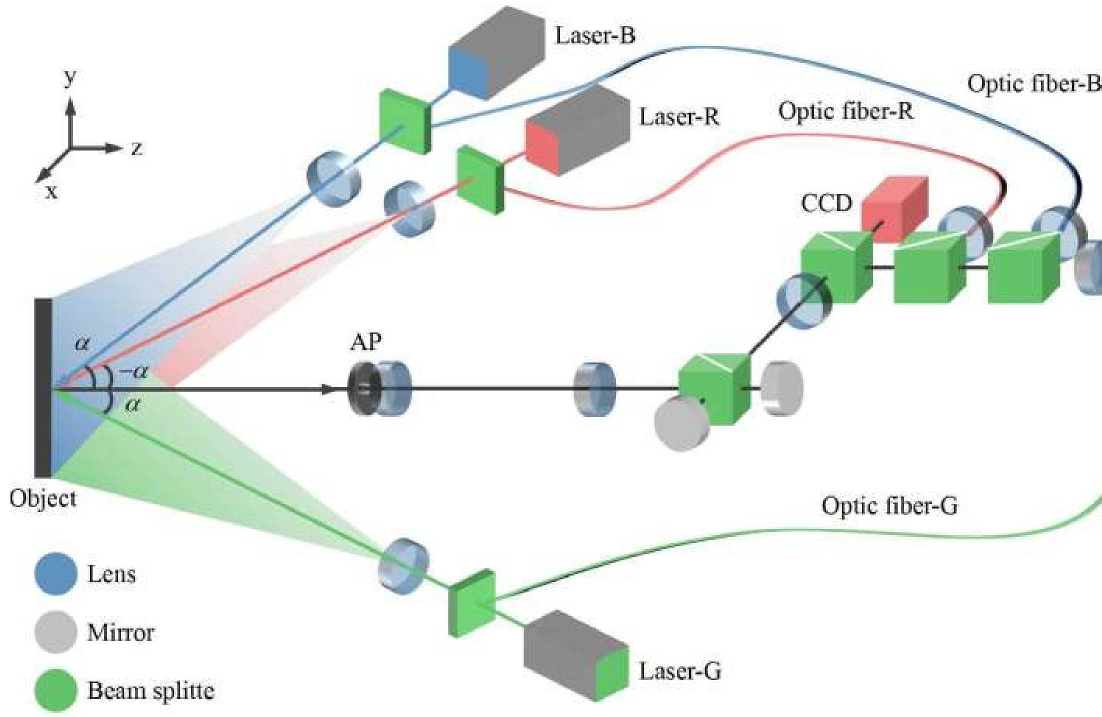

Fig 4.6 Schematic of the 3D multiplexed measurement method based on Michelson interferometer

The three lasers with different frequencies (Laser-R, Laser-G, Laser-B) emit light that is split into object light and reference light by a beam splitter. The object light, after being expanded by a beam expander, illuminates the tested object. The reference light is guided through an optical fiber to be introduced into the optical path after the shear device, and both object and reference light are received by the color camera.

By separating the color speckle interferograms generated by the color camera, the method can extract the digital speckle interferometry results and digital shear speckle interferometry results produced by each wavelength laser. From the color speckle interferograms, the individual monochromatic speckle interferograms and their corresponding frequency spectra for the RGB channels are obtained. By performing

Fourier Transform separately on each RGB channel's frequency spectrum, the frequency spectra of each individual monochromatic speckle interferogram are obtained. Fourier Inverse Transform is then applied to the selected frequency spectra to obtain the phase maps for the RGB channels.

4.2.3.2 Single laser beam

Based on the utilization of polarization technique, Boyang Zhang and his team studied the establishment of a dual-shear imaging system using a single laser and used laser polarization technology to replace multi-wavelength lasers and bandpass filters for signal separation. This approach allows for the creation of two relatively independent optical channels using a single laser. Figure 4.6 illustrates the schematic setup of this system. This system is based on an improved Michelson interferometer. The setup incorporates some ideas from the Siebert and Schmitz systems and is developed to record information from two shear directions in a single image using one camera.

A coherent laser with a wavelength of 532 nm serves as the light source, and a $\lambda/4$ waveplate is used to transform the laser from linearly polarized to circularly polarized. This is because, although a rough surface reflection can randomize a well-polarized laser into a randomly polarized one, most reflected waves will maintain their original polarization direction and are not evenly distributed. The $\lambda/4$ waveplate ensures that the light intensity is evenly divided 50:50 among each polarization direction when the light wave passes through the polarization beam splitter (PBS). AP and L1 represent the aperture and lens of the imaging system, while L2 and L3 are lenses of the 4f system used to enlarge the field of view.

The light waves reflected from the object are split into two beams by a regular beam splitter (BS). One of these two waves, not subjected to polarization processing, is named Light wave #R. It reaches the mirror M1 and is reflected back to the BS before entering the CCD. The other light wave enters a polarization Michelson interferometer consisting of PBS, M2, and M3 (as shown in Figure 4.7) and is split into two polarized sub-beams by the PBS. The sub-beam with the ordinary polarization direction is reflected by M2 and named Light wave #S. The second sub-beam with an extraordinary polarization direction reaches M3 and is named Light wave #P. By tilting M2 and M3 along the horizontal (x-shear) and vertical (y-shear) directions, carrier frequency, shear direction, and shear distance are introduced.

To separate the frequency spectrum of the two shear images in the spatial frequency domain, changes in the circular aperture's size are used to control the spectrum size, and the Fourier Transform method is applied to calculate the shear images. Finally, after the inverse Fourier Transform, the phase maps are obtained.

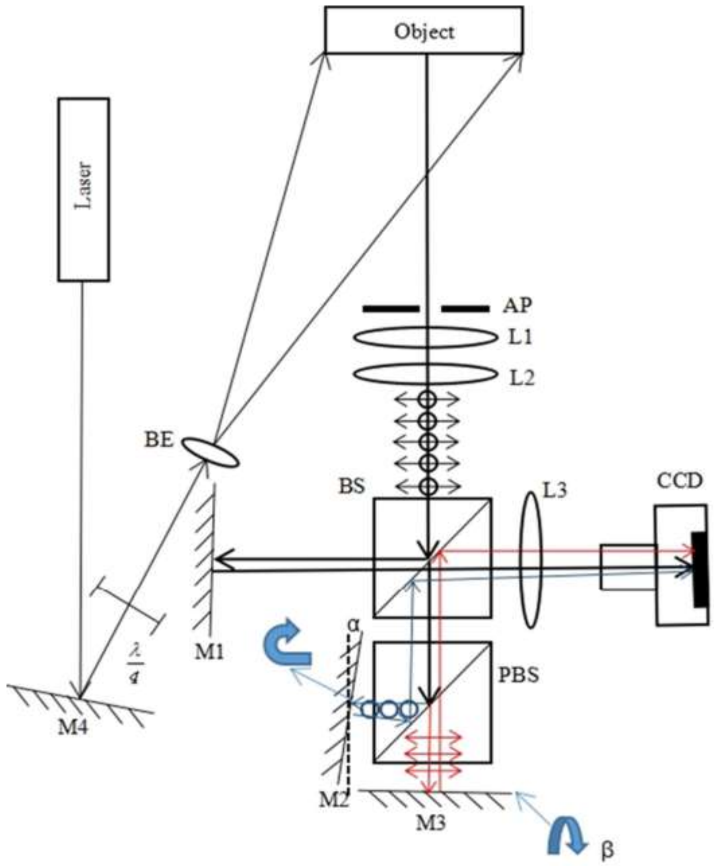

Fig 4.7 The schematic of polarized digital shearography for simultaneous dual shearing directions using modified Michelson Interferometer

4.2.4 Polarization technique

Polarization technique is a crucial method for establishing non-cross-interfering dual optical channels. Coherent light sources are used in speckle interferometry because coherent light possesses consistent spatial characteristics, frequency (wavelength), phase, and polarization states, enabling interference and measurement. Polarization is a property of transverse waves that specifies the geometric orientation of oscillation [89-93]. When coherent light is polarized, it loses its coherence as its oscillation directions are specified, and they are no longer consistent. Polarized light can be generated by allowing only one polarization wave to pass through a polarizer, as shown in Figure 4.8. The black light represents circular polarization light, which becomes two red and blue polarized lights after being polarized. The red light is ordinary light, with its oscillation direction along the y-axis, while the blue light represents extraordinary light, with its oscillation direction specified along the x-axis. These two polarized lights are incoherent and cannot interfere with each other. By utilizing these two incoherent lights to establish two independent optical channels, the interference between these two channels can be avoided. Thus, it becomes possible to create two relatively independent optical channels using a single laser.

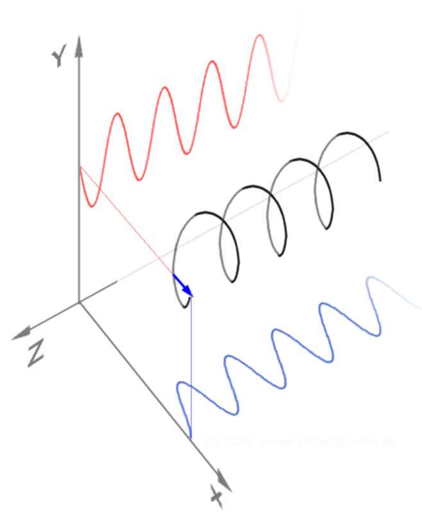

Fig 4.8 Sketch of polarization technique

4.3 The method to achieve simultaneous dual spatial resolution measurement

Simultaneous dual spatial resolution measurement is a technique that focuses on a single object but measures it at two different spatial resolutions simultaneously. This measurement requires obtaining two measurement results simultaneously. To implement synchronized dual spatial resolution measurement, two optical channels need to be designed, with each channel corresponding to a different spatial resolution. This paper developed a digital shearography measurement system and designed a digital holography measurement system to achieve dual spatial resolution optical path. The polarization techniques are used to avoid the cross interference between the two optical channels. Spatial carrier phase-shifting techniques are employed to simultaneously separate and extract the phase maps at the two spatial resolutions from one intensity image recorded by CCD. These design and key technique enable simultaneous dual spatial resolution measurement be achieved.

4.3.1 The major issue of simultaneous dual spatial resolution measurement

The main focus of this paper is on utilizing speckle interferometry for simultaneous dual spatial resolution measurement. There are three main issues that need to be addressed. The first one is how to design a speckle interferometry setup with dual spatial resolution. The second is how to design relatively independent dual optical channels. And the third is how to synchronously separate and extract the speckle information from both channels using only single intensity image.

During the detection process, as shown in Figure 4.9, when intensity subtraction or time shifting methods are used to measure the test object at different spatial resolutions, clear phase maps can be extracted from the intensity images recorded in each measurement repectively. However, if the intensity information of both spatial resolution channels is recorded simultaneously, the two speckle patterns from both channels will mix together, making it impossible to extract clear and independent phase maps at the same time.

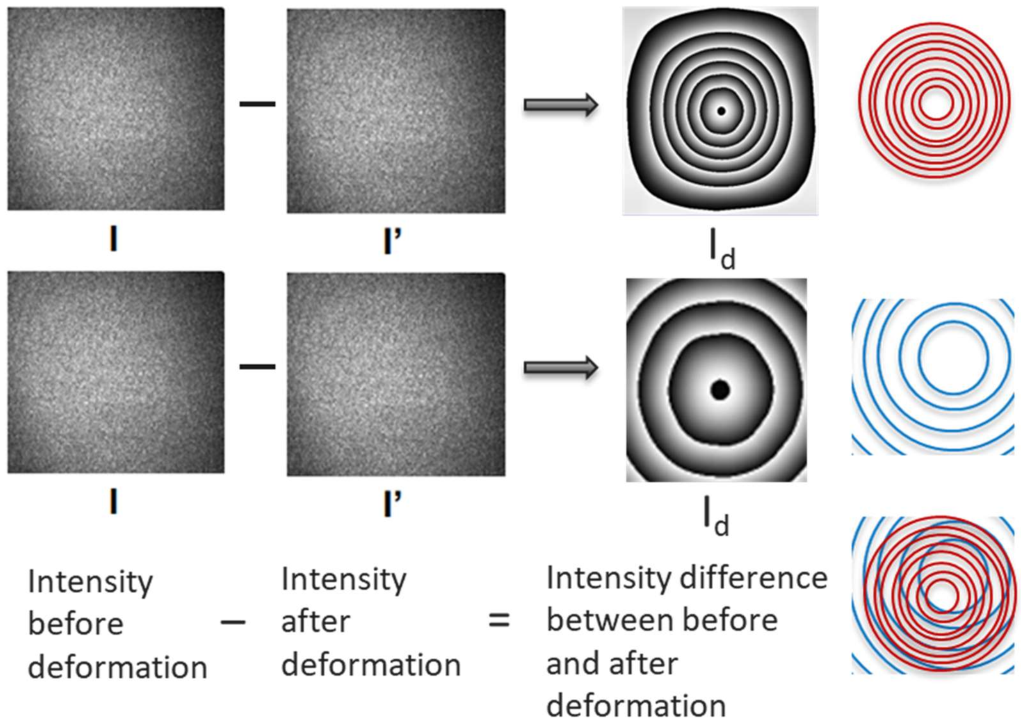

Fig 4.9 Sketch of spackle pattern overlap

Regarding the first issue, it can be resolved by using a lens system in combination with speckle technology, and the specific design approach will be detailed in Chapters 5 and 6. As for the second issue, this study employs optical equipment to polarize a single laser beam into different polarization directions. A polarization beam splitter (PBS) can transform a non-polarized wave into two polarized waves with a 90-degree polarization angle difference. The PBS has a special coating on its diagonal interface with the following characteristics: one polarization direction of polarized light can only be reflected by the interface, while the other orthogonal polarization direction of the reflected light can only pass through the interface without being reflected. Consequently, after passing through the reflection interface of the PBS, two orthogonal polarized lights are obtained, and these two polarized lights are not coherent. Figure 4.10 illustrates the working principle of the polarization beam splitter, where the circle represents the polarization direction perpendicular to the paper, and the arrow represents the polarization direction parallel to the paper. Circularly polarized light (represented by a circle and arrows) enters the PBS, and the reflected light is linearly polarized light with the polarization direction perpendicular to the paper, represented by S. The transmitted light through the PBS is linearly polarized light with the polarization direction parallel to the paper, represented by P. The detailed design of this setup will also be discussed in Chapters 5 and 6. The third issue will be addressed in the following section.

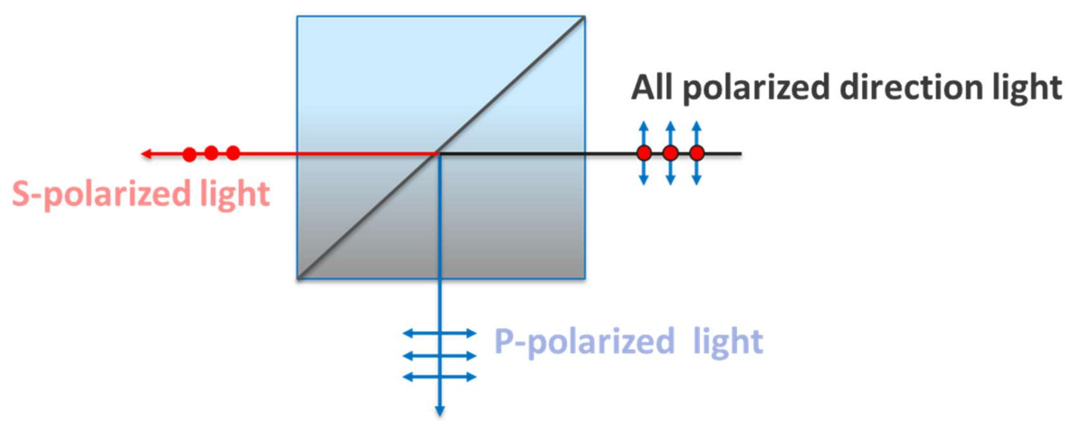

Figure 4.10. The schematic of polarized beam splitter

4.3.2 How to get dual spatial resolution results simultaneously

In 1996, the first carrier frequency spatial phase-shift shearography system was reported by Pedrini et al., which subsequently led to more consideration of spatial phase-shift techniques for NDT (Non-Destructive Testing) applications. Spatial phase-shift techniques utilize Fourier Transform (FT) to convert intensity information into spectral information shown as spectrum distribution in the frequency domain. As shown in Figure 4.11, the left image represents the intensity image, and after Fourier Transform, the intensity information from the left image is transformed into the spectral image in the spatial domain.

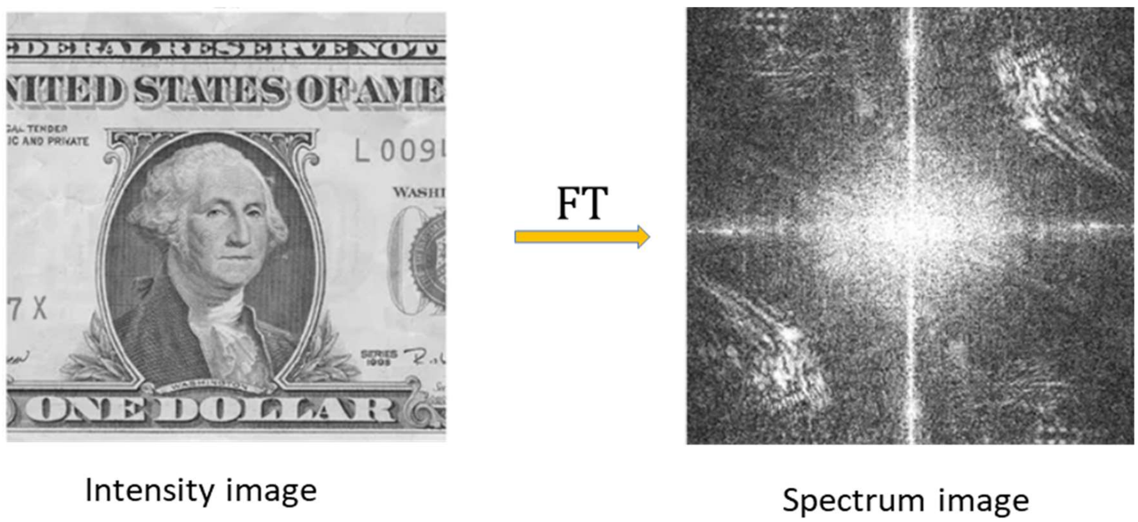

Figure 4.11 Schematic diagram of Fourier Transfer optical application

When employing spatial carrier phase-shift techniques, a carrier frequency is needed to be introduced, and after Fourier Transform, the spectrum containing intensity information is distributed in the frequency domain according to the introduced carrier frequency. This allows the speckle information mixed in the intensity image to be separated and represented as distinct spectral information in the frequency domain. By introducing different carrier frequencies in two relatively independent optical channels, separate spectral distributions can be obtained due to the different carrier frequency. Adjusting the carrier frequency enables the spectrum distribution to change in the frequency domain. Subsequently, an inverse Fourier Transform (IFT) is applied to the separated target spectra, the clear phase maps for the two channels with different spatial resolutions can be obtained. Figure 4.12 explain this processing procedure.

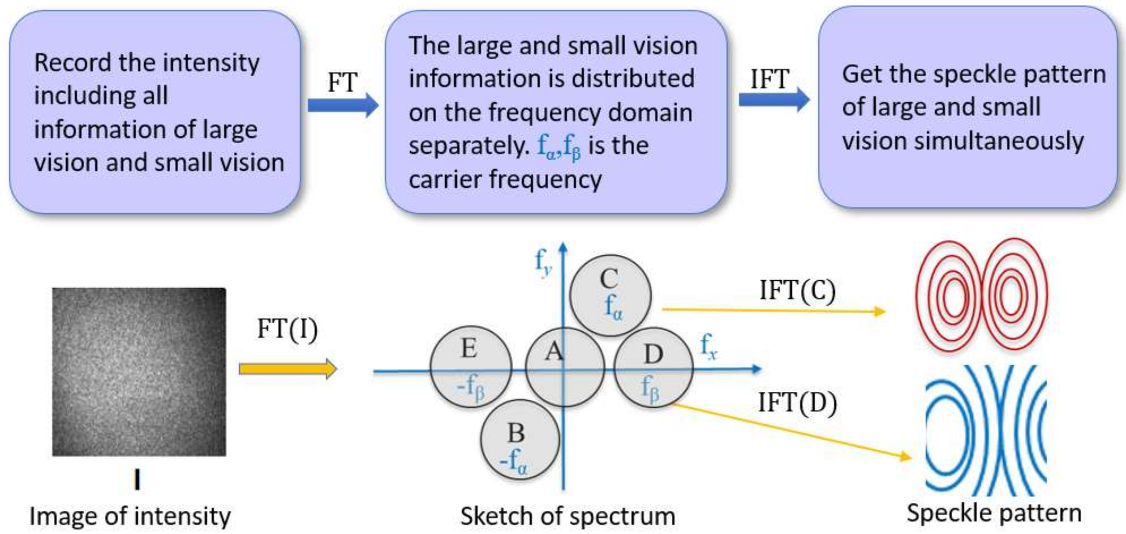

Figure 4.12 The process of extracting two phase maps simultaneously

CHAPTER FIVE

IMPROVEMENT OF DIGITAL SHEAROGRAPHY FOR DUAL SENSITIVITY SIMULTANEOUS MEASUREMENT

5.1 The review of digital shearography for simultaneous dual sensitivity measurement

Application of speckle pattern interferometry for NDT has increased in aerospace, automotive, and other industrial areas because of its advantages of full-field measurement and high sensitivity. Digital shearography, one speckle pattern interferometry technique that is becoming more popular for NDT, can directly measure the first derivative of deformation with the advantage of robustness [94,95]. The interference in digital shearography is generated by two object beams sheared by a shearing component. However, most digital sherography applications can only work in one field of view per measurement, and some small defects may not be detected as a result. Multiple measurements of different fields of view are needed to solve this issue, which will increase the measurement time and cost.

Boyang Zhang, Xiaowan Zheng et al. firstly proposed a Sagnac interferometer based dual sensitive shearography system to achieve simultaneous dual sensitive measurement. The system can perform dual sensitivity measurements on the same image plane based on the newly developed optical configuration [96].

Figure 5.1 illustrates the schematic diagram of the synchronized dual-space resolution shearography system. In the diagram, L represents an ideal convex lens. The system utilizes a coherent laser with a wavelength of 532nm as the light source, which is expanded by a beam expander before illuminating the object. The 50:50 beam splitter (BS) divides the reflected waves into two beams, marked in blue. The tilted mirrors, M2 and M3, at 45 degrees direct these two beams to the polarization beam splitter (PBS). The PBS further converts these two non-polarized waves into two polarized waves with a 90-degree phase difference. The interface of the PBS is coated with a medium that reflects the s-polarized light, represented in red, and transmits the p-polarized light, represented in green.

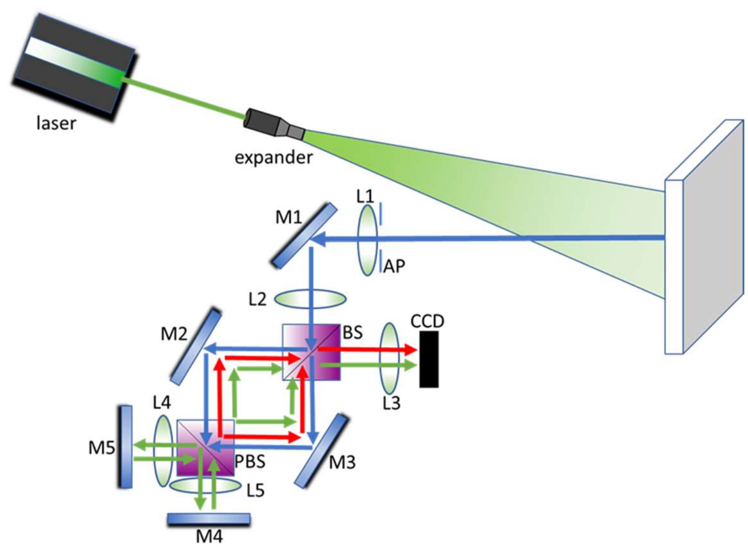

Figure 5.1 Schematic of the simultaneous dual spatial resolution shearography system.

The S-light (red) forms channel #Red, which contains information about the large field of view, while the P-light (green) forms channel #Green, which represents the small field of view or high-sensitivity view. By separately rotating the PBS and M4, shear can be introduced into channels #Red and #Green.

The green channel and the red channel respectively constitute the digital shearography system for two different sizes of the field of view.

However, the spectrum easily overlaps because all of the spectrums are located in the x-direction, which is shown in Figure 5.2. In the image, D and E represent small field of view, B and C represent large field of view. D and B, C and E mix together. The phase information cannot be extracted clearly.

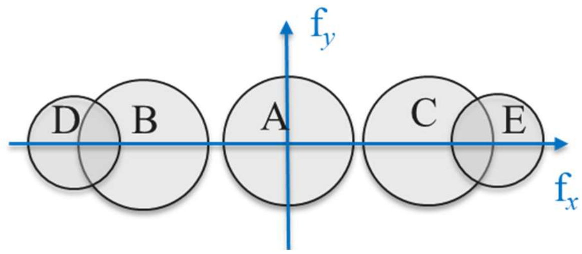

Figure 5.2 Schematic of overlapped spectrum

In this dissertation, a developed method to separate the spectrum is proposed, resulting in two fields of view that lie in the x- and y-direction respectively. It not only separates the spectrum, but also performs simultaneous dual shearing direction measurements. The theory, schematic, equation derivation, and experiment results are presented in the following section.

5.2 Theory and principle

The typical shearography setup, shown in Figure 5.3, is used in this section as an example to show the fundamentals of the frequency carrier spatial phase-shift technique [96]. A modified Michelson interferometer is used as the shearing device in the setup [97,98]. At both sides of the Michelson interferometer, two lenses (L1 and L2) with the same focus length are placed, which are used to enlarge the field of view [16]. The laser is a helium–neon laser with a wavelength of 632.8 nm. A beam expander

(BE) is used to expand the laser to illuminate the testing object. The diffused light reflected from the object then goes through the shearing device and forms the image on the CCD plane. M1 and M2 are two mirrors. When one mirror of them (M2) is tilted a small angle, the shearogram can be obtained and recorded by the CCD camera. [Xie et al, 2013] A spatial frequency shift is introduced by the shearing that results from tilting M2. Using an FT, the speckle pattern image is transferred into a spectrum on the Fourier domain which contain the phase information of the recorded shearogram.

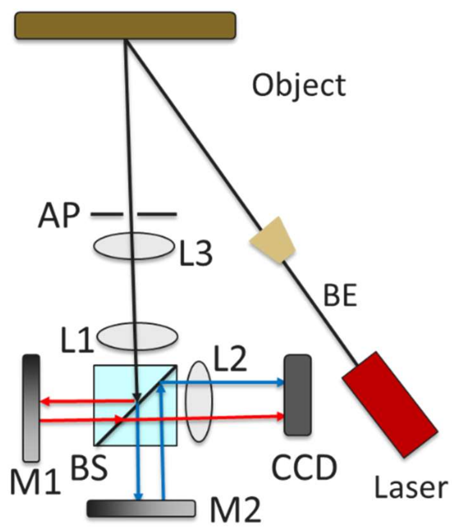

Figure 5.3. Schematic of shearography setup

The phase value can then be obtained by using an inverse FT (IFT). By analyzing the phase difference between before and after loading, the deformation gradient of the testing object due to the loading can be evaluated. The CCD camera captures two shared wave fronts from M1 and M2. These two wave fronts can be represented by Equations 5.1 and 5.2:

$$u_1 = |u_1(x,y)|\, exp[i\phi(x,y)]$$

5.1

$$u_2 = |u_2(x+\Delta x, y+\Delta y)|\, exp\{\, i[\phi(x+\Delta x, y+\Delta y) + 2\pi(f_{\alpha_x}x + f_{\alpha_y}y)]\}$$

5.2

where u_1 and u_2 are the two wave fronts reflected by the reference mirror M1 and M2, tilted mirror, respectively. Δx and Δy are the shearing distances in the x- and y-direction, respectively, while f_α, which represents the component of the spatial frequency introduced by shearing angle α, can be expressed as Equations 5.3 and 5.4:

$$f_{\alpha_x} = \frac{sin\alpha_x}{\lambda}$$

5.3

$$f_{\alpha_y} = \frac{sin\alpha_y}{\lambda}$$

5.4

where x and y are the x-direction and y-direction respectively.

The intensity can be expressed as Equation 5.5:

$$I = (u_1 + u_2)(u_1{}^* + u_2{}^*) = u_1u_1{}^* + u_2u_2{}^* + u_1u_2{}^* + u_2u_1{}^*$$

5.5

The * denotes the complex conjugate of u_i, i= 1 or 2. The Fourier Transform converts the image from the spatial domain to the Fourier domain. Application of the Fourier Transform to Equation 5.5 transforms the equation into the following form:

$$FT(I) = U_0(f_x, f_y) \otimes U_0(f_x, f_y)^* + U_r[(f_x + f_{\alpha_x}), (f_y + f_{\alpha_y})] \otimes U_r[(f_x + f_{\alpha_x}), (f_y + f_{\alpha_y})]^* + U_0(f_x, f_y) \otimes U_r[(f_x + f_{\alpha_x}), (f_y + f_{\alpha_y})]^* + U_r[(f_x + f_{\alpha_x}), (f_y + f_{\alpha_y})] \otimes U_0(f_x, f_y)^*$$

5.6

Here $\otimes$ is the convolution operation.

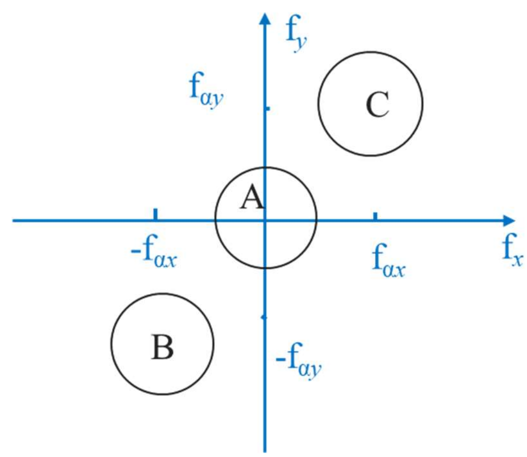

Figure 5.4. Schematic of spectrum of speckle pattern

Figure 5.4 shows the Fourier spectrum of the speckle pattern. There are three spectra on the Fourier domain, which correspond to the four terms in Eq. (6) due to different spatial frequencies. In part A, the $U_1 \otimes U_1^* + U_2 \otimes U_2^*$ terms located at the center of the frequency domain are low frequency terms mainly from the background light. Part B, where $U_1 \otimes U_2^*$ is located at $\left(-f_{\alpha_x}, -f_{\alpha_y}\right)$ and part C, where $U_2 \otimes U_1^*$ is located at $\left(f_{\alpha_x}, f_{\alpha_y}\right)$ contain the phase information of the shearogram. The part B moves due to $\left(-f_{\alpha_x}, -f_{\alpha_y}\right)$, the part C moves due to $\left(f_{\alpha_x}, f_{\alpha_y}\right)$.

$$A = U_1(f_x, f_y) \otimes U_1(f_x, f_y)^* + U_2[(f_x + f_{\alpha_x}), (f_y + f_{\alpha_y})] \otimes U_2[(f_x + f_{\alpha_x}), (f_y + f_{\alpha_y})]^*$$

5.7

$$B = U_1(f_x, f_y) \otimes U_2[(f_x + f_{\alpha_x}), (f_y + f_{\alpha_y})]^*$$

5.8

$$C = U_2[(f_x + f_{\alpha_x}), (f_y + f_{\alpha_y})] \otimes U_1(f_x, f_y)^*$$

5.9

Figure 5.5 shows that the phase distributions can be calculated by using an IFT on circled area B or C. This result is shown in the following equation:

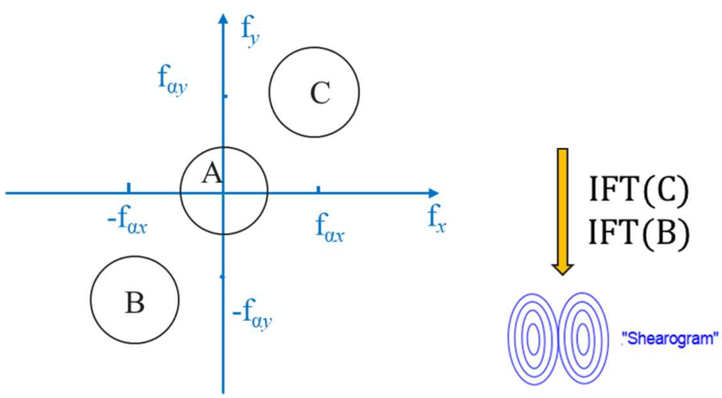

Figure 5.5. Sketch of IFT

$$\theta + 2\pi\left(f_{\alpha_x}x + f_{\alpha_y}y\right) = tan^{-1}\frac{Im[u_1u_2^*]}{Re[u_1u_2^*]}$$

5.10

$$\theta = \phi(x + \Delta x, y + \Delta y) - \phi(x, y)$$

5.11

Here, *Im* and *Re* denote the imaginary and real part of the complex numbers respectively, and θ is the phase difference between the two tilted beams reflected from M1 and M2.

With the same method, another phase distribution can be obtained after the object is loaded using the recorded images:

$$\theta' + 2\pi\left(f_{\alpha_x}x + f_{\alpha_y}y\right) = tan^{-1}\frac{Im[u_1u_2^*]}{Re[u_1u_2^*]}$$

5.12

The relative phase difference due to a deformation can then be calculated as:

$$\Delta\theta = \theta - \theta'$$

5.13

5.3 Experiment

5.3.1 Experiment setup

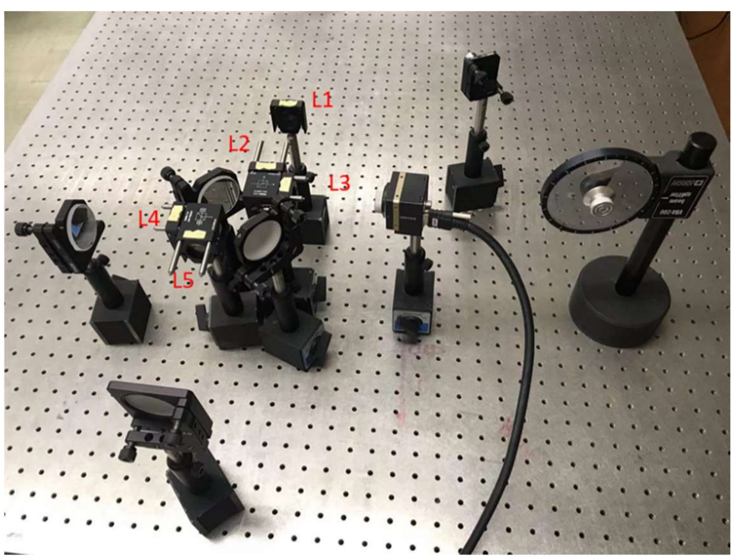

Figure 5.6. The real setup of the dual sensitivity shearography

Figure 5.6 shows a real dual resolution shearography system. The CCD camera this system used is 2453 x 2056-pixel grayscale, the pixel size is 3.45 µm in the horizontal direction and 3.45 µm in the vertical direction. The laser is a Verdi. The imaging lens, L1, was 35 mm focal length (f = 35 mm). The focal lengths of L2 and L3 were 100mm (f =100 mm) while the focal lengths of L4 and L5 were 150mm (f=150mm). The normal beam splitter and polarized beam splitter both are 50:50 split ratios.

<u>5.3.2 Spectrum adjustment</u>

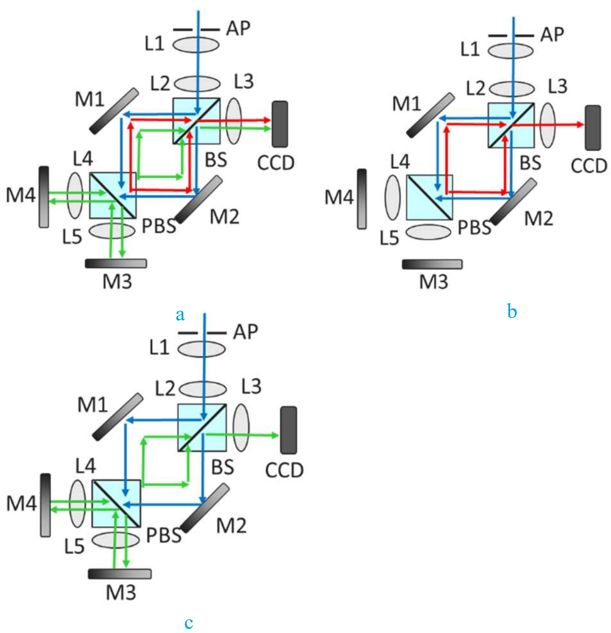

Figure 5.7. Sketch of the optical path of the setup [Zhang et al, 2022]

As discussed in literature [99], Figure 5a shows the schematic of the optical path of the dual sensitivity system. Figure 5b shows the channel of the large field of view represented by a red line and Figure 5c shows the channel of the small field of view represented by a green line. The large field of view channel is a typical Sagnac interferometer based digital shearography setup. L1 is the image lens of the system, while L2 and L3 are used to extend the image distance. The small field of view channel is a modified Michelson Interferometer. The first arm goes from BS to M2 to L5 to M4, while the second arm goes from BS to M1 to L4 to M4 [Zhang et al, 2022]. As shown in Figure 5.2, the spectrum of the large and small fields of view tended to overlap during the experiment. Here, B and C represent the spectrum of the large field of view, while D and E represent the spectrum of the small field of view.

A method is proposed to solve this issue. The spectrum will be clearly separated if the small vision spectrum is made to distribute in the x-direction while the large vision spectrum is made to distribute in the y-direction. At the same time, the setup can not only test fields of view of two different sizes, but also two shear directions, which allows for the detection of defects that lie on two different directions simultaneously. The spectrum of the simultaneous dual sensitivity shearography system is shown in Figure 5.8 a. For the spectrum map, B and C, which represent large fields of view, should be located in the y-direction as shown in Figure 5.8 b, while D and E, which represent small fields of view, should be located in the x-direction as shown in Figure 5.8 c.

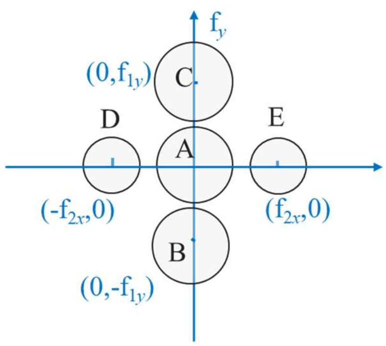

a

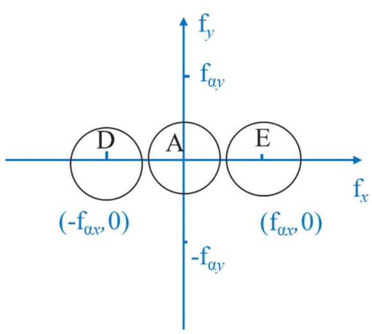

b

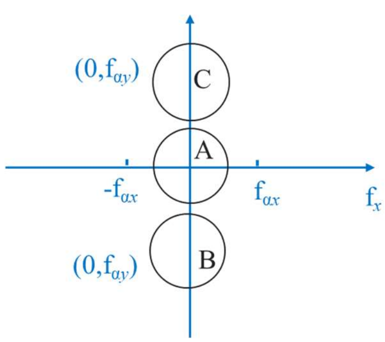

c

Figure 5.8 Sketch of the spectrum distribution

According to the principle introduced in the Theory section of this paper and Figure 2, part B moves due to $\left(-f_{\alpha_x}, -f_{\alpha_y}\right)$, while part C moves due to $\left(f_{\alpha_x}, f_{\alpha_y}\right)$. For the large field of view channel, represented in Figure 5b by the red line, the two sheared lights can be described using Equations 5.14 and 5.15:

$$u_{r1}(x,y) = |u_r(x,y)|\, exp[i\phi_r(x,y)] \tag{5.14}$$

$$u_{r2} = |u_r(x+\Delta x, y+\Delta y)|\, exp\{\, i[\phi_r(x+\Delta x, y+\Delta y) + 2\pi(f_{1_x}x + f_{1_y}y)]\} \tag{5.15}$$

We want to put the spectrums on y-direction so let $f_{1_x} = 0$ and $\Delta x = 0$, and results in Equations (16):

$$u_{r2} = |u_r(x, y+\Delta y)|\, exp\{\, i[\phi_r(x, y+\Delta y) + 2\pi f_{1_y} y]\} \tag{5.16}$$

The intensity of the red channel can be described as Equation 5.17

$$I_r = (u_{r1} + u_{r2})({u_{r1}}^* + {u_{r2}}^*) = u_{r1}{u_{r1}}^* + u_{r2}{u_{r2}}^* + u_{r1}{u_{r2}}^* + u_{r2}{u_{r1}}^* \tag{5.17}$$

Due to the above, we can shear M2 only along the y-direction. The sketch of the spectrum is shown in Figure 7c.

Similarly, for the small field of view channel, represented in Figure 5c by the green line, the two sheared lights can be described using Equations 5.18 and 5.19:

$$u_{g1}(x,y) = \left|u_g(x,y)\right| exp\left[i\phi_g(x,y)\right]$$

5.18

$$u_{g2} = |u_g(x+\Delta x, y+\Delta y)|\, exp\{\, i[\phi_g(x+\Delta x, y+\Delta y) + 2\pi(f_{2_x}x + f_{2_y}y)]\}$$

5.19

The spectrums are placed in the x-direction by setting $f_{2_x} = 0$ and $\Delta y = 0$, resulting in Equations 5.20 and 5.21:

$$u_{g2} = |u_g(x+\Delta x, y)|\, exp\{\, i[\phi_r(x+\Delta x, y) + 2\pi f_{2_x}x]\}$$

5.20

The intensity of the green channel can be described as Equation 5.21

$$I_g = \left(u_{g1} + u_{g2}\right)\left(u_{g1}{}^* + u_{g2}{}^*\right) = u_{g1}u_{g1}{}^* + u_{g2}u_{g2}{}^* + u_{g1}u_{g2}{}^* + u_{g2}u_{g1}{}^*$$

5.21

Due to the above, we can shear M4 only along the x-direction. The sketch of the spectrum is shown in Figure 7b.

The intensity of the whole system can be described as Equation 5.22

$$I = I_r + I_g$$

5.22

Applying FT to the image recorded by the whole simultaneous dual sensitivity system results in the following:

$$FT(I) = U_{r1}(f_x, f_y) \otimes U_{r1}(f_x, f_y)^* + U_{r2}(f_x, f_y + f_{1_y}) \otimes U_{r2}(f_x, f_y + f_{1_y})^*$$
$$+ U_{g1}(f_x, f_y) \otimes U_{g1}(f_x, f_y)^* + U_{g2}(f_x + f_{2_x}, f_y) \otimes U_{g2}(f_x + f_{2_x}, f_y)^*$$
$$+ U_{r1}(f_x, f_y) \otimes U_{r2}(f_x, f_y + f_{1_y})^* + U_{r2}(f_x, f_y + f_{1_y}) \otimes U_{r1}(f_x, f_y)^*$$
$$+ U_{g1}(f_x, f_y) \otimes U_{g2}(f_x + f_{2_x}, f_y)^* + U_{g2}(f_x + f_{2_x}, f_y) \otimes U_{g1}(f_x, f_y)^*$$

5.23

Equation (23) can be grouped into parts A, B, C, D, and E as follows:

$$A = U_{r1}(f_x, f_y) \otimes U_{r1}(f_x, f_y)^* + U_{r2}(f_x, f_y + f_{1_y}) \otimes U_{r2}(f_x, f_y + f_{1_y})^* + U_{g1}(f_x, f_y)$$
$$\otimes U_{g1}(f_x, f_y)^* + U_{g2}(f_x + f_{2_x}, f_y) \otimes U_{g2}(f_x + f_{2_x}, f_y)^*$$

5.24

$$B = U_{r1}(f_x, f_y) \otimes U_{r2}(f_x, f_y + f_{1_y})^*$$

5.25

$$C = U_{r2}(f_x, f_y + f_{1_y}) \otimes U_{r1}(f_x, f_y)^*$$

5.26

$$D = U_{g1}(f_x, f_y) \otimes U_{g2}(f_x + f_{2_x}, f_y)^*$$

5.27

$$E = U_{g2}(f_x + f_{2_x}, f_y) \otimes U_{g1}(f_x, f_y)^*$$

5.28

Part A represents the background information, and the remaining components represent the complex amplitudes of the interferogram. B and C represents the large field of view information, and D and E represents the small field of view information. Thus, the phase distribution in the Fourier domain can be achieved, as shown in Figure 7a.

5.3.3 Results and discussion

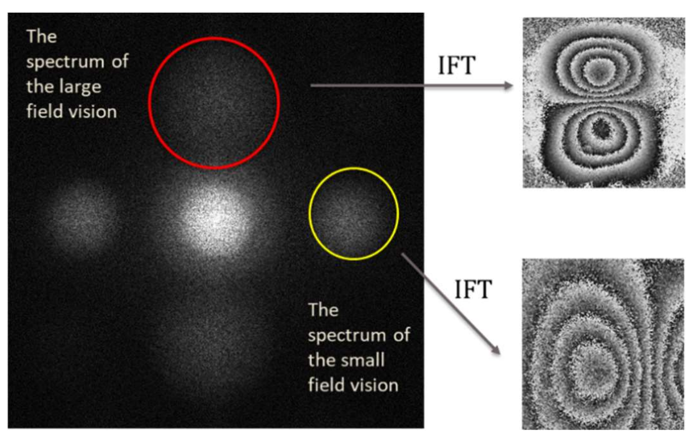

Figure 5.9 Spectrum map and two resolution shearograms

A defect-free square aluminum plate with a size of 100x100 mm was used to verify the feasibility of the method. The plate was clamped all around and loaded at the center by a screw micrometer, and images were recorded before and after loading. Applying FT, a spectrum distribution can be obtained as shown in Figure 5.9 a. Using IFT, two shearograms of two resolutions can be obtained as shown in Figures 5.9 b and 5.9 c

To verify the functionality of the method proposed in this paper, an NDT application was performed on a round aluminum plate with a small sized defect. Shown in Figure 5.10, the plate was 10 mm thick and mounted on a sealed chamberwhich was connected to a vacuum. The defect has a diameter of 8mm, and the thickness to the surface is 0.6 mm. A 10KPa pressure difference was used to detect the defect, the result of which is shown in Figure 5.11. From the image, we can find that the small size defects may be ignored using the large field of view, but the small size defects can be found using the small field of view. The accuracy of the test is increased as a result.

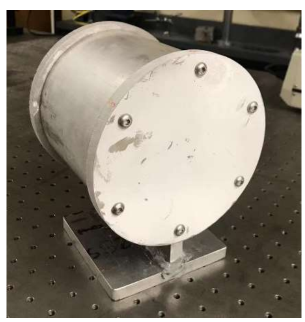

Figure 5.10. The plate with defect on a sealed chamber

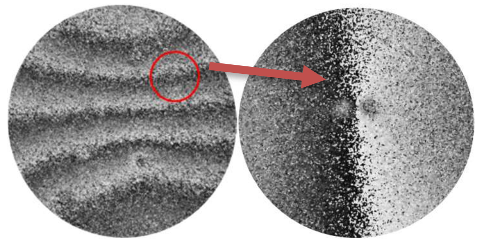

Figure 5.11. The shearograms of large field vision and small field vision

Simultaneous dual sensitivity measurements using sherography can obtain acceptable results using the new method to separate the spectrum distribution in the frequency domain. However, the setup is very complicated and requires the use of many pieces of optical equipment, resulting in an energy decrease that can affect the image quality. Future research will focus on developing the advanced setup and method further to simplify the measurement system and reduce the energy loss.

5.4 Chapter summary

This paper proposes adjusting the spectrum distribution in different directions to separate the spectrums and phase information on the spectrogram. Depending on the frequency carrier spatial technology, the setup can be adjusted to cause the large vision and c small vision spectrums to be located in two different directions, one in the horizontal direction and the other in the vertical direction. Therefore, the phase information of each interferogram can be excavated by windowing the corresponding spectrum and taking the IFT. Meanwhile, the method can enable the system to detect defects in the x- and y-direction. As shown by the experimental results, this method can increase the accuracy and efficiency of the simultaneous dual sensitivity shearography system. The experiments result show that this method can assist to develop the simultaneous dual sensitive shearograpy system.

CHAPTER SIX

DEVELOPMENT OF SIMULTANEOUS DUAL-RESOLUTION DIGITALHOLOGRAPHY SYSTEM

6.1 Digital holography for simultaneous dual sensitivity measurement

This section is focused on the development of a digital holography system for simultaneous dual-resolution measurements. Digital holography has been widely used for deformation measurements and non-destructive testing (NDT) due to its advantages of high sensitivity, high accuracy, and whole-field, non-touch measurements. This dissertation presents research on a novel digital holography system that achieves dual spatial resolution measurements simultaneously by testing different-sized fields of view with a single camera. The novel system has two optical channels with two optical layouts of holography to measure deformation. By changing the combined focus length, the two holographic setups have different fields of view, i.e., one has a large and the other has a small field of view. To realize a simultaneous test, the polarization technique is used to avoid cross-interference between the two optical layouts. Finally, spatial carrier fringes with different orientations are introduced into the two holographic setups by appropriately adjusting the reference beam of each setup. The different oriented spatial carrier fringes enable the spectrums of the two interferograms to be separated after a FT (Fourier transform) and the phase distributions of the two interferograms can be extracted and separated by windowing the spectrum to perform an IFT (inverse Fourier transform). The phase distributions can then be used to analyze and calculate the deformations. The experiment using this system is described in this paper and the practicability of this method is verified by the obtained experimental results.

6.2 Introduction

The digital holography interferometry technique is a non-contact, full-field, and highly sensitive optical measurement method. It is widely used in a variety of industrial areas, including the automotive and aerospace industries, for deformation/strain measurements and non-destructive testing (NDT) [100–105]. For this technique, one laser beam is split into two beams. One, called the object beam, illuminates the object's surface, while the other, called a reference beam, goes to a reference object, such as a mirror. These two beams meet at the CCD and interfere with each other on the CCD plane to produce an interferogram. The intensities of the interferograms can be recorded by a digital camera before and after loading. A visible fringe pattern, also called a hologram, that includes the object deformation information can be obtained to subtract the different intensity information and obtain deformation due to the applied load [106–109].

Currently, most optical inspection systems use a single camera with a fixed field of view to record images, resulting in only one resolution being obtained per measurement. However, some small defects may also be found without increasing the spatial resolution by improving the stability and the contrast of phase maps and avoiding air disturbances and environmental vibrations by a real-time phase processing method with high-frequency synchronizing trigger technology [110]. A high-spatial-resolution setup in combination with this technology would be even better for measuring smaller defects. Usually, one-resolution systems suffer from some disadvantages: (1) when measuring the deformation of an object with a strain concentration in some locations, the fringe pattern may be too dense to be resolved by the measurement system, which can cause the measurement to fail; (2) when conducting non-destructive testing, small-sized inner defects may be ignored due to a low spatial resolution. Measurements using different spatial resolutions would be necessary to solve these issues. Usually, separate multiple tests are used to observe different-sized fields of view. However, this will not only increase the labor costs and testing time, but also complicate the measurement operation. Furthermore, multiple measurements may not be achievable in some cases. Therefore, if a measurement is not repeatable, a simultaneous du-al-resolution measurement system with different fields of view is helpful. To reach this goal, two optical channels with large and small fields of view are required to achieve a simultaneous dual spatial resolution measurement using one experimental setup.

Research on simultaneous measurement with two-channel systems has been re-ported, but almost all of the existing methods use the same spatial resolution, i.e., the same field of view, to measure two targets. Examples of these are listed as follows: (1) Two-channel systems with the same spatial resolution which measure the first derivative in the x- and y- directions. In these systems, the two channels correspond to two shearographic systems, one in the x-shearing direction to measure the first derivative of deformation in the x-direction and one in the y-shearing direction to measure the first derivative of deformation in the y-direction. Three methods have been reported to separate the information from these two channels in the final results. The first one is to use a two-camera system to record the information of the two channels separately [111]. The second method is to observe different channels on one color camera using RGB channels in combination with different laser wavelengths [112]. The last method is to use one black/white camera based on the polarization technology to avoid cross-interference [113,114]. These types of two-channel digital shearographic systems can be useful for NDT because some defects are sensitive to different directions of the first derivative of deformation. (2) The second example is a two-channel system with the same spatial resolution that simultaneously measures the deformation and its first derivative. For these systems, one channel is related to a holographic/electronic speckle pattern interferometry (ESPI) system and the other is related to a shearographic sys-tem [115–117]. Such kinds of systems are used if both the deformation and its derivative are needed at the same time. (3) Our last example is two-channel systems with the same spatial resolution that simultaneously measure both out-of-plane and in-plane strains. In these systems, one channel is used for an out-of-plane shearographic system and the other for an in-plane shearographic system [118,119]. They are usually utilized for 3D strain measurements.

Another application of two-channel systems is to test only one measurement target, but with different spatial resolutions. A Sagnac interferometer-based digital shearography system has been reported by Boyang Zhang et al. [120]. They used a Sagnac interferometer-based optical layout to enable a dual spatial resolution shearography system to measure the first derivative of deformation. It was the first recorded report of a system that allows two shearograms, one for a large field of view and one for a small field of view, to be obtained simultaneously. The development of this technology advanced digital shearography for NDT. However, a deficiency of the developed technology is the phenomenon of spectrum aliasing because the two shearograms have the same shearing direction, e.g., in the x- shearing direction, and all the spectra lie on the x-axis. In shearography, the orientation and separation of the spectrum are determined by the shearing direction and shearing amounts, respectively. Avoiding the spectrum aliasing of the two shearograms requires careful selection and adjustment of the shearing amount of the two channels, which complicates the measurement. Xiaowan Zheng reported an improved method to place one spectrum on the x-axis and the other on the y-axis to avoid the overlap [121]. However, this system is a two-target measurement, i.e., one channel measures the x-direction derivative and the other channel measures the y-direction derivative. In this dissertation, we will present a novel dual-spatial-resolution holographic system to measure deformation, which has a relatively simple optical setup and can easily separate the spectra from two channels. By changing the combined focus length, the two holographic setups can observe different fields of view, i.e., one has a large and the other has a small field of view. To realize a simultaneous measurement, the polarization technique is used to avoid cross-interference between the two optical layouts [122]. Finally, based on the spatial carrier frequency technique [123], the reference beam is adjusted to introduce a different carrier frequency to obtain the spatial carrier fringes with different orientations in one speckle pattern image captured from the two holographic setups. The different oriented spatial carrier fringes enable the spectra of the two interferograms to be easily separated after a FT (Fourier transform), thus overcoming the main deficiency of spectrum aliasing reported in the dual-spatial-resolution shearographic system. The phase distributions of the two interferograms can be extracted and separated by windowing the spectrum to perform an IFT (inverse Fourier transform). The phase distributions can then be used to analyze and calculate the deformations. Different applications will be presented, and the practicability of this method is verified by the obtained experimental results.

6.3. Principle and Method

Our objective to develop a dual-resolution system is to obtain full and local measurement results simultaneously. To achieve these dual sensitive resolution, two different size fields of view are needed. Full field can be observed under the large field of view, local can be detected under the small field of view.

Figure 6.1 shows an optical setup to achieve simultaneous dual-resolution sensitivity measurements. The setup consists of a holography system using the multiple-carrier-frequency spatial-phase-shift method combined with the polarization technique. The laser beam is split by beam splitter 1 (BS1) into two beams, an object beam and a reference beam. The object beam goes to the object's surface, then is expanded through a beam expander (BE). Here, L1 to L4 are lenses with different focus lengths. Lens 1 (L1) is the image lens. Lens 2 (L2) and Lens 3 (L3) have the same focal length and are used to enlarge the field of view [124-126]. Lens 4 (L4) can enlarge the image to obtain a small field of view. The aperture (AP), placed just before the image lens (L1), is used to control the speckle size and spectrum pattern size on the Fourier domain. Beam splitter 2 (BS2) and beam splitter 3 (BS3) are beam splitters with a 50:50 ratio. Polarized beam splitter 1 (PBS 1) is a polarized beam splitter which can generate two non-coherent polarized object beams. Polarized beam splitter 2 (PBS2) is used to obtain two non-coherent polarized reference beams. The quarter-wave plate (QWP) can convert linearly polarized light to circular polarized light. A single-mode optical coupler (SOC) 50:50 splitter is used to split the reference beam into two beams that are both circular lights.

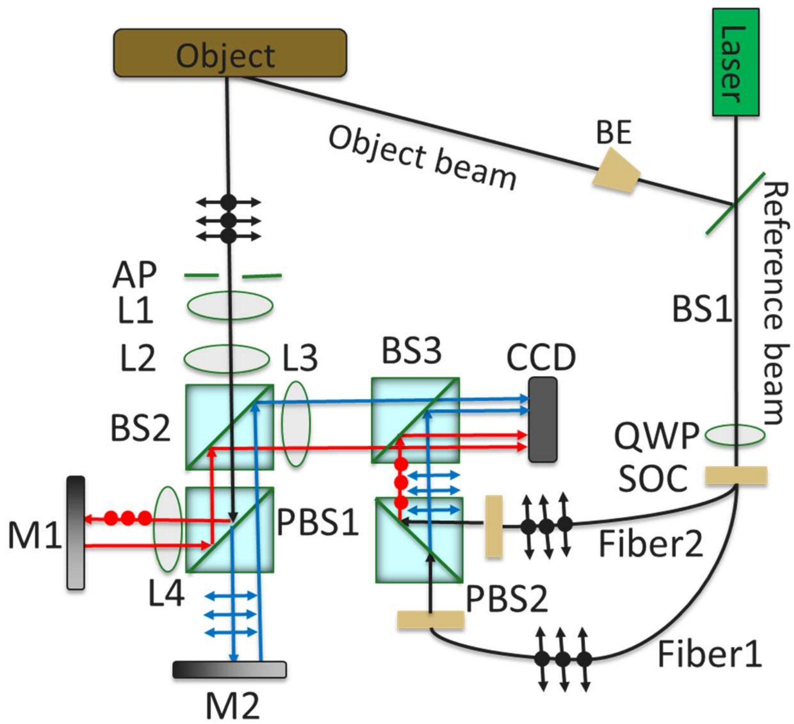

Figure 6.1. Sketch of simultaneous dual-resolution measurement system.

A frequency-doubled Nd: YAG laser (532 nm green) is used in the system. The laser is separated into an object beam and reference beam by using beam splitter 1 (BS1). The object beam is expanded by a beam expander (BE), and illuminates the object. The diffused object's light is reflected from the object, which is a circular light represented by a black line, then goes through the aperture (AP), image lens (L1), and lens L2 before arriving at the PBS. Here, the object beam is divided into two non-coherent polarized beams represented in red and blue, respectively. The red beam, or S-polarized light, is reflected by the PBS and goes through L4. It is then reflected by Mirror 1 (M1) before going into PBS1 again. After being reflected by PBS1 and BS2, the light goes through L3 and BS3 and is received by the CCD camera. The blue beam, or P-polarized light, goes through PBS1, then is reflected by mirror 2 (M2) before going into PBS1 again. The light is reflected by BS2, then goes through L3 and BS3 before arriving at the CCD camera.

The reference beam goes through a quarter-wave plate (QWP) and is converted into circular lights. It then goes into a single-mode optical coupler splitter fiber (OCS), in which the reference light is split into two identical circular lights represented by black lines. These two beams propagate through two optical fibers, then arrive at polarized beam splitter 2 (PBS2). Here, these two circular lights are converted to two non-coherent polarized lights which are represented by red and blue lines. These two polarized reference beams are independent. Different carrier frequencies can be introduced by adjusting the reference beams separately. The red line, or S-polarized light, is reflected by PBS2 and goes into BS3, where it is reflected before being received by the CCD camera. The blue line, representing P-polarized light, goes through PBS2 and is reflected by BS3 before arriving at the CCD camera. Here, the blue, P-polarized object and reference beams interfere with one another, and the red, S-polarized object and reference beams interfere with one another.

Through the design described above, the first two main goals of this research paper are been realized: (1) Two in-coherent holographic setups without cross-interference have been built in a multiplexed measurement setup, with each setup being independent and consisting of an object beam and reference beam which are split into two pairs of polarized beams; (2) the two optical channels have different fields of view, large and small. The red-S-polarized light goes through one more lens (L4) than the blue-P-polarized light, and the fields of view between the two channels can be adjusted by the focus length of L4. Next, we will discuss how to separate the measuring results from a single image recorded by one camera.

The carrier frequency used to obtain the frequency shift on the Fourier domain can be introduced by adjusting the two reference beams to change the incident angle from the normal of the CCD plane. The hologram of the large field of view is generated by interference between the blue polarized object beam and reference beam, which both represent P-polarized light. The hologram of the small field view is also obtained through interference between the red polarized object beam and the red reference beam, both S-polarized light. The holograms of the large and small fields of view are simultaneously recorded by the CCD camera in the form of an intensity difference.

These two reference beams and two object beams' wave fronts can be represented by Equations 6.1 to 6.4:

$$u_{r1} = |u_{r1}(x,y)|\, exp\{\, i[2\pi(f_{1_x}x + f_{1_y}y)]\} \tag{6.1}$$

$$u_{r2} = |u_{r2}(x,y)|\, exp\{\, i[2\pi(f_{2_x}x + f_{2_y}y)]\} \tag{6.2}$$

$$u_{o1} = |u_{o1}(x,y)|\, exp[i\phi_1(x,y)] \tag{6.3}$$

$$u_{o2} = |u_{o2}(x,y)|\, exp[i\phi_2(x,y)] \tag{6.4}$$

where u_{r1} is the wave front of the red polarized reference beam, u_{r2} is the wave front of the blue polarized reference beam, u_{o1} is the wave front of the red polarized object beam, and u_{o2} is the wave front of the blue polarized object beam. The values f_{1x}, f_{1y}, f_{2_x}, and f_{2_y} represent the components of the spatial frequency. f_{1_x} and f_{1_y} are introduced by angle α_2 between the red polarized reference beam and the normal of the CCD plane, while f_{2_x} and f_{2_y} are introduced by angle β_2 between the blue polarized reference beam and the normal of the CCD plane. These components can be expressed as Equations 6.5 to 6.8, where λ is the laser wavelength

$$f_{1_x} = \frac{sin\alpha_{2x}}{\lambda}$$

6.5

$$f_{1_y} = \frac{sin\alpha_{2y}}{\lambda}$$

6.6

$$f_{2_x} = \frac{sin\beta_{2x}}{\lambda}$$

6.7

$$f_{2_y} = \frac{sin\beta_{2y}}{\lambda}$$

6.8

The intensity image of both large and small fields of view can be recorded on the CCD camera simultaneously. u_{r1} and u_{r2}, as well as u_{o1} and u_{o2}, are non-coherent polarized lights. u_{r1} and u_{o1} are both S-polarized lights, represented by red lines, that interfere together to obtain the hologram for the small field of view, while u_{r2} and u_{o2} are P-polarized lights, represented by blue lines, that result in the hologram of the large field of view when they interfere with each other. The intensity recorded can be expressed as follows:

$$I_S = (u_{r1} + u_{o1})(u_{r1}{}^* + u_{o1}{}^*) = u_{r1}u_{r1}{}^* + u_{o1}u_{o1}{}^* + u_{r1}u_{o1}{}^* + u_{o1}u_{r1}{}^* \tag{6.9}$$

$$I_L = (u_{r2} + u_{o2})(u_{r2}{}^* + u_{o2}{}^*) = u_{r2}u_{r2}{}^* + u_{o2}u_{o2}{}^* + u_{r2}u_{o2}{}^* + u_{o2}u_{r2}{}^* \tag{6.10}$$

$$I = u_{r1}u_{r1}{}^* + u_{r2}u_{r2}{}^* + u_{o1}u_{o1}{}^* + u_{o2}u_{o2}{}^* + u_{r1}u_{o1}{}^* + u_{o1}u_{r1}{}^* + u_{r2}u_{o2}{}^* + u_{o2}u_{r2}{}^* \tag{6.11}$$

The * denotes the complex conjugate of u_{r1}, u_{r2}, u_{o1}, and u_{o2}. I_S and I_L are the intensity of the small field of view and the large field of view, respectively, while I is the total intensity recorded by the CCD camera. The intensity image is converted to the Fourier domain to obtain the phase information by applying a Fourier transform to I. Equation 6.11 is transformed into the following form:

$$\mathrm{FT}(I) = U_{r1} \otimes U_{r1}{}^{*} + U_{r2} \otimes U_{r2}{}^{*} + U_{o1} \otimes U_{o1}{}^{*} + U_{o2} \otimes U_{o2}{}^{*} + U_{r1} \otimes U_{o1}{}^{*} + U_{o1} \otimes U_{r1}{}^{*} + U_{r2} \otimes U_{o2}{}^{*} + U_{o2} \otimes U_{r2}{}^{*} \quad 6.12$$

Here $\otimes$ is the convolution operation, $U_{r1} = \mathrm{FT}(u_{r1})$, $U_{r2} = \mathrm{FT}(u_{r2})$, $U_{o1} = \mathrm{FT}(u_{o1})$, and $U_{o2} = \mathrm{FT}(u_{o2})$.

Here $\otimes$ is the convolution operation, $U_{r1} = \mathrm{FT}(u_{r1})$, $U_{r2} = \mathrm{FT}(u_{r2})$, $U_{o1} = \mathrm{FT}(u_{o1})$, and $U_{o2} = \mathrm{FT}(u_{o2})$.

Figure 3 shows a sketch of the Fourier spectrum of the intensity images. Five spectra are distributed on the Fourier domain, corresponding to the eight terms in Equation 6.12. Sections A contains $U_{r1} \otimes U_{r1}{}^{*} + U_{r2} \otimes U_{r2}{}^{*} + U_{o1} \otimes U_{o1}{}^{*} + U_{o2} \otimes U_{o2}{}^{*}$, which are low-frequency components that represent the background in the spatial domain. Sections B and C represent the $U_{r2} \otimes U_{o2}{}^{*}$ and $U_{o2} \otimes U_{r2}{}^{*}$ parts, respectively, which contain information of the hologram for the large field of view. Sections D and E represent the $U_{r1} \otimes U_{o1}{}^{*}$ and $U_{o1} \otimes U_{r1}{}^{*}$ parts, respectively. These two parts contain information of the hologram for the small field of view.

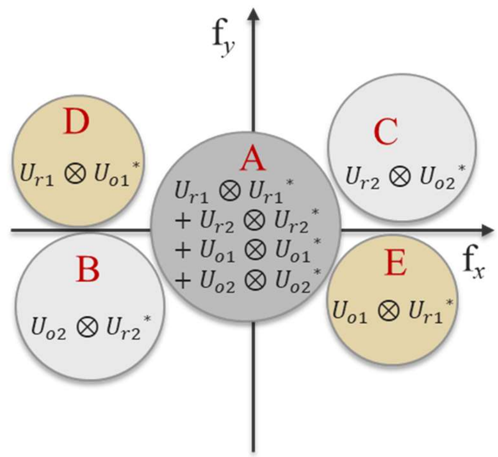

Figure 6.2. Sketch of the Fourier spectrum.

${u_{o1}u_{r1}}^*$ can be obtained by employing an inverse Fourier transform to window the spectrum of $U_{o1} \otimes {U_{r1}}^*$. Similarly, ${u_{o2}u_{r2}}^*$ can be obtained using the same method. These results are shown in the following equations:

$$\phi_1(x,y) - 2\pi\left(f_{1_x}x + f_{1_y}y\right) = tan^{-1}\frac{\mathrm{Im}[u_{o1}u_{r1}^*]}{\mathrm{Re}[u_{o1}u_{r1}^*]}$$

6.13

$$\phi_2(x,y) - 2\pi\left(f_{2_x}x + f_{2_y}y\right) = tan^{-1}\frac{\mathrm{Im}[u_{o2}u_{r2}^*]}{\mathrm{Re}[u_{o2}u_{r2}^*]}$$

6.14

Using the same method, after the object deforms, the distribution of an additional two phases can be obtained, as described in the following equations:

$$\phi_1{}'(x,y) - 2\pi\left(f_{1_x}x + f_{1_y}y\right) = tan^{-1}\frac{\text{Im}[u_{o1}u_{r1}^*]}{\text{Re}[u_{o1}u_{r1}^*]}$$

6.15

$$\phi_2{}'(x,y) - 2\pi\left(f_{2_x}x + f_{2_y}y\right) = tan^{-1}\frac{\text{Im}[u_{o2}u_{r2}^*]}{\text{Re}[u_{o2}u_{r2}^*]}$$

6.16

The relative phase difference in the large and small fields of view due to a deformation resulting from an applied load can then be calculated as follows:

$$\Delta\phi_S = \phi_1{}'(x,y) - \phi_1(x,y)$$

6.17

$$\Delta\phi_L = \phi_2{}'(x,y) - \phi_2(x,y)$$

6.18

Through the operation described above, our last goal, i.e., to separate the phase information from the two holographic setups recorded in a single image by a Fourier transform and inverse Fourier transform, is attained, and the deformations of the large and small fields of view resulting from the applied load can then be calculated by the determined phase distribution. It should be emphasized that the direction of the carrier frequency in the holographic system determines the orientation of the spectrum of the hologram after the Fourier transform. A special advantage of holography is that a direction change in the carrier frequency can easily be implemented by adjusting the incident angle of the reference beams; therefore, the spectrum aliasing reported in the shearographic system can be solved easily in the dual-channel holographic system.

6.4. Experiments and Results

Figure 6.3 shows a simultaneous dual-spatial-resolution digital holography measurement system. This system utilizes a Verdi G5 laser as well as a 2453 × 2056-pixel grayscale CCD camera. The pixel sizes of the CCD camera in the horizontal direction and the vertical directions are both 3.45 μm. L1, L2, L3, and L4 are the lenses. The focal lengths of the imaging lens, L1, is 35 mm (f1 = 35 mm). The focal lengths of L2 and L3, placed on the two sides of the beam splitter, are 100 mm (f2 = f3 = 100 mm), and the focal length of L4 is 150 mm (f4 = 150 mm). The normal beam splitter and polarized beam splitter both have split ratios of 50:50. The single-mode optical coupler splitter is 50:50.

The measurement procedure is as follows: (1) to take an image before the loading, (2) to load the object, and (3) to take an image again after the loading, then, to conduct an evaluation of the measured result by Fourier and inverse Fourier transforms. The time for the measurements is determined by steps 1 to 3. Taking two images requires just dozens of milliseconds and the loading can be conducted within dozens of seconds, therefore, the whole measurement can be performed within one minute.

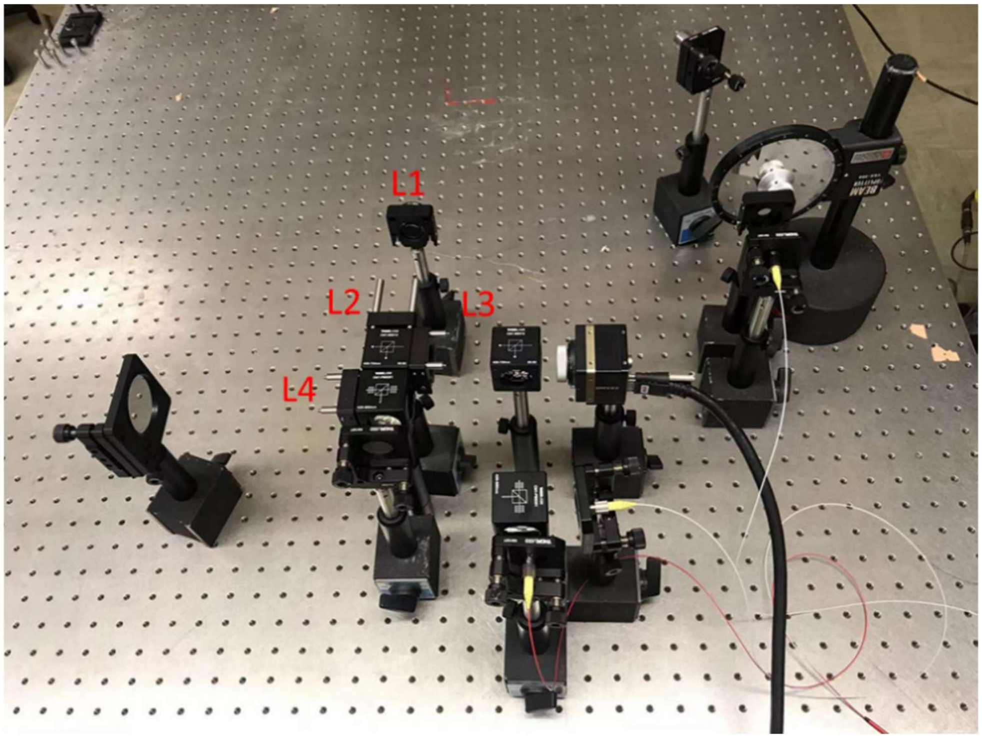

Figure 6.3. Experiment setup.

A 100 × 100 mm square aluminum plate was tested to verify the feasibility of the method. The plate was fixed along its four edges. A screw micrometer was used to apply a load to the center of the plate, and images before and after loading were captured for evaluation. A spectrum distribution was obtained, as shown in Figure 6.4a, by applying a FT. Then two holograms of two resolutions, as shown in Figure 6.4b,6.4c, were obtained by using an IFT to obtain the phase information and subtracting the phase value before and after loading.

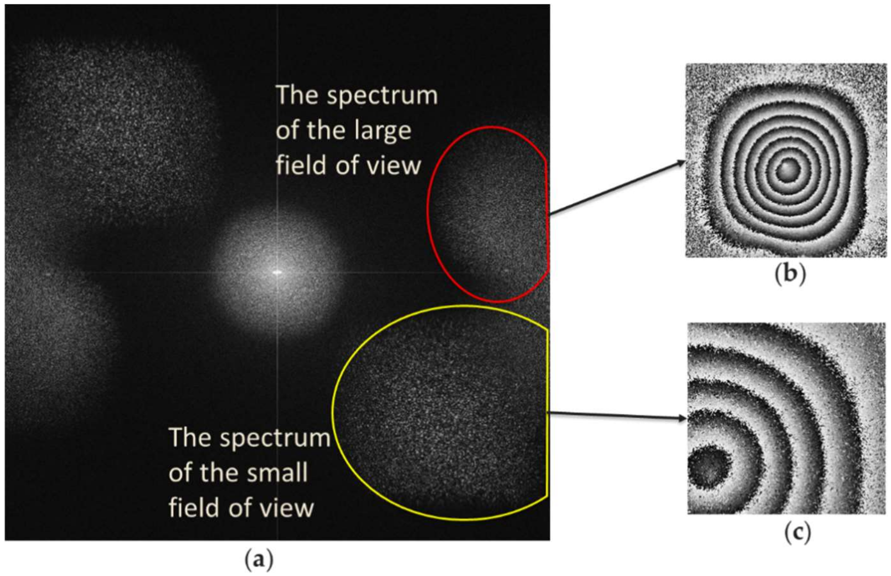

Figure 6.4. Schematic of spectrum of speckle pattern image: (a) is the spectrum, (b) is the hologram of large field of view, and (c) is the hologram of small field of view.

To verify the functionality of the digital holography system presented in this paper, an NDT application was performed on a round aluminum plate with a small-sized defect inside. The round plate had a thickness of 10 mm and was fixed on a 150 mm diameter sealed chamber. The sealed chamber was connected to a vacuum to load the round plate. The defect was a small circle with an 8 mm diameter and 0.6 mm of thickness to the surface. A 10 KPa pressure difference was applied to detect the defect, the result of which is shown in Figure 6. From the image, we can find that the whole area can be observed using the large field of view, but, as shown in Figure 6.5a, the small-sized defect may be ignored. However, the small-sized defects can be found under the small field of view, as shown as Figure 6.5b.

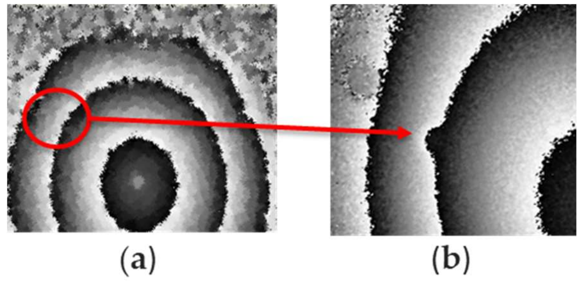

Figure 6.5. Hologram with defect using different field of view sizes. (a) Hologram of large field of view, (b) Hologram of small field of view.

Another deformation test was completed using this system and a defect-free square aluminum plate. The plate was fixed all around with screws, and the plate size was 100 × 100 mm. Figure 7 shows the phase map for the large field of view and small field of view, respectively. A load was applied at the center of the plate by a screw micrometer. Under the large field of view, the phase map, shown in Figure 7a, was very unclear because the large magnitude of the load caused the fringes to be too dense; as a result, it cannot be used to calculate the deformation. However, under the small field of view, the phase map, shown in Figure 7b, was clearer and could be used to calculate the deformation.

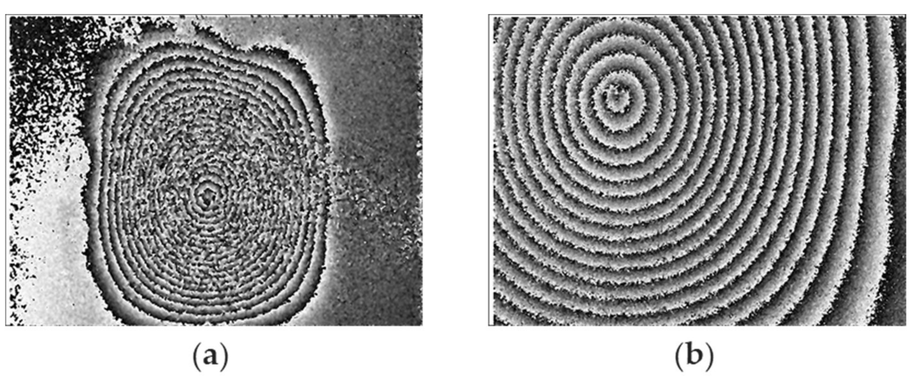

Figure 6.6. Phase map under large and small fields of view. (a) Phase map of large field of view, and (b) Phase map of small field of view.

6.5. Discussion

6.5.1. Adjustment of the System

Figure 6.7 shows the optical layouts of the two holographic setups. Figure 8a shows the setup for the large field of view and the Figure 8b shows the setup for the small field of view. The difference between them is L4, as L4 is introduced to enlarge the image to obtain the small field of view. The size of the small field of view can be changed by adjusting the position and changing the focus length of L4, and while the size of the large field of view can be adjusted by adjusting the position and changing the focus length of L1.

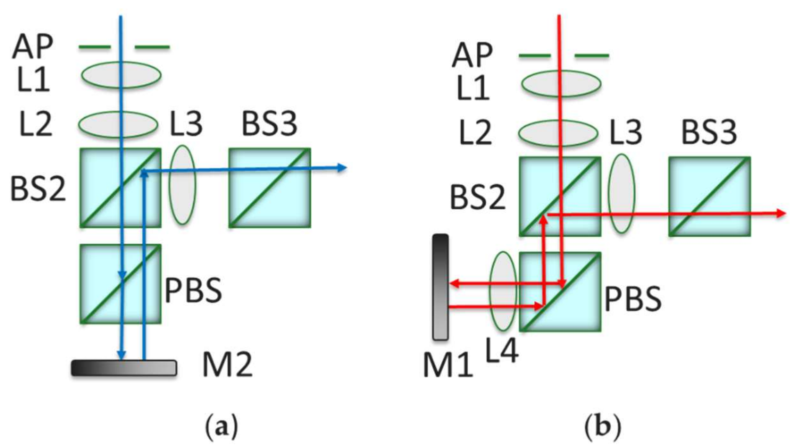

Figure 6.7. Sketch of two optical channels for two fields of view. (a) Optical channel for large field of view, and (b) Optical channel for small field of view.

The image with the large field of view must be adjusted first to make both of the different fields of view form clear images on the image plane. Adjusting the image with the large field of view is relatively easy. Adjusting the image with the small field of view on the same image plane is more challenging. It can be performed by adjusting the position of L4 in combination with that of mirror 1. Thus, it is important that mirror 1 should be able to be moved in the left and right directions.

6.5.2. Separate the Spectrums

After adjusting the two images with different fields of view into clear images on the image plane, it is also very important to adjust the reference beam of the two holographic setups to appropriate incident angles and planes. This is performed by introducing carrier fringes into the holograms. The two spectra transferred from the intensity images of the holograms should be separated to obtain good-quality phase maps. The orientation of the spectrum is determined by the direction of the carrier frequency. The advantage of the holographic system is the ease in changing the directions of carrier frequency; changing the direction is performed by adjusting the plane of the incident angle of the reference beam. The directions of the two carrier fringes should be checked before the Fourier transform is conducted. They should be orientated in different directions with a separation of at least 30 degrees. Figure 6.8 shows an ideal adjustment, in which the separation of the directions of the two carrier fringes is almost 90 degrees, resulting in two perfect mutually perpendicular spectrums. The phase distributions of the two holograms can then be easily separated by the inverse Fourier transform.

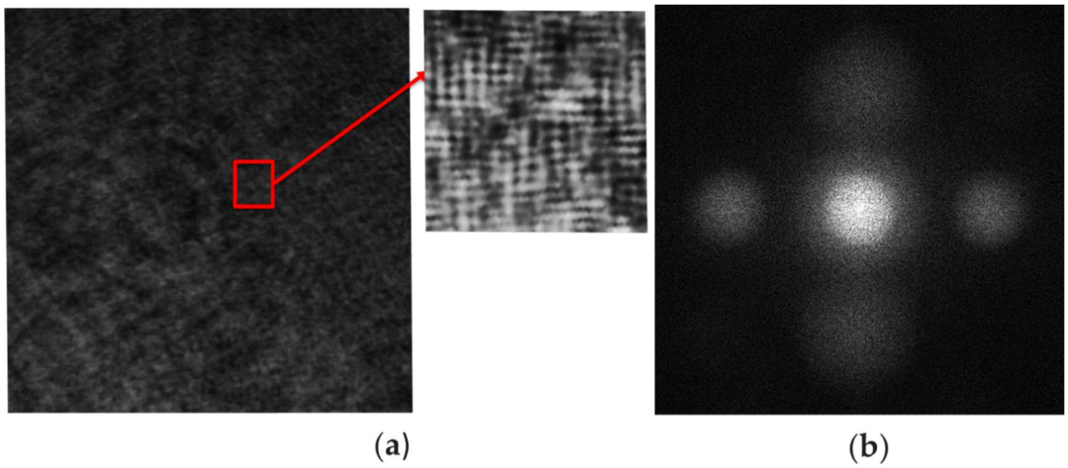

Figure 6.8. (a) Intensity image of an interferogram with carrier fringes, the area of the rectangle is magnified to show the carrier fringe. (b) Distribution of the spectrum.

The size of the aperture of the camera is also important. A big aperture size leads to more light intensity going through the lens, allowing a relatively large object to be tested. This is desired in practical applications. However, a big aperture size results in a small speckle size. According to the sampling theorem, the speckle size should cover at least two pixels theoretically [128] and two to three times more practically, or at least four to six pixels [129]. Therefore, the aperture of the camera cannot be too big. Two adjustments can be performed to ensure a good measuring result with the small aperture: (1) enhancing the laser power to increase the light intensity to allow a relatively small aperture size to be used, and (2) using a CCD camera with a high resolution that has a relatively small pixel size to allow speckling, which results in covering more pixels.

6.6. Chapter summary

A multiplexed holographic system for simultaneous dual-spatial-resolution measurements of deformation is presented in this paper. The main innovation of our research is we are the first to enable the digital holographic system to take simultaneous measurements with both the large and small fields of view and to observe whole-field deformations as well as local information, such as in the areas of strain concentration. The developed system is beneficial for deformation and strain measurements as well as for non-destructive testing, especially if the loading is not repeatable. The polarization technique is used to obtain two polarized holographic setups with two different-sized fields of view, large and small, by changing the combined focus length. The phase distributions of two holograms have been successfully extracted from one image containing two holograms recorded by a single camera through the spatial carrier fringes' phase shift method. The optical setup is relatively simple and the spectrums of two holograms can be separated easily by adjusting the orientation of the carrier fringes. This along with the good measurement results obtained from the setup increase its utility for practical applications. The special advantage of the system developed is its capability to perform simultaneous and dual-resolution measurements. This is particularly meaningful for some experiments which cannot be repeated; additionally, this can also lead to reduced labor and time costs associated with testing. The experiments conducted have demonstrated that the developed system is an effective tool to measure both whole and local information, especially in cases in which more detailed information is required for areas with a strain concentration and in cases in which smaller defects need to be found.

CHAPTER SEVEN

CONCLUSION

Spackle interferometry measurement technology is an optical detection method that offers advantages such as full-field, high sensitivity, high accuracy, and non-contact capabilities. After decades of development, this technology now mainly comprises digital holography and digital shearography techniques. These two methods have found widespread applications in aviation, automotive, and industrial sectors for deformations or stress detection in advanced materials and non-destructive testing.

Typically, electronic scatter interferometry measurements are performed at a fixed spatial resolution for each measurement. However, this single-resolution detection system has the following drawbacks:

When measuring the deformation of objects with strain concentration at specific locations, the fringe patterns may become too dense for the measurement system to handle, leading to measurement failures.

In non-destructive testing, low spatial resolution may overlook small-sized internal defects.

Therefore, using measurements with different spatial resolutions is an effective approach to address these issues. Usually, this involves multiple separate tests to observe different spatial resolutions, which not only increases labor and testing time but also complicates the measurement process. Additionally, in some cases, multiple measurements may not be feasible.

This dissertation primarily focuses on synchronized dual-resolution measurements. Firstly, it establishes two independent optical channels using polarization techniques to simultaneously observe two different-sized fields of view, achieving dual resolutions by observing these different-sized fields. Then, it introduces spatial carrier techniques to introduce carriers of different frequencies, transforming the intensity information that overlaps into spectrum distributions separated by different carriers in the spatial domain through Fourier transformation. Subsequently, it extracts scatter phase information from the separated spectra through inverse Fourier transformation, enabling synchronized dual-resolution measurements.

Based on these key technologies, this thesis primarily concentrates on proposing a novel holography system. It is the first to utilize digital holography technology to achieve synchronized dual spatial sensitivity measurements. Furthermore, this thesis enhances a shearography system, addressing the issue of spectrum distribution only along the x-axis, which leads to overlap, and increasing the number of parameters that can be simultaneously detected.

However, both systems still have some issues. For the shearography system, the optical path design is complex, and it involves the use of multiple optical devices leading to a decrease in optical intensity. As for the holography system, the use of two sets of polarization optics results in significant energy loss, leading to lower precision in experimental results. Additionally, its resistance to interference is inferior to the shearography system.

In future research work, emphasis should be placed on addressing these shortcomings. This includes simplifying system design, reducing optical energy loss, improving detection precision, and enhancing interference resistance.

REFERENCE

[1] Hung, Y.Y., A speckle-shearing interferometer: A tool for measuring derivatives of surface displacements. Optics Communications, 1974. 11(2): p. 132-135.

[2] Burch J.M., Leendertz J.A. Speckle pattern and holographic techniques in engineering metrology. Optics and Laser Technology, 1971, 3(1): 26-30.

[3] Nakadate S., Yatagai T., Saito H. Electronic speckle pattern interferometry using digital image processing techniques. Applied Optics, 1980, 19(11): 1879-1883.

[4] Creath K. Phase-shifting speckle interferometry. Applied Optics, 1985, 24(18):3053-3058.

[5] Hung Y.Y. A speckle-shearing interferometer: a tool for measuring derivatives of surface displacements[J]. Optics Communications, 1974, 11(2): 132-135.

[6] Hung Y.Y. Shearography: a new optical method for strain measurement and nondestructive testing[J]. Optical Engineering, 1982, 21(3): 391-395.

[7] Steinchen, W.; Yang, L. Digital Shearography: Theory and Application of Digital Speckle Pattern Shearing Interferometry; SPIE Press: Bellingham, WA, USA, 2003; Volume 93.

[8] Wang, Y.; Gao, X.; Xie, X.; Wu, S.; Liu, Y.; Yang, L. Simultaneous dual directional strain measurement using spatial phase-shift digital shearography. Opt. Lasers Eng. 2016, 87, 197–203.

[9] Siebert, T.; Schmitz, B. New shearing setup for simultaneous measurement of two shear directions. In Practical Holography XIII; SPIE: 1999; Volume 3637, pp. 225–230.

[10] Xie, X.; Lee, C.P.; Li, J.; Zhang, B.; Yang, L. Polarized digital shearography for simultaneous dual shearing directions meas-urements. Rev. Sci. Instrum. 2016, 87, 083110.

[11] Bhaduri, B.; Mohan, N.K.; Kothiyal, M.P. Simultaneous measurement of out-of-plane displacement and slope using a multi-aperture DSPI system and fast Fourier transform. Appl. Opt. 2007, 46, 5680–5686.

[12] Qihan, Z.; Chen, W.; Sun, F.; Yan, P.; Ye, B.; Wang, Y. Simultaneous 3D measurement of deformation and its first derivative with speckle pattern interferometry and shearography. Appl. Opt. 2019, 58, 8665–8672.

[13] Hooshmand-Ziafi, H.; Hassani, K.; Dashtdar, M. Dual-sensitive spatial phase-shifting shearography based on a common-path configuration. Opt. Eng. 2019, 58, 114104.

[14] Francis, D.; Tatam, R.P.; Groves, R.M. Shearography technology and applications: A review. Meas. Sci. Technol. 2010, 21, 102001.

[15] Dong, J.; Wang, S.; Lu, M.; Jakobi, M.; Liu, Z.; Dong, X.; Pöller, F.; Bilgeri, L.M.; Bloise, F.S.; Yetisen, A.K.; et al. Real-time du-al-sensitive shearography for simultaneous in-plane and out-of-plane strain measurements. Opt. Express 2019, 27, 3276–3283.

[16] Zhang, B.; Zheng, X.; Guo, B.; Fang, S.; Sia, B.; Yang, L. Sagnac interferometer based digital shearography for simultaneous dual sensitivity measurement. Opt. Lasers Eng. 2022, 152, 106984.

[17] Wang, Y.; Gao, X.; Xie, X.; Wu, S.; Liu, Y.; Yang, L. Simultaneous dual directional strain measurement using spatial phase-shift digital shearography. Opt. Lasers Eng. 2016, 87, 197–203.

[18] Kujawinska, M.; Wojciak, J. Spatial-carrier phase-shifting technique of fringe pattern analysis. In Industrial Applications of Holographic and Speckle Measuring Techniques; SPIE: 1991; Volume 1508, pp. 61–67.

[19] Rigden, J.D. and E.I. Gordon. Granularity of Scattered Optical Maser Light [J]. Proc. Inst. Radio Eng. 1962. 50: 2367-2368.

[20] Yu Qifeng, Fu Sihua. ESPI and InSAR Interferogram Processing Method Based on Fringe Orientation and Fringe Contour [M]. Beijing: Science Press. 2007.

[21] Fang Qiang, Chen Jiabi. Holographic Speckle Metrology [M]. Beijing: Science Press. 1995.

[22] G. Pedrini, H. J. Tiziani. Quantitative evaluation of two dimensionals dynamical deformations using digital holography [J]. Optics & Laser Technology. 1997. 29(5): 249-256.

[23] G. Pedrini, I. Alexeenko, W. Osten & H. J. Tiziani. Temporal phase unwrapping of digital hologram sequences. Applied Optics. 2003. 42: 5846-5854.

[24] Qin Yuwen, Dai Jiabin, Chen Jinlong. Advances in Electronic Speckle Methods [J]. Experimental Mechanics. 1996.

[25] L.X. Yang and Thorsten Siebert, Digital Speckle Interferometry in Engineering of New Directions of Holography and Speckles [M]. American Scientific Publishers. 2008.

[26] Goodman. Speckle Phenomena in Optics: Theory and Applications [M]. Beijing: Science Press. 2009.

[27] Y.H. Wang, D. Thomas, P. Zhang, H. Yokota, and L.X. Yang. Whole Field Strain Measurement on Complex Surfaces by Digital Speckle Pattern Interferometry. Materials Evaluation. 2008.66(5): 507-512.

[28] Moore, A.J. and J.R. Tyrer, An Electronic Speckle Pattern Interferometer for Complete in Plane Displacement Measurement. Measurement Science & Technology, 1999. 1(10): p. 1024.

[29] Jingbo and Zhang, Two-dimensional in-plane electronic speckle pattern interferometer and its application to residual stress determination. Optical Engineering, 1998. 37(8): p. 2402-2409

[30] Santos, F., M. Vaz, and J. Monteiro, A new set-up for pulsed digital shearography applied to defect detection in composite structures. Optics & Lasers in Engineering, 2004. 42(2): p. 131-140.

[31] Yang, L., Digital Shearography: Theory and Application of Digital Speckle Pattern Shearing Interferometry. 2003.

[32] Brug, H.V., Temporal phase unwrapping and its application in shearography systems. Applied Optics, 1998. 37(28): p. 6701.

[33] Xie, X., et al., Spatial Phase-Shift Digital Shearography for Out-of-Plane Deformation Measurement. Sae International Journal of Materials & Manufacturing, 2014. 7(2): p. 402-405.

[34] S.J. Wu, L.Q. Zhu, Q.B. Feng, and L.X. Yang. Digital Shearography with In Situ Phase Shift Calibration, Optics and Lasers in Engineering. 2012. 5(9): 1260-1266

[35] Huang J.R., Ford H.D., Tatam R.P. Phase-stepped speckle shearing interferometer by source wavelength modulation[J]. Optics Letters, 1996, 21(18):.1421-1423.

[36] Qian Kemao, Xu Boqin, Wu Xiaoping. "Phase Measurement Methods in Optical Interferometric Metrology." Experimental Mechanics, 2001, 16(3): 239-249.

[37] Zhu L.Q., Wang Y.H., Xu N., Wu S.J., Dong M.L., Yang L.X. Real-time monitoring of phase maps of digital shearography[J]. Optical Engineering, 2013, 52(10): 101902.

[38] Wang Yonghong, Feng Jiaya, Wang Xin, Liu Pei, Li Junrui, Yang Lianxiang. "Dynamic Measurement of Shear Speckle Interferometry Based on Slit Light Stop." Optics and Precision Engineering, 2015, 23(3): 645-651.

[39] Wang Y.H., Gao X.Y., Xie X., Wu S.J., Liu Y.X., Yang L.X. Simultaneous dual

[40] directional strain measurement using spatial phase-shift digital shearography[J]. Optics and Lasers in Engineering, 2016, 87: 197-203.

[41] Zhou Hualong. "Research on Digital Image Processing System Based on ESPI." [Dissertation]. Hefei: School of Instrument Science and Opto-electronics Engineering, Hefei University of Technology, 2012.

[42] Bu Weihua. "Research on Surface Measurement Technology Based on Electronic Speckle Interferometry." [Dissertation]. Hefei: School of Instrument Science and Opto-electronics Engineering, Hefei University of Technology, 2013.

[43] Li Nan. "Research on Digital Speckle Interferometric Fringe Information Processing Technology." [Dissertation]. Hefei: School of Instrument Science and Opto-electronics Engineering, Hefei University of Technology, 2012.

[44] Yang, L. and X. Xie, Principles of Temporal Phase Shift Shearography. 2016.

[45] Xie, Xin, Lianxiang Yang, Xu Chen, Nan Xu, and Yonghong Wang. "Review and comparison of temporal-and spatial-phase shift speckle pattern interferometry for 3D deformation measurement." In Sixth International Symposium on Precision Mechanical Measurements, International Society for Optics and Photonics, 2013. 8916, p.89260D.

[46] Zhu, Lianqing, Yonghong Wang, Nan Xu, Sijin Wu, Mingli Dong, and Lianxiang Yang. "Real-time monitoring of phase maps of digital shearography." Optical Engineering, 2013. 52(10), p. 101902.

[47] Yang, L. X., W. Steinchen, M. Schuth, and G. Kupfer. "Precision measurement and nondestructive testing by means of digital phase shifting speckle pattern and speckle pattern shearing interferometry." Measurement, 1995. 16(3), p. 149- 160.

[48] Kao C.C., Yeh G.B., Lee S.S., Lee C.K., Yang C.S., Wu K.C. Phase-shifting algorithms for electronic speckle pattern interferometry[J]. Applied Optics, 2002, 41(1): 46-54.

[49] Bi H.B., Zhang Y., Ling K.V., Wen C.Y. Class of 4+1-phase algorithms with error compensation[J]. Applied Optics, 2004, 43(21): 4199-4207.

[50] Sun C., Chen J.L., Lu H. Improved phase-shifted digital speckle shearography for time-dependent deformation measurement[J]. Optical Engineering, 2008,47(8): 065601.

[51] Takeda, Mitsuo, Quan Gu, Masaya Kinoshita, Hideaki Takai, and Yosuke Takahashi. "Frequency-multiplex Fourier-transform profilometry: a singleshot three-dimensional shape measurement of objects with large height discontinuities and/or surface isolations." Applied optics,1997. 36(22), p. 5347-5354.

[52] Kolenovic, Ervin, Wolfgang Osten, Reiner Klattenhoff, Songcan Lai, Christoph von Kopylow, and Werner Jüptner. "Miniaturized digital holography sensor for distal three-dimensional endoscopy." Applied optics, 2003. 42(25), p. 5167- 5172.

[53] Gong, X. L., and S. Toyooka. "Investigation on mechanism of plastic deformation by digital speckle pattern interferometry." Experimental mechanics, 1999. 39(1), p. 25-29.

[54] Restivo, Gaetano, Gary L. Cloud, Rob M. Beaudry, and Basavaraju B. Raju. 3-D Strain fields using embedded DSPI: pilot study. ARMY TANK AUTOMOTIVE RESEARCH DEVELOPMENT AND ENGINEERING CENTER WARREN MI, 2004.

[55] Baik, Sung-Hoon, Seung-Kyu Park, Cheol-Jung Kim, and Soo-Yong Kim. "Twochannel spatial phase shifting electronic speckle pattern interferometer." Optics communications, 2001. 192(3), p. 205-211.

[56] Fu, Yu, Min Guo, and Huan Liu. "Determination of instantaneous curvature and twist by digital shearography." Optical Engineering, 2012. 51(8), p. 083602.

[57] Pedrini, G., Y. L. Zou, and H. J. Tiziani. "Quantitative evaluation of digital shearing interferogram using the spatial carrier method." Pure and Applied Optics: Journal of the European Optical Society Part A, 1996. 5(3), p. 313.

[58] Pedrini, Giancarlo, Wolfgang Osten, and Mikhail E. Gusev. "High-speed digital holographic interferometry for vibration measurement." Applied optics, 2006. 45(15), p. 3456-3462.139

[59] Bhaduri, Basanta, N. Krishna Mohan, M. P. Kothiyal, and R. S. Sirohi. "Use of spatial phase shifting technique in digital speckle pattern interferometry (DSPI) and digital shearography (DS)." Optics express, 2006 14(24), p. 11598-11607.

[60] Bhaduri, Basanta, Nandigana Krishna Mohan, and Mahendra Prasad Kothiyal. "Simultaneous measurement of out-of-plane displacement and slope using a multiaperture DSPI system and fast Fourier transform." Applied optics, 2007. 46(23), p. 5680-5686.

[61] Pedrini, G., Y-L. Zou, and H. J. Tiziani. "Simultaneous quantitative evaluation of inplane and out-of-plane deformations by use of a multidirectional spatial carrier." Applied optics, 1997. 36(4), p. 786-792

[62] Santos, F., M. Vaz, and J. Monteiro, A new set-up for pulsed digital shearography applied to defect detection in composite structures. Optics & Lasers in Engineering, 2004. 42(2): p. 131-140.

[63] Jiancheng, et al., Algorithm for multiple-beam Fizeau interferograms with arbitrary phase shifts. Optics Express, 2008.

[64] Smythe R., Moore R. Instantaneous phase measuring interferometry[J]. Optical Engineering, 1984, 23(4): 361-364.

[65] J, A., et al., Real-time displacement measurement using a multicamera phase-stepping speckle interferometer. Applied Optics, 1994.

[66] Pedrini, G., Y.-L. Zou, and H.J. Tiziani, Quantitative evaluation of digital shearing interferogram using the spatial carrier method. Pure & Applied Optics Journal of the European Optical Society Part A, 1996. 5(3): p. 313.

[67] Baik, S.H., et al., Two-channel spatial phase shifting electronic speckle pattern interferometer. Optics Communications, 2001. 192(3): p. 205-211.

[68] Takeda, M., Performance of spatial vs. temporal phase shifting in ESPI. Proceedings of Spie Interferometry, 1999. 3744.

[69] Pedrini, G., Y. L. Zou, and H. J. Tiziani. "Quantitative evaluation of digital shearing interferogram using the spatial carrier method." Pure and Applied Optics: Journal of the European Optical Society Part A, 1996. 5(3), p. 313.

[70] Pedrini, Giancarlo, Wolfgang Osten, and Mikhail E. Gusev. "High-speed digital holographic interferometry for vibration measurement." Applied optics, 2006. 45(15), p. 3456-3462.

[71] Kohler, Christian, Matias R. Viotti, and G. Armando Albertazzi Jr. "Measurement of three-dimensional deformations using digital holography with radial sensitivity." Applied optics, 2010. 49(20), p. 4004-4009.

[72] Bhaduri, Basanta, Nandigana Krishna Mohan, and Mahendra Prasad Kothiyal. "Simultaneous measurement of out-of-plane displacement and slope using a multiaperture DSPI system and fast Fourier transform." Applied optics, 2007. 46(23), p. 5680-5686.

[73] Xie, Xin, Nan Xu, Jianfei Sun, Yonghong Wang, and Lianxiang Yang. "Simultaneous measurement of deformation and the first derivative with spatial phase-shift digital shearography." Optics Communications, 2013. 286, p. 277-281.140

[74] Schedin, Staffan, Giancarlo Pedrini, Hans J. Tiziani, and Fernando Mendoza Santoyo. "Simultaneous three-dimensional dynamic deformation measurements with pulsed digital holography." Applied optics, 1999. 38(34), p.7056-7062.

[75] Li Yanhua, "Research on Filtering and Skeletonization Algorithms for Optical Interferometric Images." Harbin Institute of Technology.

[76] Tang, C., et al., Denoising by coupled partial differential equations and extracting phase by backpropagation neural networks for electronic speckle pattern interferometry. Applied Optics, 2007. 46(30): p. 7475-84.

[77] Aebischer, H.A. and S. Waldner, Simple and effective method for filtering speckle-interferometric phase fringe patterns. Optics Communications, 1999. 162(4): p. 205-210.

[78] Pedrini, G., W. Osten, and M.E. Gusev, High-speed digital holographic interferometry for vibration measurement. Applied Optics, 2006. 45(15): p. 3456-62.

[79] Pedrini, Zou, and Tiziani, Simultaneous quantitative evaluation of in-plane and out-of-plane deformations by use of a multidirectional spatial carrier. Applied Optics, 1997.

[80] Pedrini, G., Y.-L. Zou, and H.J. Tiziani, Quantitative evaluation of digital shearing interferogram using the spatial carrier method. Pure & Applied Optics Journal of the European Optical Society Part A, 1996. 5(3): p. 313.

[81] Boyang Zhang, Fangyuan Sun, Lei Yang, and Lianxiang Yang, "Spatial-light-modulator-based dual shearing direction shearography," Appl. Opt. 59, 11080-11086 (2020)

[82] Xie, Xin, et al. "Simultaneous measurement of deformation and the first derivative with spatial phase-shift digital shearography." Optics Communications 286 (2013): 277-281.

[83] Qihan Zhao, Weijie Chen, Fangyuan Sun, PeiZheng Yan, Bing Ye, and Yonghong Wang, "Simultaneous 3D measurement of deformation and its first derivative with speckle pattern interferometry and shearography," Appl.Opt. 58, 8655-8672 (2019)

[84] Hooshmand-Ziafi, Helia, Khosrow Hassani, and Masoomeh Dashtdar. "Dual-sensitive spatial phase-shifting shearography based on a common-path configuration." Optical Engineering 58.11 (2019): 114104.

[85] Yang L, Chen F, Steinchen W, Huang MY. Digital shearography for nondestructive testing: potentials, limitations, and applications. JOHAS 2004;1(2):69–79.

[86] Steinchen W, Yang L. Digital shearography: theory and application of digital speckle pattern shearing interferometry. SPIE Optical Engineering Press; 2003.

[87] Siebert T, Schmitz B. New shearing setup for simultaneous measurement of two shear directions. SPIE 1999; 3637:225–30.

[88] Xie, Xin, et al. "Simultaneous measurement of deformation and the first derivative with spatial phase-shift digital shearography." Optics Communications 286 (2013): 277-281

[89] Shipman, James; Wilson, Jerry D.; Higgins, Charles A. (2015). An Introduction to Physical Science, 14th Ed. Cengage Learning. p. 187. ISBN 978-1-305-54467-3.

[90] Muncaster, Roger (1993). A-level Physics. Nelson Thornes. pp. 465–467. ISBN 0-7487-1584-3.

[91] Singh, Devraj (2015). Fundamentals of Optics, 2nd Ed. PHI Learning Pvt. Ltd. p. 453. ISBN 978-8120351462.

[92] Jump up to:a b Avadhanulu, M. N. (1992). A Textbook of Engineering Physics. S. Chand Publishing. pp. 198–199. ISBN 8121908175.

[93] Desmarais, Louis (1997). Applied Electro Optics. Pearson Education. pp. 162–163. ISBN 0-13-244182-9.

[94] Hung YY. Shearography: a new optical method for strain measurement and nondestructive testing. Opt. Eng. 1982; 21:213391.

[95] Yang L, Xie X. Digital Shearography–New Developments and Applications. SPIE Press 2016.

[96] Zhang, Boyang, Xiaowan Zheng, Bicheng Guo, Siyuan Fang, Bernard Sia, and Lianxiang Yang. "Sagnac Interferometer Based Digital Shearography for Simultaneous Dual Sensitivity Measurement." Optics and Lasers in Engineering 152 (2022): 106984. Xie, Xin, Lianxiang Yang, Nan Xu, and Xu Chen. "Michelson interferometer based spatial phase shift shearography." Applied optics 52, no. 17 (2013): 4063-4071.

[97] W. Steinchen and L. Yang, Digital Shearography: Theory and Application of Digital Speckle Pattern Shearing Interferometry (SPIE, 2003), pp. 116–122

[98] X. Xie, N. Xu, J. Sun, Y. Wang, and L. Yang, "Simultaneous measurement of deformation and the first derivative with spatial phase-shift digital shearography," Opt. Commun. 286, 277–281 (2013).

[99] Zhang, Boyang, Xiaowan Zheng, Bicheng Guo, Siyuan Fang, Bernard Sia, and Lianxiang Yang. "Sagnac Interferometer Based Digital Shearography for Simultaneous Dual Sensitivity Measurement." Optics and Lasers in Engineering 152 (2022): 106984.

[100] Yang, L. and Xie, X., 2016. Digital shearography: new developments and applications. SPIE press.

[101] Zhang, B., Zheng, X., Xu, W. and Yang, L., 2020. Overview of digital shearography for NDT. Materials Evaluation, 78(3).

[102] Wang, B., Zhong, S., Lee, T.L., Fancey, K.S. and Mi, J., 2020. Non-destructive testing and evaluation of composite materials/structures: A state-of-the-art review. Advances in mechanical engineering, 12(4), p.1687814020913761.

[103] Gupta, R., Mitchell, D., Blanche, J., Harper, S., Tang, W., Pancholi, K., Baines, L., Bucknall, D.G. and Flynn, D., 2021. A review of sensing technologies for non-destructive evaluation of structural composite materials. Journal of Composites Science, 5(12), p.319.

[104] Wang, B., Zhong, S., Lee, T.L., Fancey, K.S. and Mi, J., 2020. Non-destructive testing and evaluation of composite materials/structures: A state-of-the-art review. Advances in mechanical engineering, 12(4), p.1687814020913761.

[105] Gryzagoridis, J. and Findeis, D., 2010. Impact damage detection on composites using optical NDT techniques. Insight-Non-Destructive Testing and Condition Monitoring, 52(5), pp.248-251.

[106] Hariharan, P., 2002. Basics of holography. Cambridge university press.

[107] Ettemeyer, A., 2000. Combination of 3-D deformation and shape measurement by electronic speckle pattern interferometry for quantitative strain-stress analysis. Optical Engineering, 39(1), pp.212-215.

[108] Collier, Robert. Optical holography. Elsevier, 2013.

[109] Schnars, Ulf, Claas Falldorf, John Watson, Werner Jüptner, Ulf Schnars, Claas Falldorf, John Watson, and Werner Jüptner. Digital holography. Springer Berlin Heidelberg, 2015.

[110] Dong, J., Wang, S., Lu, M., Jakobi, M., Liu, Z., Dong, X., Pöller, F., Bilgeri, L.M., Bloise, F.S., Yetisen, A.K. and Koch, A.W., 2019. Real-time dual-sensitive shearography for simultaneous in-plane and out-of-plane strain measurements. Optics Express, 27(3), pp.3276-3283.

[111] Bhaduri, B., Mohan, N.K. and Kothiyal, M.P., 2007. Simultaneous measurement of out-of-plane displacement and slope using a multiaperture DSPI system and fast Fourier transform. Applied optics, 46(23), pp.5680-5686.

[112] Hooshmand-Ziafi, H., Hassani, K. and Dashtdar, M., 2019. Dual-sensitive spatial phase-shifting shearography based on a common-path configuration. Optical Engineering, 58(11), pp.114104-114104.

[113] Francis, D., Tatam, R.P. and Groves, R.M., 2010. Shearography technology and applications: a review. Measurement science and technology, 21(10), p.102001.

[114] Yang, L., Chen, F., Steinchen, W. and Hung, M.Y., 2004. Digital shearography for nondestructive testing: potentials, limitations, and applications. Journal of Holography and Speckle, 1(2), pp.69-79.

[115] Steinchen, W. and Yang, L., 2003. Digital shearography: theory and application of digital speckle pattern shearing interferometry (Vol. 93). Bellingham, WA: SPIE press.

[116] Siebert, T. and Schmitz, B., 1999, March. New shearing setup for simultaneous measurement of two shear directions. In Practical Holography XIII (Vol. 3637, pp. 225-230). SPIE.

[117] Pedrini, G., Zou, Y.L. and Tiziani, H.J., 1996. Quantitative evaluation of digital shearing interferogram using the spatial carrier method. Pure and Applied Optics: Journal of the European Optical Society Part A, 5(3), p.313.

[118] Kujawinska, M. and Wojciak, J., 1991, October. Spatial-carrier phase-shifting technique of fringe pattern analysis. In Industrial Applications of Holographic and Speckle Measuring Techniques (Vol. 1508, pp. 61-67). SPIE.

[119] Goldberg, K.A. and Bokor, J., 2001. Fourier-transform method of phase-shift determination. Applied optics, 40(17), pp.2886-2894.

[120] Wang, Y., Gao, X., Xie, X., Wu, S., Liu, Y. and Yang, L., 2016. Simultaneous dual directional strain measurement using spatial phase-shift digital shearography. Optics and Lasers in Engineering, 87, pp.197-203.

[121] Zhao, Qihan, Weijie Chen, Fangyuan Sun, PeiZheng Yan, Bing Ye, and Yonghong Wang. "Simultaneous 3D measurement of deformation and its first derivative with speckle pattern interferometry and shearography." Applied Optics 58, no. 31 (2019): 8665-8672.

[122] Xie, X., Lee, C.P., Li, J., Zhang, B. and Yang, L., 2016. Polarized digital shearography for simultaneous dual shearing directions measurements. Review of Scientific Instruments, 87(8), p.083110.

[123] Zhang, B., Zheng, X., Guo, B., Fang, S., Sia, B. and Yang, L., 2022. Sagnac interferometer based digital shearography for simultaneous dual sensitivity measurement. Optics and Lasers in Engineering, 152, p.106984.

[124] Xiaowan Zheng, Bicheng Guo, Siyuan Fang, Bernard Sia, and Lianxiang Yang. Development of Digital Shearography for dual sensitivity simultaneous measurement using carrier frequency spatial phase shift technology. No. 2023-01-0068. SAE Technical Paper, 2023.

[125] Xie, X., Xu, N., Sun, J., Wang, Y. and Yang, L., 2013. Simultaneous measurement of deformation and the first derivative with spatial phase-shift digital shearography. Optics Communications, 286, pp.277-281.

[126] Cai, C. and He, L., 2012. Improved Mach–Zehnder interferometer-based shearography. Optics and Lasers in Engineering, 50(12), pp.1699-1705.

[127] Wu, S., He, X. and Yang, L., 2011. Enlarging the angle of view in Michelson-interferometer-based shearography by embedding a 4f system. Applied optics, 50(21), pp.3789-3794.

[128] Boudebs, G., Besse, V., Cassagne, C., Leblond, H. and de Araújo, C.B., 2013. Nonlinear characterization of materials using the D4σ method inside a Z-scan 4f-system. Optics letters, 38(13), pp.2206-2208.

[129] Schnars, U., Kreis, T.M. and Jüptner, W.P., 1996. Digital recording and numerical reconstruction of holograms: reduction of the spatial frequency spectrum. Optical Engineering, 35(4), pp.977-982.